2013 Volume 1

The Journal on Advanced Studies in Theoretical and Experimental Physics, including Related Themes from Mathematics

PROGRESS IN PHYSICS

"All scientists shall have the right to present their scientific research results, in whole or in part, at relevant scientific conferences, and to publish the same in printed scientific journals, electronic archives, and any other media."
— Declaration of Academic Freedom, Article 8

ISSN 1555-5534

The Journal on Advanced Studies in Theoretical and Experimental Physics, including Related Themes from Mathematics

PROGRESS IN PHYSICS

A quarterly issue scientific journal, registered with the Library of Congress (DC, USA). This journal is peer reviewed and included in the abstracting and indexing coverage of: Mathematical Reviews and MathSciNet (AMS, USA), DOAJ of Lund University (Sweden), Zentralblatt MATH (Germany), Scientific Commons of the University of St. Gallen (Switzerland), Open-J-Gate (India), Referativnyi Zhurnal VINITI (Russia), etc.

Electronic version of this journal:
http://www.ptep-online.com

Postal Address

Department of Mathematics and Science,
University of New Mexico,
705 Gurley Ave., Gallup, NM 87301, USA

ISSN: 1555-5534 (print)
ISSN: 1555-5615 (online)

Standard Address Number: 297-5092
Printed in the United States of America

JANUARY 2013 **VOLUME 1**

CONTENTS

Information for Authors and Subscribers

Progress in Physics has been created for publications on advanced studies in theoretical and experimental physics, including related themes from mathematics and astronomy. All submitted papers should be professional, in good English, containing a brief review of a problem and obtained results.

All submissions should be designed in LaTeX format using *Progress in Physics* template. This template can be downloaded from *Progress in Physics* home page http://www.ptep-online.com. Abstract and the necessary information about author(s) should be included into the papers. To submit a paper, mail the file(s) to the Editor-in-Chief.

All submitted papers should be as brief as possible. We accept brief papers, no larger than 8 typeset journal pages. Short articles are preferable. Large papers can be considered in exceptional cases to the section *Special Reports* intended for such publications in the journal. Letters related to the publications in the journal or to the events among the science community can be applied to the section *Letters to Progress in Physics*.

All that has been accepted for the online issue of *Progress in Physics* is printed in the paper version of the journal. To order printed issues, contact the Editors.

This journal is non-commercial, academic edition. It is printed from private donations. (Look for the current author fee in the online version of the journal.)

Some Expressions for Gravity without the Big G and their Possible Wave-Theoretical-Explanation

Hasmukh K. Tank
Indian Space Research Organization, 22/693, Krishna Dham-2, Vejalpur, Ahmedabad-380015, India
E-mail: tank.hasmukh@rediffmail.com, hasmukh.tank1@gmail.com

This letter presents some new expressions for gravity without the big G and proposes their possible wave-theoretical-explanation. This attempt leads to some insight that: (i) We need the proportionality-constant G because we measure masses and distances in our arbitrarily-chosen units of kg and meters; but if we measure "mass" as a fraction of "total-mass of the universe" M_0 and measure distances as a fraction of "radius-of-the-universe" R_0 then there is no need for the proportionality-constant G. However, large uncertainties in the M_0 and R_0 limit the general application of this relation presently. (ii) The strength of gravity would be different if the total-mass of the universe were different. Then this possibility is supported with the help of wave-theory. (iii) This understanding of G leads to an insight that Plancks-length, Planck-mass and Planck's unit of time are geometric-mean-values of astrophysical quantities like: total-mass of the universe and the smallest-possible-mass hH_0/c^2. (iv) There appears a law followed by various systems-of-matter, like: the electron, the proton, the nucleus-of-atom, the globular-clusters, the spiral-galaxies, the galactic-clusters and the whole universe; that their ratio $\text{Mass}/\text{Radius}^2$ remains constant. This law seems to be more fundamental than the fundamental-forces because it is obeyed irrespective of the case, whether the system is bound by strong-force, electric-force, or gravitational-force.

1 Introduction

Sir Isaac Newton presented the quantitative description of gravitational attraction between two massive bodies, that the force of attraction is directly proportional to the product of two masses, and inversely proportional to the square of centre-to-centre distance between them; and the value of proportionality-constant G was found to remain the same even in the case of planets. But there has been no explanation for why the value of G is this much. Einstein also made extensive use of G by treating it as a fundamental-physical-constant. Based on my previous works, [1-5] and the works of researchers cited in these papers, this paper presents some alternative expressions for gravity, without the big G, and proposes a wave-theoretical-explanation for gravity.

2 New expressions of gravity without the big G

(i) R.K. Adair, in his book "Concepts in Physics" [6] has given a derivation, that the sum of "gravitational-potential-energy" and "energy-of-mass" of the whole universe is, strikingly, zero! i.e.

$$M_0c^2 - \frac{GM_0M_0}{R_0} = 0$$

where M_0 and R_0 are total-mass and radius of the universe respectively, and G is Newton's gravitational constant; i.e.

$$\frac{GM_0^2}{R_0} = M_0c^2$$

i.e.

$$G = \frac{R_0c^2}{M_0}.$$

So, by substituting R_0c^2/M_0 for G in Newton's formula, the gravitational potential energy U_g stored in a system of masses M and m separated by a distance r can be expressed as:

$$U_g = \frac{\frac{M}{M_0}mc^2}{r/R_0}. \quad (1)$$

Newton's law when expressed as shown in the expression-1, shows that: if we measure masses as a fraction of total-mass of the universe M_0 and measure distances as a fraction of radius of the universe R_0 then we do not need the big G.

However, large uncertainties in the M_0 and R_0 limit the general application of this relation presently.

A brief discussion will be in order, how the "total-mass-of-the-universe" and "radius-of-the-universe" are derived; and what would be the uncertainties of these?

Total-mass-of-the-universe:

E.P. Hubble's experimental-observations of the "cosmological-red-shift", when interpreted in terms of "recession-of-galaxies", gives a linear relation:

$$v = H_0D$$

where: v is the "velocity-of-recession" of a galaxy, H_0 is Hubble's constant and D the luminosity-distance of a galaxy. From this relation we can get an estimate of "sum-total-of-kinetic-energy-of-the-universe" K_u. This recession-of-galaxies, also known as: "expansion-of-the-universe", can stop if

and when "kinetic-energy-of-the-universe" K_u becomes equal to "gravitational-potential-energy-of-the-universe" U_u. By equating $K_u = U_u$, cosmologists have derived the value of "total-mass-of-the-universe" M_0.

It has been estimated [7] that the universe would have collapsed to hot-death much sooner than the present-age of the universe if total-mass of the universe were more than M_0; and it would have cooled down to cold-death much earlier than the present-age of the universe if its total-mass were less than M_0. The present-age, of 14 billion years, imply that the total-mass of the universe is indeed M_0. $M_0 = 10^{82}$ pion-masses.

It is surprising [8] that cosmologists are so far able to experimentally detect only the baryonic-matter, which is hardly 4% of the total-mass M_0! At least 70% of the total-mass M_0 is believed to be in the form of "dark-energy", and remaining 26% in the form of "dark-matter". "Dark-matter" is needed to explain the "flattening-of-galaxies-rotation-curves". That is, the estimates of total-mass of the universe depend on 26% share from "dark-matter", and 70% share from "dark-energy" which are yet to be detected.

Radius-of-the-universe:

The distance at which a galaxy can attain the velocity-of-light, that is, when Hubble's expression becomes: $H_0R_0 = c$, where c is the speed-of-light, this distance R_0 is called: "the-radius-of-the-universe". Even if universe-tip may be moving with speed higher than light-speed, the "visible" horizon will be limited by the equation $c = H_0R_0$ [8]. So, the value of radius of the universe is taken as 10^{26} meters, i.e. $= 10^{40}$ classical-radius of the electron. Here H_0 is Hubble's constant.

As far as accuracy of the values of M_0 and R_0 are concerned, there must be large amount of uncertainties. We can not expect to improve current value of G form them. Our expression of gravity without G can only help us to gain an insight, that the strength of gravitational-force seems to depend on total-mass and radius of the universe. Similarly, we can gain some insight in to Planck's natural units, and Milgrom's new constant of nature a_0, termed as the "critical-acceleration" of Modified Newtonian Dynamics (MOND).

Now, let us move to some more expressions without the big G.

(ii) Milgrom's expression for the constant velocity v of the stars at the out-skirts of a spiral-galaxy of mass M is conventionally expressed as [7]:

$$v = (GMa_0)^{1/4}\,. \tag{2}$$

Since: $G = R_0c^2/M_0$, and $a_0 = c^2/R_0$, as discussed in [9], the expression-2 can be re-expressed without G as:

$$v = \left[\frac{R_0c^2}{M_0}M\frac{c^2}{R_0}\right]^{1/4}$$

i.e.

$$v = [M/M_0]^{1/4}c. \tag{3}$$

In the expression-3, c is the speed of light in vacuum, and M_0 and R_0 are total-mass and radius of the universe respectively.

(iii) We can express the radii of the globular-clusters, the spiral-galaxies and the galactic-clusters as:

$$R_{globu} = \left[\frac{M_{globu}}{M_0}\right]^{1/2} R_0 = [r_{Gglo}R_0]^{1/2}, \tag{4}$$

where r_{Gglo} is gravitational-radius of the globular-cluster.

$$R_{galaxy} = \left[\frac{M_{galaxy}}{M_0}\right]^{1/2} R_0 = [r_{Ggal}R_0]^{1/2}, \tag{5}$$

where r_{Ggal} is gravitational-radius of the galaxy.

$$R_{gal-clust} = \left[\frac{M_{gal-clust}}{M_0}\right]^{1/2} R_0 = [r_{Ggal-clust}R_0]^{1/2}, \tag{6}$$

where $r_{Ggal-clust}$ is gravitational-radius of the galactic-cluster.

Even the classical-radius of the electron $r_e = e^2/m_ec^2$ can also be expressed as:

$$r_e = \left[\frac{m_e}{M_0}\right]^{1/2} R_0 = [r_{G-e}R_0]^{1/2}, \tag{7}$$

where r_{G-e} is gravitational-radius of the electron.

Radius of the pi-meson $r_{pi} = Ng^2/m_{pi}c^2$ can also be expressed as:

$$r_{pi} = \left[\frac{m_{pi}}{M_0}\right]^{1/2} R_0 = [r_{G-pi}R_0]^{1/2}, \tag{8}$$

where r_{G-pi} is gravitational-radius of the pi-meson.

And the radius of nucleus of an atom r_n can also be expressed as:

$$r_n = \left[\frac{m_n}{M_0}\right]^{1/2} R_0 = [r_{G-n}R_0]^{1/2}, \tag{9}$$

where r_{G-n} is gravitational-radius of the nucleus-of-atom.

The expressions (4) to (9) can be jointly expressed as [8]:

$$\frac{M_0}{R_0^2} = \frac{m_P}{r_P^2} = \frac{me}{r_e^2} = \frac{m_n}{r_n^2} = \frac{M_{gc}}{R_{gc}^2} = \frac{M_{gal}}{R_{gal}^2} = \frac{M_{cg}}{R_{cg}^2} = \frac{H_0c}{G}.$$

We shall consider a possible "wave-theoretical-explanation" for the expressions (4) to (9) in the section-4.

Since the classical-radius of the electron $r_e = e^2/m_ec^2$, radius of the pi-meson $r_{pi} = Ng^2/m_{pi}c^2$ and the radius of nucleus of an atom r_n can also be expressed in the similar manner by inserting the masses of the electron, the pi-meson and the nucleus in the right-hand-sides of the above expressions, though they are bound by electric-force, strong-force and the nuclear-force respectively, it suggests a possibility that the currently-believed fundamental-forces may not be truly fundamental; rather, the law followed by them, as expressed in

the expressions (4) to (9), may be more fundamental than the "fundamental-forces"; and the strengths of forces may be getting decided by these expressions (4) to (9). It also suggests a possibility that when a "black-hole" has some "mass" then it has to have a "radius".

(iv) We can express the cosmological red-shift z_c smaller than unity as:

$$z_c = \frac{D}{R_0}. \tag{10}$$

And we can express the accelerated-expansion of the universe, the deceleration of the cosmologically red-shifted photon, the deceleration of the Pioneer-10, 11, Galileo and Ulysses space-probes and the "critical-acceleration" of MOND as [9]:

$$a_0 = \frac{c^2}{R_0}. \tag{11}$$

3 Some insight into Planck's units

From the law of equality of gravitational-potential-energy and energy-of-mass of the universe we found that: $G = R_0c^2/M_0$. Now let us make use of this expression to get some insight into Planck's units of length, mass and time:
Planck's-length $L^* = [hG/c^3]^{1/2}$.

Substituting R_0c^2/M_0 for G in the above expression,
Planck's-length $L^* = [hR_0c^2/M_0c^3]^{1/2}$;
i.e. Planck's-length

$$L^* = \left[\frac{h}{M_0c}R_0\right]^{1/2}; \tag{12}$$

i.e. Planck's-length L^* is a geometric-mean of: Compton-wavelength and Gravitational radius of total-mass of the universe, because $R_0 = GM_0/c^2$.
Planck-mass $M^* = [hc/G]^{1/2}$;
i.e. Planck-mass $M^* = [(h/R_0c)(M_0)]^{1/2}$; i.e. Planck-mass

$$M* = \left[\frac{hH_0}{c^2}M_0\right]^{1/2}. \tag{13}$$

That is Planck's unit of mass is a geometric-mean of: total-mass of the universe and smallest-possible-mass, corresponding to Hubble's constant (hH_0/c^2). Similarly, Planck's unit of time T^* is a geometric-mean of: age-of-the-universe T_0 and the period (h/M_0c^2): i.e.

$$T^* = \left[T_0\frac{h}{M_0c^2}\right]^{1/2}. \tag{14}$$

4 Possible wave-theoretical explanation for gravity

Let us assume that there are some most-fundamental-particles, and a long-range fundamental-force. We can take the mass of the "most-fundamental-particle" as a unity, and think that all the massive objects are collections of the "most-fundamental-particles".

Now, by a "particle" we mean an entity which is localized in an extremely small space; so, a "particle" can be mathematically represented in the space-domain as an impulse-function. This impulse-function can be Fourier-transformed into the "wave-number-domain". Then assuming a constant velocity of transmission of these waves, at the velocity of light, we can represent these waves in the "frequency-domain" as a wide band of frequencies. A particle of matter has a wide band of frequency-spectrum and a definite phase-spectrum. When this wide band of waves travels in space, then a "particle" becomes manifest only at a place and time when-and-where all the spectral-components add constructively, and have a particular, definite phase-relation, otherwise the particle remains dissolved in the un-manifest-state.

Secondly, we can not expect any coherence between the spectral-components of one and the other "particle". That means, that when two or more such fundamental-particles come close to each-other, the wide bands of their waves add like the incoherent superimposition of wideband-noise.

We know that the superimposition of n number of wide-band noise-sources of unit-amplitude is square-root-of n; like the vector-sum of n mutually orthogonal unit-vectors. That is:

$$N(t) = \left[(N_1(t))^2 + (N_2(t))^2 + (N_3(t))^2 \cdots + (N_n(t))^2\right]^{1/2}.$$

Now, if the strength of "coupling-constant" of a fundamental-force is, say, e^2, which is the strength of electric-force of the proton, then the strength of "coupling-constant" of a new "fundamental-force", which is actually due to "incoherent-superimposition", within the system of n fundamental-particles will be: $(n^{1/2}e^2)/n$. Since the total-mass of the universe M_0 is 10^{80} proton-masses, the strength of gravitational-force between the two protons is expected to be:

$$GM_0m_p = (\text{Total}-\text{number of protons in the universe})^{1/2}\ e^2$$

i.e.

$$Gm_p^2 = \frac{\sqrt{10^{80}}e^2}{10^{80}}$$

i.e.

$$Gm_p^2 = 10^{-40}e^2. \tag{15}$$

[Note: This is just an order-of-magnitude-estimate.]

Now, if the force within a system is stronger than gravity by a multiplication-factor, say, k-times, then the density of matter within that system is also logically expected to be k-times higher. That is, in our example of proton and the universe:

$$\frac{e^2}{Gm_p^2} = \left[\frac{M_0}{m_p}\right]^{1/2} = \frac{\frac{m_p}{\frac{4}{3}\pi r_p^3}}{\frac{M_0}{\frac{4}{3}\pi R_0^3}}$$

i.e.

$$\frac{e^2}{Gm_p^2} = \left[\frac{M_0}{m_p}\right]^{1/2} = \frac{m_pR_0^3}{M_0r_p^3}$$

i.e.

$$\left[\frac{M_0}{m_p}\right]^{3/2} = \frac{R_0^3}{r_p^3}$$

i.e.

$$\left[\frac{M_0}{m_p}\right]^{1/2} = \frac{R_0}{r_p} = \frac{e^2}{Gm_p^2} \tag{16}$$

i.e.

$$\frac{M_0}{R_0^2} = \frac{m_p}{r_p^2}. \tag{17}$$

The expression-16 was noticed as the "large-number-coincidence" [LNC], whereas here we derived it with the help of wave-theory.

Sivaram [10] had noticed a relation between masses and radii of the electron, the proton the nucleus-of-atoms, the globular-clusters, the spiral-galaxies, the galactic-clusters and the universe as shown in the expression-18 below. The expression-18 is similar to the expression-17 derived by us using wave-theory. So our derivation based on wave-theory matches with the observations presented by Sivaram.

$$\frac{M_0}{R_0^2} = \frac{M_{gal-clust}}{R_{gal-clust}^2} = \frac{M_{gal}}{R_{gal}^2} = \frac{M_{globu}}{R_{globu}^2} = \frac{m_n}{r_n^2} = \frac{m_{pi}}{R_{pi}^2} = \frac{m_e}{r_e^2} = \frac{H_0 c}{G} \tag{18}$$

Even the mysterious-looking Weinberg-formula can be re-written, and explained, as follows: Weinberg's formula is: $m_{pi}^3 = h^2 H_0/c\, G$, which can be re-written as: $m_{pi}/(h/m_{pi}c)^2 = H_0 c/G$. Weinberg's formula has an imbalance of one order of magnitude which can be corrected by replacing Compton-wavelength of the pion by radius of the pion, i.e. $m_{pi}/R_{pi}^2 = H_0 c/G$. So the mysterious-looking Weinberg-formula is also a part of the expression-18.

5 Conclusion

Now we have an explanation for why we need the gravitational constant G. The strength of gravity seems to depend on the total-mass M_0 and radius R_0 of the universe. However, large uncertainties in the M_0 and R_0 limit the general application of this relation presently. Secondly, gravity may not be an independent "fundamental-force"; it may be arising due to "in-coherent super-imposition" of wave-amplitudes of very wide-band of waves of total number of fundamental-particles contained in the universe. The theory also explained the large-number-coincidence, and the mysterious-looking Weinberg formula. We also gained some insight into Planck's units that: Planck-length, Planck-mass and Planck's unit of time are geometric-mean-values of astrophysical quantities like: total-mass of the universe and the smallest-possible-mass hH_0/c^2.

Submitted on: September 20, 2012 / Accepted on: September 28, 2012

References

1. Tank H.K. Explanation for the recurrences of large-number 10^{40} in astrophysics, and some insight into the nature of fundamental forces. *Proceedings of Indian National Science Academy*, 1997, v. 63A, no. 6, 469–474.
2. Tank H.K. An Explanation for the Relative Strengths of 'Gravitational' and 'Electric' Forces Suggesting Equality of the 'Electrostatic-potential-energy', 'Gravitational-potential-energy' and 'Energy of Mass' of the Universe. *Science and Culture*, 2009, v. 75 (searchable from google).
3. Tank H.K. A new law emerging from the recurrences of the "critical-acceleration" of MOND, suggesting a clue to unification of fundamental forces. *Astrophysics and Space Science*, 2010, v. 330, 203–205.
4. Tank H.K. Wave-theoretical explanation for the newly-emerged-law of equality of potential-energy and energy-of-mass of reasonably independent systems of matter. *Advanced Studies in Theoretical Physics*, 2011, v. 5, 45–55.
5. Tank H.K. Some clues to understand MOND and the accelerated expansion of the universe. *Astrophysics and Space Science*, 2011, v. 336, no. 2, 341–343.
6. Adair R.K. Concepts in Physics. Academic Press, New York, (1969), p. 775.
7. Gupta R.C. and Pradhan, Anirudh. A Theoretically-explained New-variant of Modified Newtonian Dynamics (MOND). *Astrophysics and Space Science*, 2011, v. 333, 311–316.
8. Rees M. Just Six Numbers. Orion Books, London, (2000), p. 81–82.
9. Tank H.K. Genesis of the critical-acceleration of MOND and its role in formation of structures. *Progress in Physics*, 2012, v. 4, 36–38.
10. Sivaram C. Some aspects of MOND and its consequences for cosmology. *Astrophysics and Space Science*, 1994, v. 215, 185–189.

A Theoretical Description of U(5)-SU(3) Nuclear Shape Transitions in the Interacting Boson Model

A.M. Khalaf* and T.M. Awwad†

*Physics Department, Faculty of Science, Al-Azhar University, Egypt. E-mail: Ali-Khalaf43@hotmail.com
†Department of Physics, Faculty of Girls, Ain Shams University, Egypt. E-mail: tawwad12@hotmail.com

We investigated the evaluation of nuclear shape transition from spherical to axially rotational shapes using the Coherent state formalism of the first version of interacting boson model (sd IBM). The validity of such model is examined for rare-earth Nd/Sm/Gd/Dy isotopic chains by analyzing the potential energy surface (PES's). In this region, a change from spherical to well-deformed nuclei is observed when moving from the lighter to heavier isotopes.

1 Introduction

In recent years, the study of quantum phase transition (QPT) is an important topic in the research of nuclear structure. Some evidence of nuclear shape transition have been observed. For instance, several isotopes have been found to undergo shape phase evolution of first order from spherical vibrator to deformed axially symmetric rotor and phase transition of second order from spherical vibrator to deformed $\gamma-$ soft [1–3].

The Hamiltonian describing this transition is a repulsive boson pairing Hamiltonian that has the particularity of being exactly solvable allowing the study of very large systems. The study of phase shape transitions in nuclei can be best done in the interacting boson model (IBM) [4] which reproduces well the data in all transition regions [5–11].

The possible phases that can occur in the IBM have been classified in a triangular Casten diagram [12], the three phases correspond to the breaking of U(6) into its three subalgebras U(5), SU(3) and O(6) [13]. The $X(5)$ critical point symmetry [14] was developed to describe analytically the structure of nuclei at the critical point of the transition from vibrational U(5) to prolate axially symmetric SU(3) shapes. In addition the symmetry E(5) [15, 16] have been introduced to describe the nuclei at the critical point corresponding to second order transition, nuclear examples of which were used [17]. Recently, the critical point in the phase transition from axially deformed to triaxial nuclei called Y(5), has been analyzed [18]. In all these cases, critical points are defined in the context of the collective Bohr Hamiltonian [19].

Since the IBM was formulated from the beginning in terms of creation and annihilation boson operators, its geometric interpretation in terms of shape variables is usually done by introducing a boson condensate with two shape parameters β and γ. The parameter β is related to the axial deformation of the nucleus, while γ measures the deviation from axial symmetry. The equilibrium shape of the nucleus is obtained by minimizing the expectation value of the Hamiltonian in the intrinsic state.

In this paper, we discuss some aspects of the nuclear shape phase transition in even-even nuclei using the IBM with the intrinsic state formalism. The outline of the present paper is as follows: In Section 2, we construct the IBM Hamiltonian in terms of Casimir operators and using coherent state to get the potential energy surface (PES). In section 3, we check that results of the IBM with coherent state to agree for dynamical limits U(5), SU(3) and O(6) in the limit of large N. In section 4 we applied our model to the rare earth Nd/Sm/Gd/Dy isotopic chains which evolve a rapid structural changes from spherical to well-deformed nuclei when moving from lighter to the heavier isotopes.

2 Coherent State Potential Energy Surface

We start by considering a general standard two-body sd IBM Hamiltonian in the Casimir forms as:

$$\begin{aligned} H &= \epsilon C_1[U(5)] + K_1 C_2[U(5)] \\ &\quad + K_2 C_2[O(5)] + K_3 C_2[O(3)] \\ &\quad + K_4 C_2[SU(3)] + K_5 C_2[O(6)] \end{aligned} \tag{1}$$

Here $C_n[G]$is the n-rank Casimir operator of the Lie group G, with

$$C_1[U(5)] = \hat{n}_d \tag{2}$$

$$C_2[U(5)] = \hat{n}_d(\hat{n}_d + 4) \tag{3}$$

$$C_2[O(5)] = 4[\frac{1}{10}(\hat{L}\,\hat{L}) + \hat{T}_3\,\hat{T}_3] \tag{4}$$

$$C_2[O(3)] = 2(\hat{L}\,\hat{L}) \tag{5}$$

$$C_2[SU(3)] = \frac{2}{3}\left[2\left(\hat{Q}\,\hat{Q}\right) + \frac{3}{4}(\hat{L}\,\hat{L})\right] \tag{6}$$

$$C_2[O(6)] = 2\left[N(N+4) - 4(\hat{P}\,\hat{P})\right] \tag{7}$$

where $\hat{n}_d, \hat{P}, \hat{L}, \hat{Q}, \hat{T}_3$ and $\hat{T}_4$ are the boson number, pairing, angular momentum, quadrupole, octupole and hexadecapole operators defined as:

$$\hat{n}_d = (d^\dagger\,\tilde{d})^{(0)} \tag{8}$$

$$\hat{P} = \frac{1}{2}(\tilde{d}\,\tilde{d}) - \frac{1}{2}(\tilde{s}\,\tilde{s}) \tag{9}$$

$$\hat{L} = \sqrt{10}\left[d^{\dagger}\times\tilde{d}\right]^{(1)} \tag{10}$$

$$\hat{T}_3 = \left[d^{\dagger}\times\tilde{d}\right]^{(3)} \tag{11}$$

$$\hat{T}_4 = \left[d^{\dagger}\times\tilde{d}\right]^{(4)} \tag{12}$$

where $s^{\dagger}(s)$and $d^{\dagger}(\tilde{d})$ are monopole and quadrupole boson creation (annihilation) operators, respectively. The scalar product is defined as

$$\hat{T}_L\,\hat{T}_L = \sum_M (-1)^M \hat{T}_{L,M}\,\hat{T}_{L,-M} \tag{13}$$

where $\hat{T}_{L,M}$ corresponds to the M component of the operator $\hat{T}_L$. The operator $\tilde{d}_m(-1)^m d_{-m}$ and $\tilde{s} = s$ are introduced to ensure the correct tensorial character under spatial rotations.

The Connection between the IBM, PES, geometric shapes and phase transitions can be investigated by introducing a coherent, or intrinsic state which is expressed as a boson condensate [20]

$$|N,\beta,\gamma\rangle = \frac{1}{\sqrt{N!}}\left(b_c^{\dagger}\right)^N|0\rangle \tag{14}$$

with

$$b_c^{\dagger} = \frac{1}{\sqrt{1+\beta^2}}\left(s^{\dagger}+\beta\cos\gamma\, d_o^{\dagger} + \frac{1}{\sqrt{2}}\beta\sin\gamma(d_2^{\dagger}+d_{-2}^{\dagger})\right). \tag{15}$$

$|0\rangle$ is the boson vacuum and the variables β and γ determine the geometry of nuclear surface. Spherical shapes are characterized by $\beta = 0$ and deformed ones by $\beta > 0$. The angle γ allows one to distinguish between axially deformed nuclei $\gamma = 0^{\circ}$ for prolate and $\gamma = 60^{\circ}$ for oblate deformation and triaxial nuclei $0^{\circ} < \gamma < 60^{\circ}$.

The expectation values of the Casimir operators equations (2–7) in the ground state equation (14) is:

$$\langle C_1[U(5)]\rangle = \frac{N}{1+\beta^2}\beta^2 \tag{16}$$

$$\langle C_2[U(5)]\rangle = \frac{5N}{1+\beta^2}\beta^2 + \frac{N(N-1)}{(1+\beta^2)^2}\beta^4 \tag{17}$$

$$\langle C_2[O(5)]\rangle = \frac{8N}{1+\beta^2}\beta^2 \tag{18}$$

$$\langle C_2[O(3)]\rangle = \frac{12N}{1+\beta^2}\beta^2 \tag{19}$$

$$\begin{aligned}\langle C_2[SU(3)]\rangle &= \frac{20}{3}N + \frac{4}{3}\frac{N(N-1)}{(1+\beta^2)^2}\cdot\\ &\left(4\beta^2 + \frac{1}{2}\beta^4 + 2\sqrt{2}\beta^3\cos(3\gamma)\right)\end{aligned} \tag{20}$$

$$\langle C_2[O(6)]\rangle = 2N(N+4) - \frac{1}{2}\frac{N(N-1)}{(1+\beta^2)^2}\left(1-\beta^2\right)^2. \tag{21}$$

The PES associated with the IBM Hamiltonian of equation (1) is given by its expectation value in the coherent state and can be written as:

$$\begin{aligned}V(\beta,\gamma) &= a_{\circ}\frac{N}{1+\beta^2}\beta^2\\ &+\frac{N(N-1)}{(1+\beta^2)^2}\left(a_1 + a_2\beta^2 +\right.\\ &\left. a_3\beta^3\cos(3\gamma) + a_4\beta^4\right)\end{aligned} \tag{22}$$

where the coefficients a_i are linear combinations of the parameters of the Hamiltonian and terms which do not depend on β and/or γ have not been included.

3 Shape Structure of the Dynamical Symmetries

The analysis of the three dynamical symmetry limits of the IBM provides a good test of the formalism presented in the previous section.

3.1 The U(5) Symmetry

The Hamiltonian of the vibrational limit $U(5)$ can be written down by putting $k_4 = k_5 = 0$ in equation (1). This has the consequence that in H remain only the terms which conserve both the number of d-bosons and the one of the s-bosons. The Hamiltonian operator of this approximation reads:

$$\begin{aligned}H[U(5)] &= \epsilon C_1[U(5)] + K_1C_2[U(5)] +\\ &K_2C_2[O(5)] + K_3C_2[O(3)].\end{aligned} \tag{23}$$

This yields the PES

$$E(N,\beta) = \epsilon_d\frac{N}{1+\beta^2}\beta^2 + f\frac{N(N-1)}{(1+\beta^2)^2}\beta^4. \tag{24}$$

This energy functional is $\gamma-$ independent and has a minimum at $\beta = 0$, Special case for $U(5)$ limit, when

$$H = \epsilon C_1[U(5)], \tag{25}$$

$$E(N,\beta) = \epsilon\frac{N}{1+\beta^2}\beta^2. \tag{26}$$

3.2 The SU(3) Symmetry

In the parametrization equation (1), the $SU(3)$ limit corresponds to $\epsilon = K_1 = K_2 = K_5 = 0$ and the Hamiltonian reads:

$$H[SU(3)] = K_3C_2[O(3)] + K_4C_2[SU(3)]. \tag{27}$$

This yields the PES

$$\begin{aligned}&E(N,\beta,\gamma) =\\ &3(4k_3+k_4)\frac{N}{1+\beta^2}\beta^2 + \frac{4}{3}k_4\left[\frac{N}{1+\beta^2}\left(5+\frac{11}{4}\beta^2\right)\right.\\ &\left.+\frac{N(N-1)}{(1+\beta^2)^2}\left(4\beta^2 + 2\sqrt{2}\beta^3\cos(3\gamma) + \frac{1}{2}\beta^4\right)\right].\end{aligned} \tag{28}$$

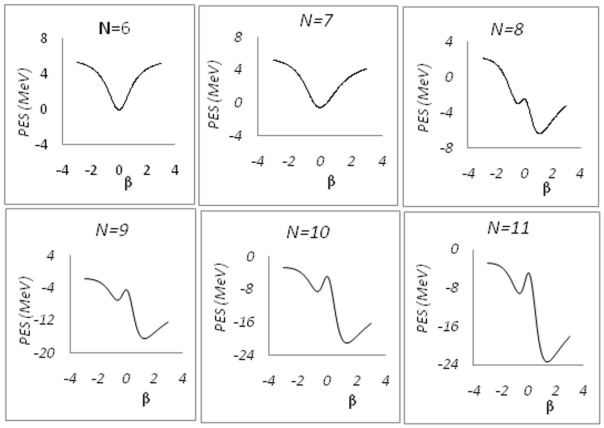

Fig. 1: Calculated PES's as a function of the deformation parameter β in U(5)-SU(3) transition for $^{144-154}$Nd (with $N_\pi = 5$ and $N_\nu = 1-6$ neutron bosons) isotopic chain. The total number of bosons N=6-11 and $\chi = -\sqrt{7}/2$).

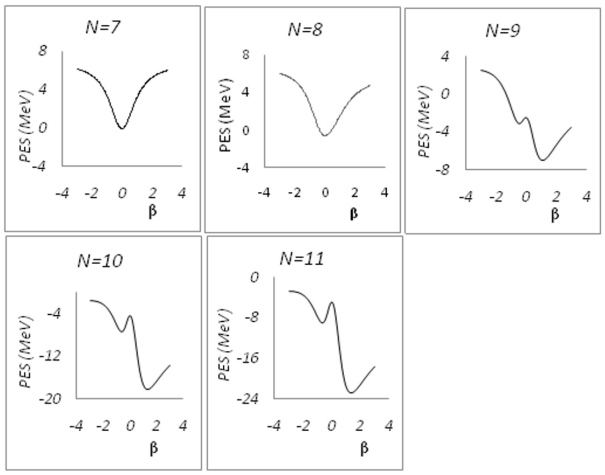

Fig. 2: Calculated PES's as a function of the deformation parameter β in U(5)-SU(3) transition for $^{146-154}$Sm (with $N_\pi = 6$ and $N_\nu = 1-5$) isotopic chain. The total number of bosons N=6-11 and $\chi = -\sqrt{7}/2$).

This energy functional has a shape minimum at $\gamma = 0$ and at a value $\beta \neq 0$.

Special case for SU(3) limit, when

$$H = a\hat{Q}\,\hat{Q} \tag{29}$$

and if we eliminate the contribution of the one-body terms of the quadrupole -quadrupole interaction, then, the PES reads

$$E(N,\beta,\gamma) = a\frac{N(N-1)}{(1+\beta^2)^2}(4\beta^2 \pm 2\sqrt{2}\beta^3\cos(3\gamma) + \frac{1}{2}\beta^4). \tag{30}$$

The equilibrium values are obtained by solving

$$\frac{\partial E}{\partial \beta} = \frac{\partial E}{\partial \gamma} = 0 \tag{31}$$

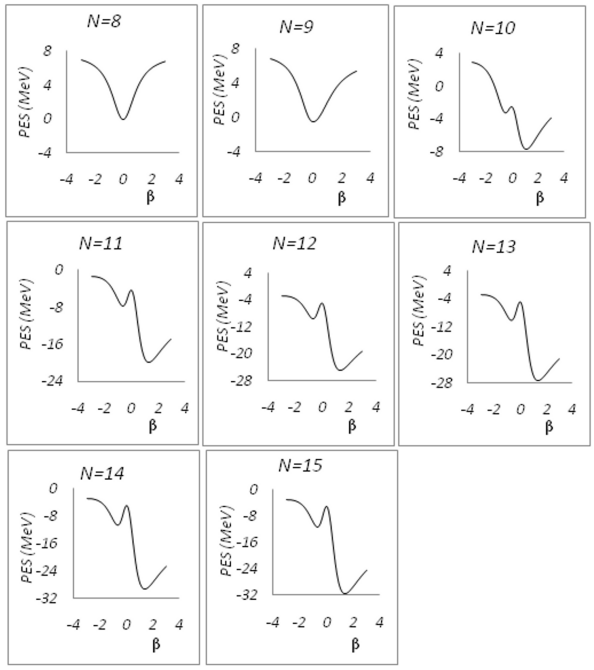

Fig. 3: Calculated PES's as a function of the deformation parameter β in U(5)-SU(3) transition for $^{148-162}$Gd (with $N_\pi = 7$ and $N_\nu = 1-8$) isotopic chain. The total number of bosons N=6-11 and $\chi = -\sqrt{7}/2$).

to give $\beta_e = \sqrt{2}$ and $\gamma = 0°$ and $\gamma = 60°$.

3.3 The O(6) Symmetry

For the O(6) limit $\epsilon = K_1 = K_2 = 0$ and the Hamiltonian takes the form

$$H[O(6)] = K_2C_2[O(5)] + K_3C_2[O(3)] + K_5C_2[O(6)]. \tag{32}$$

One then obtains the PES

$$\begin{aligned} E(N,\beta) &= 12(2K_2 + K_3)\frac{N}{1+\beta^2}\beta^2 - \\ &\quad 2k_5N(N-1)\left(\frac{1-\beta^2}{1+\beta^2}\right)^2. \end{aligned} \tag{33}$$

This energy functional is $\gamma-$independent and has a minimum at a value $|\beta| \neq 0$. For large N, the minimum is at $|\beta| = 1$.

Special case for $O(6)$ limit, when

$$H = a\hat{Q}(\chi)\,\hat{Q}(\chi) \tag{34}$$

$$\chi = 0 \tag{35}$$

and if we eliminate the contribution of the one-body term of the quadrupole-quadrupole interaction, then

$$E(N,\beta) = 4aN(N-1)\left(\frac{\beta}{1+\beta^2}\right)^2 \tag{36}$$

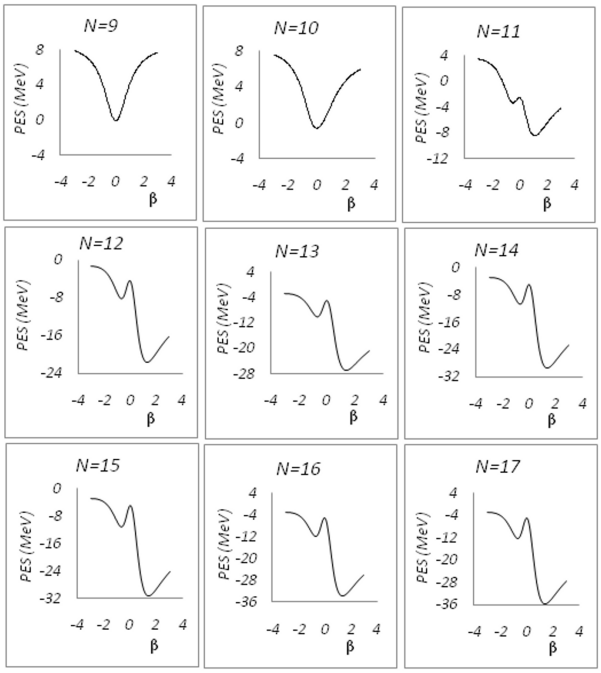

Fig. 4: Calculated PES's as a function of the deformation parameter β in U(5)-SU(3) transition for $^{150-166}$Dy (with $N_\pi = 8$ and $N_\nu = 1-9$) isptopic chain. The total number of bosons N=6-11 and $\chi = -\sqrt{7}/2$).

the equilibrium value is given by $\beta = 1$ corresponding to a γ-unstable deformed shape.

4 Application to Rare-Earth Isotope Chains

Nuclei in the region of Sm are well known examples of U(5)-SU(3) transition going from a vibrational into a rotational behavior. The validity of our model is examined for typical various even-even Nd/Sm/Gd/Dy isotopic chains with total number of bosons from N=6 to N=17.

The set of parameters of the model for each nucleus are adjusted by using a computer simulated search program in order to describe the gradual change in the structure as boson number is varied and to reproduce the properties of the selected states of positive parity excitation ($2_1^+, 4_1^+, 6_1^+, 8_1^+, 0_2^+$, $2_3^+, 4_3^+, 2_2^+, 3_1^+$ and 4_2^+) and the two neutron separation energies of all isotopes in each isotopic chain. The best fitting parameters obtained for each nucleus are given explicitly in Tables (1,2).

The PES's versus deformation parameter β for rare earth isotopic chain of nuclei evolving from spherical to axially symmetric well deformed nuclei are illustrated in figures (1-4). A first order shape phase transition with changes in number of bosons when moving from the lighter to heavier isotopes i.e. U(5)-SU(3) transitional region are observed. In our selected region we assumed a value $\chi = -\sqrt{7}/2$ because some *Gd* isotopes clearly exhibit the character of the SU(3) dynamical symmetry. Around $N = 90$ these seems to be the $X(5)$critical point symmetry. Each PES displays a relatively similar shape with only a small increase in the sharpness of the potential for increasing boson number.

5 Conclusion

In conclusion, the paper is focused on the properties of quantum phase transition between spherical U(5) and prolate deformed SU(3) in framework of the simple version of interacting boson model IBM-1 of nuclear structure.

The Hamiltonian was studied in the three different limits of the IBM and formed by laking. A systematic study of rare earth Nd/Sm/ Gd/Dy isotope chains was done using the coherent states. Nuclei located at or very close to the first order transition were the N=90 isotones ^{150}Nd, ^{152}Nd, ^{154}Nd and ^{156}Nd. They also follow the $X(5)$ pattern in ground state energies. The geometric character of the nuclei was visualizes by plotting the potential energy surface (PES's). parameters of our model were adjusted for each nucleus by using a computer simulated search program, while the parameter X in the quadrupole operator was restricted to fixed value $x = -\sqrt{7}/2$.

Submitted on: September 24, 2012 / Accepted on: September 27, 2012

References

1. Jolie J. et al. Triple Point of Nuclear Deformation. *Physical Review Letters*, 2002, v. 89, 182502–182504.
2. Arios J.M., Dukelsky J., and Garcia-Ramos J.E. Quantum Phase Transitions in the Interacting Boson Model: Integrability, Level Repulsion and Level Crossing. *Physical Review Letters*, 2003, v. 91, 162502–162504.
3. Turner P.S. and Rowe D.J. Phase Transitions and Quesidynamical Symmetry in Nuclear Collective Model, II. The Sperical vibrator to gamma-soft rotor Transition in an O(5)-invariant Bohr Model. *Nuclear Physics*, 2005, v. A756, 333–355.
4. Iachello F. and Arima A. The Interacting Boson Model. Cambridge University Press, Cambridge, England, 1987.
5. Scholten O., Iachello F. and Arima A. Interacting Boson Model of Collective Nuclear State III. The Transition from SU(5) to SU(3). *Annals of Physics*, 1978, (N.Y.) v. 115, 325–366.
6. Castonos O., Frank A. and Federman, A. The shape transition in the Sm isotopes and the structure of the IBA hamiltonian. *Physics Letters*, 1979, v. B88, 203–206.
7. Cejnar P. and Jolie J. Quantum Phase Transition Studied within the Interacting Boson Model, *Physical Review*, 2000, v. E61, 6237–6247.
8. Cejnar P., Heinze S., and Jolie J. Ground-State Shape Phase Transitions in Nuclei: Thermodynamic analogy and fitie N-effects. *Physical Review*, 2003, v. C68, 034326–034326.
9. Rowe D.J. and Thiamova G. The many relationships between the IBM and the Bohr Model. *Nuclear Physics*, 2005, v. A760, 59–81.
10. Cejnar P., Heinze S. and Dobes J. Thermodynamic analogy for quantum phase transitions at zero temperature. *Physical Review*, 2005, v. C71, 011304R–011309R.
11. Heinze S. et al. Evolution of spectral properties along the O(6)-U(5) transition in the interacting boson model. I. Level dynamics. *Physical Review*, 2006, v. C73, 014306–014316.
12. Casten R.F. Nuclear Structure from a Simple Prespective. Oxford University, Oxford, 1990.

Table 1: Values of the parameter a_o and the total number of boson for the Nd/Sm/Gd/Dy isotopic chain.

No. of Neutrons	$_{60}$Nd	$_{62}$Sm	$_{64}$Gd	$_{66}$Dy
84	1161.91775(6)	1112.0059(7)	1130.70265(8)	1174.6685(9)
86	1082.31775(7)	1078.2059(8)	1160.10265(9)	1223.4685(10)
88	1121.01775(8)	974.0059(9)	1060.40265(10)	1178.2685(11)
90	1078.51735(9)	895.5059(10)	951.80265(11)	1119.7685(12)
92	1011.71775(10)	843.3059(11)	872.90265(12)	1076.8685(13)
94	1071.51775(11)	877.2059(12)	825.80265(13)	1043.5685(14)
96	−−	996.9059(13)	813.40265(14)	1029.2685(15)
98	−−	1136.7059(14)	827.90265(15)	1025.0685(16)
100	−−	−−	−−	1058.9685(17)

Table 2: Values of the parameters a_1, a_2, a_3, and a_4 describing the IBM Hamiltonian for Nd/Sm/Gd/Dy isotopic chains.

Isotopic chains	a_1	a_2	a_3	a_4
$^{144-154}$Nd	20.93825	−110.4805	−48.51035	−84.10182
$^{146-160}$Sm	13.30225	−85.3005	−41.50433	−61.52960
$^{148-162}$Gd	11.30175	−75.1195	−37.13441	−75.61475
$^{150-166}$Dy	9.66275	−73.8775	−38.57408	−81.01053

13. Arima A. and Iachello F. Interacting Boson Model of Collective States I. The Vibrational Limit. *Annals of Physics*, 1976, (N.Y.) v. 99, 253–317; Arima A. and Iachello F. Interacting Boson Model of Collective States II. The Rotational Limit. *Annals of Physics*, 1978, (N.Y.) v. 111, 201–238.
14. Iachello F. Analytic Prescription of Critical Point Nuclei in a Spherical Axially Deformed Shape Phase Transtion. *Physical Review Letters*, 2001, v. 87, 052502–052506.
15. Iachello F. Dynamic Symmetrcies at the Critical Point. *Physical Review Letters*, 2000 v. 85, 3580–3583.
16. Leviatan A. and Ginocchio J.N. Critical Point Symmetry in a Finite System. *Physical Review Letters*, 2005, v. 90, 212501–212505.
17. Casten R.F. and Zamfir N.V. Evidence for a Possible E(5) Symmetry in ^{134}Ba. *Physical Review Letters*, 2000 v. 85, 3584–3586, Casten R.F. and Zamfir N.V. Empirical Realization of a Critical Point Description in Atomic Nuclei. *Physical Reviw Letters*, 2001 v. 87, 052503–052507.
18. Iachello F. Phase Transition an Angle Variables. *Physical Review Letters*, 2003, v. 91, 132502–132507.
19. Bohr A. and Mottelson, Nuclear Structure, Benjamin, New York, 1975, Vol. II.
20. Dieperink A.E.L., Scholten O. and Iachello F. Classical Limit of the Interacting Boson Model. *Physical Reviw Letters*, 1980, v. 44, 1747–1750.
21. Dieperink A.E.L and Scholten O. On Shapes and Shase Transition in the Interacting Boson Model. *Nuclear Physics*, 1980, v. A346, 125–138.

Fine Structure Constant as a Mirror of Sphere Geometry

Janez Špringer
Cankarjeva cesta 2, 9250 Gornja Radgona, Slovenia, EU. E-mail: janez_springer@t-2.net

A path is defined as the vector's sum of the translation and rotation component of the length unit belonging to the mass entity in motion on the sphere. The fine structure constant is an irrational number being a mirror of the path complexity as well as the sphere curvature where the path is made. The inverse value in the Euclidean plane yields $\alpha^{-1} = \sqrt{\pi^2 + 137^2}$. The inverse fine structure constant on the elliptic sphere is smaller and on the hyperbolic sphere is greater. The electron in the Hydrogen atom should move on the elliptic sphere of the radius of 3679 Compton wavelengths of the electron according to the CODATA 2012 recommended empirical value $\alpha^{-1} = 137.035999074$. Such a small sphere radius implies the heterogeneous curvature of the present universe.

1 Theoretical background

In motion is an entity having some mass. Respecting Compton the length unit is attributed to that mass:

$$\lambda = \frac{h}{mc} = 1\,. \tag{1}$$

The infinite mass and zero length unit are objectively unreachable. Nevertheless both can be theoretically approached arbitrarily close by the sufficiently great finite mass.

A curved motion obeys the path complexity: it has the translation and rotation component. Describing the curved path the length unit becomes not only the translation unit but the rotation unit, too. By the circumference of a circle concluded path s, for instance, only apparently equals the translation n, actually it is greater for the average rotation π made around the start point of the length unit:

$$\pi = \frac{0 + 2\pi \times 1}{2}\,. \tag{2}$$

The actual path is the vectorial sum of both components: the rotation π as well as translation n:

$$\overrightarrow{s} = \overrightarrow{\pi} + \overrightarrow{n}\,. \tag{3}$$

The total rotation of the length unit π equals the total Berry phase at spin $\frac{1}{2}$ [1].

1.1 Path in the Euclidean plane

By the circumference of a circle concluded path s in the Euclidean plane is calculated with the help of Pythagoras' theorem:

$$s^2 = \pi^2 + n^2. \tag{4}$$

1.2 Path on the elliptic sphere

By the circumference of a circle concluded path s on the elliptic sphere is calculated with the help of the spherical law of cosines.

On the elliptic sphere of radius R holds:

$$\cos\frac{s}{R} = \cos\frac{\pi}{R}\,\cos\frac{n}{R}\,, \tag{5}$$

$$\cos x = \sqrt{1 - \sin^2 x}\,, \tag{6}$$

$$\frac{1}{R^2} = \frac{1}{k_1^2\pi^2} + \frac{1}{k_2^2 n^2} - \frac{k_3^2 s^2}{k_1^2\pi^2 \times k_2^2 n^2} = \frac{k_1^2\pi^2 + k_2^2 n^2 - k_3^2 s^2}{k_1^2\pi^2 \times k_2^2 n^2}\,. \tag{7}$$

The coefficients are expressed as

$$k_1 = \frac{\sin\frac{\pi}{R}}{\frac{\pi}{R}}\,, \quad k_2 = \frac{\sin\frac{n}{R}}{\frac{n}{R}} \quad \text{and} \quad k_3 = \frac{\sin\frac{s}{R}}{\frac{s}{R}}\,. \tag{8}$$

They are arranged by size

$$1 \geqslant k_1 \geqslant k_2 \geqslant k_3\,. \tag{9}$$

In the case of R^2 being a positive number Pythagoras' theorem holds only exceptionally. The next condition has to be satisfied:

$$k_1^2\pi^2 + k_2^2 n^2 \geqslant k_3^2 s^2 \quad \text{or} \quad \frac{k_1^2}{k_3^2}\,\pi^2 + \frac{k_2^2}{k_3^2}\,n^2 \geqslant s^2. \tag{10}$$

The ratios of coefficients $\frac{k_1^2}{k_3^2}$ and $\frac{k_2^2}{k_3^2}$ are according to (non) equation (9) greater than 1 or at least equal 1, therefore we write:

$$\frac{k_1^2}{k_3^2}\,\pi^2 + \frac{k_2^2}{k_3^2}\,n^2 \geqslant \pi^2 + n^2 \geqslant s^2. \tag{11}$$

At the finite elliptic sphere radius R Pythagoras' theorem fails, because at non-equal coefficients (9) the square area upon hypotenuse is smaller than the sum of square areas upon catheters:

$$s^2 < \pi^2 + n^2. \tag{12}$$

At $R = \infty$ and equal coefficients (9) the elliptic sphere transforms into the Euclidean plane and Pythagoras' theorem begins to rule again (4).

1.2.1 Approximation for cos *x*

Hardy's approximation [2] is close to the function $\cos\frac{t}{r}$:

$$H\left(\frac{2t}{\pi R}\right) = \cos\frac{t}{R} \approx 1 - \frac{\left(\frac{2t}{\pi R}\right)^2}{\frac{2t}{\pi R} + \left(1 - \frac{2t}{\pi R}\right)\sqrt{\frac{2 - \frac{2t}{\pi R}}{3}}}. \tag{13}$$

At very large R Hardy's approximation can be simplified:

$$H\left(\frac{2t}{\pi R}\right) = \cos\frac{t}{R} \approx 1 - \left(\frac{2t}{\pi R}\right)^2. \tag{14}$$

The spherical law of cosines (5) with the help of the simplified Hardy approximation (14) enables to calculate the approximate value of the sphere radius in cases of a tiny curvature where Pythagoras' theorem approximately rules. The explicit relation is expressed as

$$R^2 \approx \frac{(2n)^2}{n^2 + \pi^2 - s^2}\,. \tag{15}$$

The similar approximation is obtained with the help of equation (7) at the assumption of coefficients approximate equality:

$$1 \approx k_1 \approx k_2 \approx k_3\,. \tag{16}$$

Then the sphere radius is expressed as

$$R^2 \approx \frac{(\pi n)^2}{n^2 + \pi^2 - s^2}\,. \tag{17}$$

1.3 Path on the hyperbolic sphere

By the circumference of a circle concluded path s on the hyperbolic sphere is calculated with the help of the hyperbolic law of cosines.

On the hyperbolic sphere of radius R holds:

$$\cosh\frac{s}{R} = \cosh\frac{\pi}{R}\cosh\frac{n}{R}\,, \tag{18}$$

$$\cosh x = \sqrt{1 + \sinh^2 x}, \tag{19}$$

$$\frac{1}{R^2} = -\frac{1}{k_1^2\pi^2} - \frac{1}{k_2^2 n^2} + \frac{k_3^2 s^2}{k_1^2\pi^2 \times k_2^2 n^2} = \\ = \frac{-k_1^2\pi^2 - k_2^2 n^2 + k_3^2 s^2}{k_1^2\pi^2 \times k_2^2 n^2}\,. \tag{20}$$

The coefficients are expressed as

$$k_1 = \frac{\sinh\frac{\pi}{R}}{\frac{\pi}{R}}, \quad k_2 = \frac{\sinh\frac{n}{R}}{\frac{n}{R}} \quad \text{and} \quad k_3 = \frac{\sinh\frac{s}{R}}{\frac{s}{R}}\,. \tag{21}$$

They are arranged by size

$$1 \leqslant k_1 \leqslant k_2 \leqslant k_3\,. \tag{22}$$

In the case of R^2 being a positive number Pythagoras' theorem holds only exceptionally.

The next condition has to be satisfied:

$$k_3^2 s^2 \geqslant k_1^2\pi^2 + k_2^2 n^2 \quad or \quad s^2 \geqslant \frac{k_1^2}{k_3^2}\pi^2 + \frac{k_2^2}{k_3^2}n^2. \tag{23}$$

The ratios of coefficients k_1^2/k_3^2 and k_2^2/k_3^2 are according to (non)equation (22) smaller than 1 or at most equal 1, therefore we write:

$$\frac{k_1^2}{k_3^2}\pi^2 + \frac{k_2^2}{k_3^2}n^2 \leqslant \pi^2 + n^2 \leqslant s^2. \tag{24}$$

At the finite hyperbolic sphere radius R Pythagoras' theorem fails, because at non-equal coefficients (22) the square area upon hypotenuse is greater than the sum of square areas upon catheters:

$$s^2 > \pi^2 + n^2. \tag{25}$$

At $R = \infty$ and equal coefficients (22) the hyperbolic sphere transforms into the Euclidean plane and Pythagoras' theorem begins to rule again (4).

2 Fine structure constant and sphere radius

In the ground state of the Hydrogen atom the electron path around the nucleus equals the ratio of the Compton wavelength of the electron λ and the fine structure constant α. The wavelength equals the unit, so the circular path equals the inverse fine structure constant:

$$s = \alpha^{-1}. \tag{26}$$

2.1 Inverse fine structure constant on the non-Euclidean sphere and Euclidean plane

At the finite sphere radius R two possibilities are allowed according the non-equations (12) and (25).

On the elliptic sphere holds:

$$\alpha^{-2} < \pi^2 + n^2. \tag{27}$$

On the hyperbolic sphere holds:

$$\alpha^{-2} > \pi^2 + n^2. \tag{28}$$

At $R = \infty$ both non-Euclidean spheres transform into the Euclidean plane and according to the equation (4) holds:

$$\alpha^{-2} = \pi^2 + n^2. \tag{29}$$

2.2 Calculation of the theoretical inverse fine structure constant in the Euclidean plane

In the hydrogen atom the number $n = 137$ is to the inverse fine structure constant α^{-1} the closest natural number which concludes the start and end point of Bohr orbit. The number π is the total average rotation component of the length unit.

The theoretical inverse fine structure constant in the Euclidean plane is calculated with the help of the equation (29). Its value is an irrational number:

$$\alpha^{-1}{}_{\text{EUCLID}} = \sqrt{n^2 + \pi^2} \approx 137.036015720. \tag{30}$$

2.3 Calculation of the sphere radius on the atomic level

The inverse fine structure constant should be according to the equations (27) and (28) on the elliptic sphere smaller and on

the hyperbolic sphere greater than $\alpha^{-1}_{\text{EUCLID}}$.

The recommended CODATA 2012 value of the inverse fine structure constant is smaller than the theoretical value in the Euclidean plane:

$$\alpha^{-1}_{\text{CODATA}} = 137.035999074 < \alpha^{-1}_{\text{EUCLID}} \approx 137.036015720. \quad (31)$$

This implies the elliptic sphere in the Hydrogen atom.

The calculus of the radius of the elliptic sphere with the help of the equation (5) yields:

$$R = 3679 \text{ Compton wavelengths of the electron.} \quad (32)$$

The estimate of the radius of the elliptic sphere with the help of the simplified Hardy approximation (15) yields a little bit greater value:

$$R \approx \frac{2.137}{\sqrt{137^2 + \pi^2 - \alpha^{-2}_{\text{CODATA}}}} = 4057. \quad (33)$$

2.4 Estimation of the inverse fine structure constant on the macro level

Let us consider the radius of the observable universe of about 4×10^{26}m [3] as the sphere radius:

$$R \approx 2 \times 10^{38} \text{ Compton wavelengths of the electron.} \quad (34)$$

This is a huge radius. A common calculator supports the spherical law of cosines only for radius up to $\sim 10^{15}$ Compton wavelengths of the electron.

Fortunately a huge sphere radius is given by the simplified Hardy approximation (15) in the explicit relation with the inverse fine structure constant:

$$R^2 \approx \frac{(2.137)^2}{\pi^2 + 137^2 - \alpha^{-2}}, \quad (35)$$

$$\alpha^{-1} \approx \sqrt{\pi^2 + 137^2\left(1 - \frac{4}{R^2}\right)} = \sqrt{\pi^2 + 137^2\left(1 - 10^{-76}\right)} \approx$$
$$\approx \sqrt{\pi^2 + 137^2}. \quad (36)$$

If the sphere curvature on the atomic level equals the curvature of the hypothetical elliptic observable universe, the inverse fine structure constant should not significantly differ from the theoretical constant in the Euclidean plane.

3 Conclusion

If the inverse fine structure constant is a mirror of the path complexity as well as the curvature of the sphere where the path is made, its theoretical inverse value in the Euclidean plane $\alpha^{-1} = \sqrt{\pi^2 + 137^2}$ and the recommended empirical CODATA 2012 value $\alpha^{-1} = 137.035999074$ express the electron motion on the elliptic sphere of the radius of 3679 Compton wavelengths of the electron. This implies a huge curvature of the atomic world. If the sphere curvatures in the atomic and the macro-world would be the same, the inverse fine structure constant should not significantly differ from the theoretical one in the Euclidean plane.

Submitted on: October 15, 2012 / Accepted on: October 23, 2012

References

1. Binder B. Berry's Phase and Fine Structure. http://philsci-archive.pitt.edu/682/1/alfa137MN5p.pdf. Retrieved September 2012.
2. Weisstein E. W. Cosine. http://mathworld.wolfram.com/Cosine.html. Retrieved October 2012.
3. WolframAlpha. http://www.wolframalpha.com/input/?i=size+of+ universe. Retrieved November 2011.

The Poisson Equation, the Cosmological Constant and Dark Energy

Jeffrey P. Baugher

Wright State University, Department of Electrical Engineering, 311 Russ Engineering Center, 3640 Colonel Glenn Highway, Dayton, Ohio 45449, USA. E-mail: baugher.3@wright.edu

The Cosmological Constant Λ within the modified form of the Einstein Field Equation (EFE) is now thought to best represent a "dark energy" responsible for a repulsive gravitational effect, although there is no accepted argument for its magnitude or even physical presence. In this work we compare the origin of the Λ argument with the concept of unimodular gravity. A metaphysical interpretation of the Poisson equation during introduction of Λ could account for the confusion.

1 Introduction

In 1916, Einstein introduced his general theory of relativity as a geometrical theory of gravity [4] resulting in the Einstein field equation (EFE),

$$R_{\mu\nu} - \frac{1}{2}\, g_{\mu\nu}R = G_{\mu\nu} = \frac{8\pi G}{c^4}\, T_{\mu\nu}. \tag{1}$$

It has been well documented and studied that the EFE did not predict a stable static universe, as it was theorized to be at the time [3]. The equation, however, did accurately predict gravitational redshift, magnitudes of gravitational lensing and account for Mercury's precessing orbit, which the Newtonian equation could not. In order to manufacture an equation that could account for a static universe, but still be empirically accurate, it is often stated that Einstein ad hoc threw in another constant Λ which is known as the cosmological constant. This would have been placed back into the EFE with the metric $g_{\mu\nu}$ as

$$R_{\mu\nu} - \frac{1}{2}\, g_{\mu\nu}R + g_{\mu\nu}\Lambda = G_{\mu\nu}. \tag{2}$$

Once it was discovered that the universe actually appeared to be in a decelerating or coasting expansion mode, Einstein quickly removed the Λ term. Today, though, there is empirical evidence that a very small magnitude Λ exists, but some quantum field theorists estimate it as being over 120 orders of magnitude smaller than their calculations, "probably the worst theoretical prediction in the history of physics" [3]. In addition, the observed small value of Λ requires an extremely high level of arbitrary fine tuning "for no good reason" and is a "cosmologist's worst nightmare come true" [6]. This transformation from a minor but rich interest exploded (5000 papers submitted to date [10]) near the end of the past millennium due to a startling simultaneous discovery of positive acceleration from two teams [7, 8].

The source of this unforeseen positive acceleration has come to be known as "dark energy". The lack of progress in explaining the phenomena led to the creation of a Dark Energy Task Force in 2006 which stated in a report [1]:

> "Most experts believe that nothing short of a revolution in our understanding of fundamental physics will be required to achieve a full understanding of the cosmic acceleration."

This dark energy is currently expected to contribute over 73.4% [5] of the mass-energy of the universe, and there is no sound logical theory for what it is. Consider that this leaves some type of mysterious never-observed particle known as dark matter to contribute another 22.2%, leaving only 4.4% for the normal matter we are familiar with. With this in mind, we propose that it is reasonable to re-examine any argument that has lead us to our current state of physics.

2 Poisson Equation and Gauss' Theorem

The Poisson equation,

$$-\nabla^2 u = \mathbf{f}, \tag{3}$$

is well known to relate the function f as the "source" or "load" of the effect on u of the left hand side. Let us examine what this means *exactly* more in depth and what we can conclude from this tool. As an example, for a function f given on a three dimensional domain denoted by $\Omega \subset \mathbb{R}^3$ we have

$$\alpha u + \beta\, \frac{\partial u}{\partial \mathbf{n}} = \mathbf{g} \quad \text{on} \quad \partial\Omega. \tag{4}$$

This is a solution u satisfying boundary conditions on the boundary $\partial\Omega$ of Ω. α and β are constants and $\frac{\partial u}{\partial \mathbf{n}}$ represents the directional derivative in the direction normal $\mathbf{n}$ to the boundary $\partial\Omega$ which by convention points outwards. Although if $\alpha = 0$ is referred to as a Neumann boundary condition, even with $\alpha = constant$ the solution is said to only be unique up to this additive constant. Let us examine whether this statement is entirely accurate.

2.1 Graphical Meaning of Poisson Equation

Let us take the divergence of $\mathbf{g}$ so that

$$\nabla \cdot \alpha u + \nabla \cdot \beta\, \frac{\partial u}{\partial \mathbf{n}} = \nabla \cdot \mathbf{g} \tag{5}$$

and

$$0 + \nabla \cdot \beta\, \frac{\partial u}{\partial \mathbf{n}} = \nabla \cdot \mathbf{g}. \tag{6}$$

We can see that the presence of αu seems arbitrary since it has no effect. Let us examine a two dimensional slice of scalar values in $\mathbb{R}^3$ to graphically give a better understanding. In Fig. 1 we have an example of Eq. 4 using a Euclidean coordinate system.

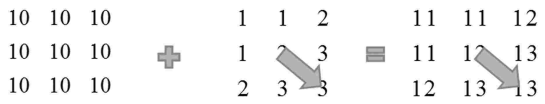

Fig. 1: Two Dimensional Scalar Field

For any derivative of Eq. 5, the constant term of course would result in no vector since there is no directional derivative from αu.

We note that this equation can also be written as

$$\alpha u - \beta \frac{-\partial u}{\partial \mathbf{n}} = \mathbf{g}, \tag{7}$$

shown in Fig. 2, which does not mathematically make a difference but can, however, introduce a question of uniqueness.

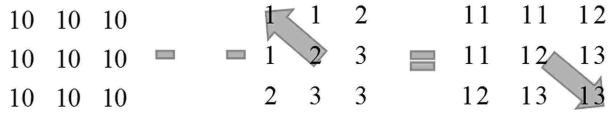

Fig. 2: Alternate Two Dimensional Scalar Field

Let us define the previous scalar field u as u_1 and a second scalar field as u_2. If ξ and γ are constants, then Eq. 8 and Fig. 3 present a dilemma. While there may be no directional derivatives from the constant term, we could also equivalently model this as orthogonal vectors with the sum of 0.

$$\xi u_2 - \gamma \frac{\partial u_2}{\partial \mathbf{n}} = \mathbf{g}_2 \tag{8}$$

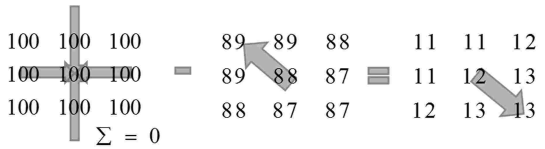

Fig. 3: Second Two Dimensional Scalar Field

From this we can see that there are no unique solutions of u for **g** from the Poisson equation, if

$$\alpha u_1 + \beta \frac{\partial u_1}{\partial \mathbf{n}} = \mathbf{g}_1 \tag{9}$$

and

$$\xi u_2 - \gamma \frac{\partial u_2}{\partial \mathbf{n}} = \mathbf{g}_2 \tag{10}$$

but also

$$\nabla \cdot (\alpha u_1 + \beta \frac{\partial u_1}{\partial \mathbf{n}}) = \nabla \cdot \mathbf{g}_1 = \nabla \cdot \mathbf{g} \tag{11}$$

and

$$\nabla \cdot (\xi u_2 - \gamma \frac{\partial u_2}{\partial \mathbf{n}}) = \nabla \cdot \mathbf{g}_2 = \nabla \cdot \mathbf{g} \tag{12}$$

if

$$\beta \frac{\partial u_1}{\partial \mathbf{n}} = -\gamma \frac{\partial u_2}{\partial \mathbf{n}}. \tag{13}$$

2.2 Gauss Theorem

Like our above illustration of the Poisson equation, a misunderstanding of Gauss' Theorem,

$$-\int_{\partial\Omega} \frac{\partial u}{\partial \mathbf{n}} = -\int_{\Omega} \nabla^2 u = \int_{\Omega} f \tag{14}$$

could also cause confusion if

$$-\int_{\partial\Omega} \beta \frac{\partial u_1}{\partial \mathbf{n}} = -\int_{\partial\Omega} \left(\xi u_2 - \gamma \frac{\partial u_2}{\partial \mathbf{n}}\right) \tag{15}$$

and

$$-\int_{\Omega} \nabla^2 \beta u_1 = -\int_{\Omega} \left(\nabla^2 \xi u_2 - \nabla \cdot \gamma \frac{\partial u_2}{\partial \mathbf{n}}\right). \tag{16}$$

Equations 15 and 16 are easily understood graphically as taking the second derivatives of the plots in Fig. 4.

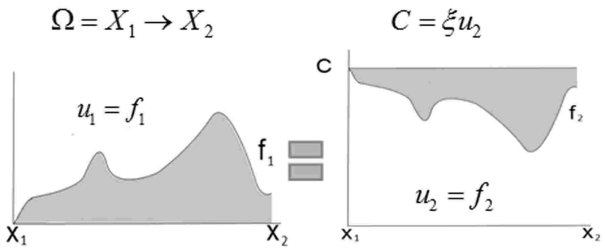

Fig. 4: Equivalent Areas From Gauss' Theorem

3 Conclusion

Although we can assume that some function **g** is causal to the appearance of a vector, does the vector appear from nothing or is it result of a change in what is already at that point? If *au* exists, what does it physically represent? Calling any field "attractive" or "repulsive" is nothing more than a metaphysical convention, i.e. does the load function cause a change in ϕ resulting in an attraction or a reduced repulsion, as in Fig. 5? From this, we can conclude that although we may possess measurements ∇u and $\nabla^2 u$, we cannot determine the nature of the scalar field u simply from the Poisson equation or Gauss' Theorem.

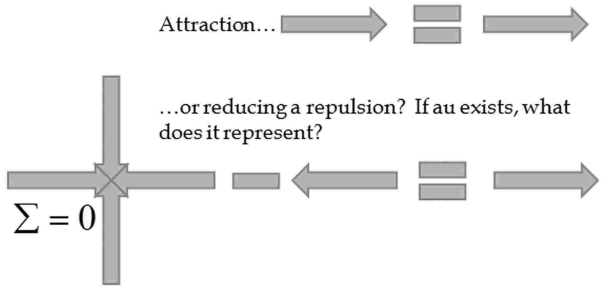

Fig. 5: Attraction or Reduced Repulsion?

4 Motivation: Cosmological Constant and General Relativity

Why is the previous figure important? Although there is a great deal of literature concerning Λ, in order to start a new perspective and to utilize the previous section, we re-examine the first known published physical meaning of the constant. In Einstein's 1917 paper *Cosmological Considerations On The General Theory of Relativity* [2] the first equation Einstein presents is the Poisson equation version of Newton's Law of Gravity

$$\nabla^2\phi = 4\pi\kappa\rho. \tag{17}$$

Citing Newtonian concerns over the limiting value of ϕ at "spatial infinity" he proposes a modification of the equation to

$$\nabla^2\phi - \lambda\phi = 4\pi\kappa\rho. \tag{18}$$

This was from an early difficulty in that the derivation required $R_{\mu\nu} = 0$ when matter or energy was not present. Due to cosmological observations though, and despite the rigor of the derivation, this requirement was eventually relaxed [4, see for relation to $G_{\mu\nu} = 0$, p. 410] allowing the introduction of a cosmological constant, even if it is not physically understood.

Setting the Poisson equation aside for the moment, it is also known that one of the interpretations of Λ or λ in Riemannian geometry is as a four dimensional constant of integration, through what is referred to as Unimodular Gravity [9]. This interpretation restricts allowable diffeomorphisms to only those preserving the four volume, but to date this has been treated as but a curious equivalent to General Relativity.

5 Introducing the Lorentz Tensor

Let us take a constant multiple of the metric $g_{\mu\nu}$ and refer to it as Ω. We do not utilize Λ or λ so as not to cause confusion and to allow us to more easily retain a difference in our understanding. Let us enforce $R_{\mu\nu} = 0$ such that

$$\Omega g_{\mu\nu} = G_{\mu\nu} + L_{\mu\nu} \tag{19}$$

where $G_{\mu\nu}$ is the Einstein tensor and $L_{\mu\nu}$ is a tensor we propose to call the "Lorentz" tensor. We shall expand on our reasoning for calling it this in subsequent papers. We can readily see that

$$G_{\mu\nu} = \Omega g_{\mu\nu} - L_{\mu\nu} \tag{20}$$

and that if $\Omega = 0$ then the Lorentz tensor is simply the negative of the Einstein tensor,

$$G_{\mu\nu} = -L_{\mu\nu}, \tag{21}$$

and should have the same important properties, i.e.

$$G_{\mu\nu;\mu} = -L_{\mu\nu;\mu}. \tag{22}$$

This of course results in

$$R_{\mu\nu} - \frac{1}{2}\, g_{\mu\nu}R = G_{\mu\nu} = \Omega g_{\mu\nu} - L_{\mu\nu}. \tag{23}$$

Note that for now cosmological models that rely on only a multiple of the metric remaining with no matter present, such as deSitter space, are not possible since $R_{\mu\nu} = 0$.

Although there are physical arguments for equating the Einstein tensor to the energy momentum tensor ($G_{\mu\nu} = \kappa T_{\mu\nu}$), and thus into analogues for Newton's Law of Gravity, we note simply in this paper that Eq. 17 is ultimately arrived at through $G_{\mu\nu}$. By the symmetry present in Eq. 23 and our arguments concerning the Poisson equation and Gauss' Theorem, our future objective is to use our understanding of Fig. 6 to obtain a rigorous derivation of Fig. 7.

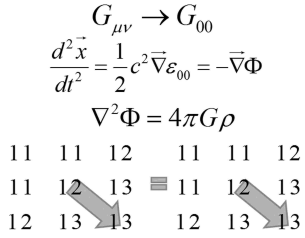

Fig. 6: Einstein Tensor to Poisson

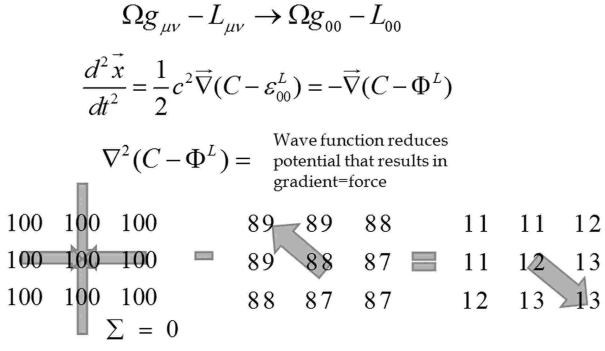

Fig. 7: Alternate EFE to Reduced Repulsive Poisson

We do this also in order to ask, should matter subject to the force represented by the vector present in Fig. 7 become

zero after traveling a certain radius from a massive body, what occurs at radii larger than this? It is our motivation to determine whether this is a plausible explanation for phenomena attributed to positive accelerating expansion.

Submitted on: October 11, 2012 / Accepted on: October 17, 2012

Acknowledgements

The author would like to thank Dr. Marian Kazimierczuk and Dmitri Rabounski.

References

1. Albrecht A., Bernstein G., Cahn R., Freedman W. L., Hewitt J., Hu W., Huth J., Kamionkowski M., Kolb E. W., Knox L. Report of the dark energy task force. arXiv: astro-ph/0609591.
2. Einstein A., Davis F.A. The principle of relativity. Dover Publications, New York, 1952.
3. Hobson M. P., Efstathiou G., Lasenby A. N., General relativity: an introduction for physicists. Cambridge University Press, Cambridge, UK ; New York, 2006.
4. Misner C. W., Thorne K. S., Wheeler J. A., Gravitation. W.H. Freeman, San Francisco, 1973.
5. NASA. Seven Year Results: Wilkinson Microwave Anisotropy Probe. 2011.
6. Padmanabhan T. Cosmological constant: the weight of the vacuum. *Physics Reports*, 2003, v. 380 (5), 235–320.
7. Perlmutter S., Aldering G., Goldhaber G., Knop R.A., Nugent P., Castro P.G., Deustua S., Fabbro S., Goobar A., Groom D.E. Measurements of Ω and Λ from 42 high-redshift supernovae. *The Astrophysical Journal*, 1999, v. 517 (2), 565–586.
8. Riess A. G., Filippenko A. V., Challis P., Clocchiatti A., Diercks A., Garnavich P. M., Gilliland R. L., Hogan C. J., Jha S., Kirshner R. P. Observational evidence from supernovae for an accelerating universe and a cosmological constant. *The Astronomical Journal*, 1998, v. 116 (3), 1009–1038.
9. Weinberg S. The cosmological constant problem. *Reviews of Modern Physics*, 1989, v. 61 (1), 1–23.
10. Author not listed. The dark side of the universe. *Economist*, 2012, v. 402 (8772), 79–81.

Magnetic Fields and Directional Spectral Emissivity in Sunspots and Faculae: Complimentary Evidence of Metallic Behavior on the Surface of the Sun

Pierre-Marie Robitaille

Department of Radiology, The Ohio State University, 395 W. 12th Ave, Columbus, Ohio 43210, USA. E-mail: robitaille.1@osu.edu

Sunspots and faculae are related phenomena and constitute regions of elevated magnetic field intensity on the surface of the Sun. These structures have been extensively studied in the visible range. In this regard, it has been recognized that the intensity contrast of faculae, relative to the photosphere, increases considerably as the line of observation moves from the center to the limb of the Sun. Such center to limb variation (CLV) suggests that the directional spectral emissivity of the faculae increases at the same time that photospheric directional emissivity decreases. Since the directional spectral emissivity of faculae increases towards the limb, these structures, along with sunspots, provide strong evidence for metallic behavior at the level of the solar surface. This further strengthens claims that the body of the Sun is not gaseous, but rather, comprised of condensed matter.

1 Introduction

In his popular work, *The Birth and Death of the Sun*, George Gamow justified the gaseous nature of the Sun as follows: "*. . . at 6000 degrees all the materials from which a furnace might be constructed, including even such refractory substances as platinum or carbon, will be not only melted but completely evaporated. No material can exist at these high temperatures in a state other than gaseous, and this is exactly what we find on the surface of the Sun, where all elements are present in vapour form*" [1, p. 4–5]. Several prominent members of the astronomy community, by utilizing similar logic, had previously laid the foundation for a gaseous Sun in the mid-1800s [2]. The contention that the Sun was too hot to be anything but gaseous would persist throughout the 20th century [3]. Conversely, experiments had long indicated that the phases of matter did not depend solely on temperature, but on factors such as external pressure, internal atomic composition, and the nature of the lattice adopted in the condensed phase. Yet, using a single justification, the possibility that certain materials might exist in liquid form within the Sun continued to be ignored. Gamow's argument [1, p. 4–5] would discount Wigner and Huntington's 1935 proposal [4] that metallic hydrogen, a material existing in the condensed phase, could be created at elevated temperatures and pressures [5–7].

2 Metallic hydrogen on the Sun

Liquid metallic hydrogen [4] is a particularly alluring substance relative to condensed solar models [5–7], especially given the observation that the Sun appears to be primarily composed of this element [8–11]. Although metallic hydrogen was first proposed nearly eighty years ago [4], it remains an elusive material in the laboratory [5]. Some claims of synthesis have received broad international acclaim [12, 13], often followed, by controversy [14–17] and slow dismissal. Others, such as claims that certain forms of metallic hydrogen can be produced in Rydberg matter, have received less attention [18].

There has recently been a new flurry of activity in the quest to produce metallic hydrogen [4] in the laboratory. In November 2011, Mikhail Eremets and Ivan Troyan published a provocative report in *Nature Materials* [19] which strongly suggested that metallic hydrogen had indeed been synthesized for the first time on the Earth. Nonetheless, given the nature of the quest for metallic hydrogen [5], it seemed crucial that more evidence be acquired [20–22]. Perhaps this time, the synthesis of metallic hydrogen will be affirmed [5].

Beyond metallic hydrogen itself, dense hydrogen could play an important role in the Sun, since the photosphere appears to be less metallic in nature than sunspots [5]. The author has advanced arguments that the photosphere adopts a layered lattice resembling graphite (a Type-1 lattice [5]), while the lattice in sunspots has more metallic character (a Type 2 lattice [5]). This is presumably due to slightly decreased inter-atomic distances within the layered lattice of sunspots. It is noteworthy that a report has recently demonstrated that dense hydrogen could adopt a graphene-like structure at 220 GPa and 300 K [23, 24]. The need for emitting a thermal spectrum provides strong motivation for considering graphite-like layered structures, which can lead to hydrogen in the metallic state, within liquid models of the Sun [5].

3 A liquid Sun

The idea that the Sun could be liquid dates back at least to the days of Gustav Kirchhoff [2] and Sir James Hopwood Jeans was its last major scientific champion [3]. Jeans was a distinguished physicist [25] and Physical Sciences Secretary of the Royal Society from 1919 to 1929 [26]. He was also Sir Arthur Eddington's principle antagonist [3]. For much of his scientific career, Jeans advanced that heavy metals such as uranium comprised the building blocks for a liquid Sun,

in opposition to Eddington's gaseous models [3]. When the Sun was determined to be principally composed of hydrogen [9–11], Jeans was left without a structural material. Eddington's gaseous Sun went on to be widely accepted by astronomy. Neither Jeans nor Eddington had anticipated the postulate that metallic hydrogen could be formed at elevated pressures [4]. For his part, Jeans abandoned the liquid model [3], apparently without sufficiently considering that the observational evidence for condensed matter might continue to mount [5–7, 27–29]. At the time, he had elucidated only fragmentary proof for a liquid state (see [3] and references therein).

Today, not a single observational line of evidence supports the idea that the Sun is gaseous, as simple temperature arguments are fallacious. Much of the scientific discussion appears centered on endowing gaseous solar models with the ability to behave as condensed matter (e.g. [30]). By dismissing the facts, the existence of the solar surface has been discounted [3], precisely because the gaseous models have no means of accounting for such a structure [29]. All structural features associated with solar activity (sunspots, faculae, prominences, flares, spicules, etc. . .) tend to be explained using magnetic fields, as the only means to impart structural features to a gaseous entity which, in reality, can support none.

In sharp contrast, observational facts point to a liquid Sun, including more than one dozen proofs for a condensed matter [5–7, 27–29]. Though the most convincing line of evidence for a liquid Sun will always remain the thermal appearance of the photospheric spectrum in the visible range [27], some may not be able to appreciate the power and sufficiency of this proof. In part, this is due to the introduction of local thermal equilibrium reasoning in solar science [30]. Local thermal equilibrium has come to cloud the requirements for producing a thermal spectrum and mask the need for condensed matter [30]. Nonetheless, the arguments which support a liquid Sun based on its thermal emission are definitive [30–33]. Thermal evidence will always remain paramount, because it points to the existence of lattice order on the surface of the Sun [31]. Nothing further is required to demonstrate the presence of condensed matter, as Kirchhoff himself indirectly understood in the mid-1800s [2]. For those who require additional illustrations, sunspots and faculae provide an interesting proving ground.

4 Directional spectral emissivity of sunspots and faculae

As key structural elements on the surface of the Sun, sunspots and faculae provide solar physicists ample opportunity for observation and discussion. In the days of Galileo and Scheiner, even the association of sunspots with the solar body was cause for extensive debate [34]. Since that time, sunspots and faculae have come to reveal much about the Sun, despite the belief that their visual appearance on the photosphere remains an optical illusion in modern solar theory [29].

4.1 Sunspots

As early as 1774, Alexander Wilson [35] noted that sunspots appeared as slight depressions relative to the solar surface. Wilson reached this conclusion based on geometry [35]. Accepted solar models currently account for the visual depression of sunspots, or "Wilson effect", using optical depth arguments (e.g [36, p. 189–190] and [37, p. 46]). Such complexity must be invoked because modern theories are built around a gaseous solar body. Since these models have long deprived the Sun of a true surface [2,29], they cannot rest upon geometrical arguments to account for the Wilson effect [35] and must have recourse to explanations based on optical depth (e.g [36, p. 189–190] and [37, 46]). Conversely, the author has argued in favor of an authentic solar surface, thereby directly challenging accepted models [29]. Hence, the Wilson effect [35], one of the oldest and simplest sunspot observation, has provided a basis for questioning the established gaseous models of the Sun.

Modern astrophysics has advanced an understanding of sunspots which, on cursory examination at least, appears to be complete. In reality, the true physical nature of these structures has remained elusive, despite our arsenal of data. Still, much has been learned about sunspots. The Wilson effect was established at the end of the 18th century [35]. Schwab discovered the eleven year sunspot cycle in 1843 [38]. In the same period, Carrington used sunspot observations and outlined the differential rotation of the Sun in great detail [39].

In 1908, George Ellery Hale discovered that sunspots are regions of powerful magnetic activity [40]. The intensity of magnetic fields at the center of sunspots has been determined to be primarily vertical and known to increase in the dark nuclei of the umbra (e.g. [37, p. 75] and [41, p. 80]). Helioseismic analysis of the Sun has revealed that sound waves travel faster within sunspots relative to the photosphere [42,43]. All of these phenomena are highly suggestive of increased density and metallicity within sunspots and have been utilized to support the idea that the Sun is condensed matter [28]. Strong magnetic fields and the science of seismology are always associated with condensed matter, not the gaseous state of solar models.

Sunspots have also been reported to have directional emissivities that increase with angle of observation, as the observer follows their movement towards the limb of the Sun [41, p. 75–77]. One of the earliest reports of increased sunspot emissivity relative to the photosphere dates back to 1875 and Samuel Langley*: "*With larger images and an improved instrument, I found that, in a complete ring of the solar surface, the photosphere, still brilliant, gave near the limb absolutely less heat than the umbra of the spots*" [44, p. 748]. Edwin Frost would soon echo Langley: "*A rather surprising result of these observations was that spots are occasionally*

*Translations from French of Langley's work [44] were executed by the author, P. M. Robitaille.

relatively warmer than the surrounding photosphere" [45, p. 143].

Should the directional emissivity of sunspots truly increase near the limb, such behavior would be highly supportive of metallic character [28]. Non-metals usually display directional spectral emissivities that tend to decrease with increasing angle of observation [46–48]. Metals often possess lower normal emissivities with respect to their directional spectral emissivities. The directional spectral emissivities of metals typically rise with increasing angle, then fall precipitously with orthogonal viewing [46–48]. Thus, a careful analysis of emissivities can provide important clues as to whether sunspots (or faculae) are behaving as metals, potentially generating strong evidence for condensed matter on the surface of the Sun.

Truly gaseous objects should be devoid of emissivities which are directionally dependent. Thus, the increased directional spectral emissivity in sunspots could only be explained with extreme difficulty using gaseous solar models and often attributed to the effect of "stray light" [41, p. 75–77]. Stray light arguments have played an important role in the modern dismissal of increased emissivity in sunspots towards the solar limb. Thus, despite 100 years of study, the exact directional emissivity within these objects remains an unresolved issue in solar physics. The same cannot be said of facular directional spectral emissivity.

4.2 Faculae

The directional spectral emissivity contrast of faculae, with respect to the photosphere, has long been known. George Ellery Hale wrote, relative to the emissivity of the faculae: "*The bright faculae, which rise above the photosphere, are conspicuous when near the edge of the Sun, but practically invisible when they happen to lie near the center of the disk...*" [49, p. 85–86]. Hale later re-emphasized the changing emissivity of the faculae as a function of position on the solar disk: "*Mention has already been made of the faculae, which are simply regions in the photosphere that rise above the ordinary level. Near the edge of the Sun, their summits lie above the lower and denser part of that absorbing atmosphere which so greatly reduced the Sun's light near the limb, and in this region the faculae may be seen visibly. At times they may be traced to considerable distances from the limb, but as a rule they are inconspicuous or wholly invisible towards the central part of the solar disk*" [49, p. 90].

In 1961, Rogerson presented an elegant summary of the increase in facular directional emissivity observed near the solar limb [50]. This work was complemented with theory and a few photographs [50]. Rogerson noted that the contrast variation between the faculae and photosphere increased to a maximum of about 64% near the very limb of the Sun [50]. Today, the center to limb variation (CLV) of facular emissivity is widely accepted and studied [51–54], as has the grouping of faculae with sunspots (e.g. [55, p. 42–43] and [56, p. 248–249]), and the identification of faculae as regions of intense magnetic activity [57–59].

The association of bright faculae with sunspots can be traced at least to the middle of the 19th century. According to de la Rue and his team, in 1865: "*It would thus appear as if the luminous matter being thrown up into a region of greater absolute velocity of rotation fell behind to the left; and we have thus reason to suppose that the faculous matter which accompanies a spot is abstracted from that very portion of the Sun's surface which contains the spot, and which has in this manner been robbed of its luminosity*" [60]. This direct association of sunspot and facular matter has recently been re-emphasized as a result of studying large flares on the solar surface [61].

While faculae display CLV with respect to their spectral emissivity, their emissivity contrast remains highly associated with the magnetogram signal [59]. Facular contrast, after increasing to a maximum near $\mu = 0.2$ (where $\mu = \cos\theta$ and θ is the heliocentric angle between the pixel of interest and direction of the Earth; r, the distance from the disk center, is given by $r = R\sin\theta$, if R represents the solar radius) has been observed to drop rapidly when moving even closer towards the limb [52]. This finding [52] appears to be in agreement with Spruit's "*hot wall*" model of facular emissivity [62, 63].

Spruit's "*hot wall*" model stated that faculae appeared darker when viewed directly from above because very little of the "*hot wall*" was visible. As the faculae moved towards the limb, the "*hot wall*" became increasingly visible and, hence, the structures appeared bright. With increasing distance towards the limb, the "*hot wall*" once again fell out of the line of sight, being obscured by the trailing wall, and the faculae once again appeared darker (see [53] for additional detail). Others have reported that facular contrast continues to increase towards the limb (e.g. [51]). This behavior would be more consistent with the "*hot cloud*" model [50, 64, 65]wherein the faculae are viewed as floating above the photosphere [53]. Today, Spruit's "*hot wall*" model has gained almost universal acceptance, as more in accordance with observation (e.g. [66, 67]).

Alternatively, it is herein proposed that the directional spectral emissivity observed in faculae constitutes one of the most elegant proofs that the Sun is comprised of condensed matter. The reasoning remains that advanced in section 3.1 (see also [28]), with the important distinction that the directional spectral emissivity changes in faculae, unlike sunspots, are uncontested [51–54, 57–59, 66, 67]. Moreover, the observation that directional spectral emissivity contrast in faculae increase towards the limb, before rapidly subsiding at the very edge of the Sun [52], strongly supports metallic behavior in these structures [28, 46–48].

On the Earth, the existence of directional spectral emissivity in condensed matter has been established [46–48, 68]. Materials display emissivities which always manifest their

atomic nature and structure, in addition to the temperature of observation [46–48, 68]. Every material possesses a unique signature and this constitutes a powerful lesson from the study of condensed matter [46–48, 68].

The idea that faculae are condensed matter based on directional emissivities also gains support from the realization that these objects, like sunspots, are regions of intense magnetic activity [57–59]. The ideal means of accounting for this activity remains the invocation of conduction bands. A solar body which is comprised of liquid metallic hydrogen and adopts a layered graphite-like lattice presents a wonderful material to account both for the directional spectral emissivities of faculae and the associated high magnetic field [5, 28]. While condensed matter can easily support such fields, there remains no evidence on the Earth that gases, in isolation, can generate powerful magnetic fields. While it is true that gaseous plasmas respond to the presence of magnetic fields, they certainly do not possess the required structure to create such phenomena.

5 Conclusion

Despite the wide acceptance of Spruit's "*hot wall*" model of facular emissivity [62] numerous problems exist with such approaches.

First, modern models of solar emissivity are fundamentally dependent on elemental and ionic opacities within the Sun. However, the solar spectrum cannot be generated using the sum of individual opacities. The author has designated solar opacity as the Achilles' heel of the gaseous solar models [30]. It is not reasonable to account for solar emission with phenomena which cannot explain the simple emissivity found on the Earth within graphite [30].

Second, a discussion of facular emissivity often focuses on local thermal equilibrium (LTE) arguments (e.g. [66]) and such arguments are not applicable to the Sun [30]. The Sun operates well outside the confines of local thermal equilibrium and Milne's argument in support of such a regimen [69–72] leads to conduction, not equilibrium [30].

Third, the assignment of temperatures, based on emissivities on the solar surface, constitutes a direct violation of the principles associated with thermal emission [30–33], as has been highlighted by Max Planck himself [73, §101] and discussed in detail [74].

Finally, the idea that a fully gaseous object can support structure remains contrary to the known principles of physics. Objects such as "*walls*", even when only considering emissivity, require condensed matter. They cannot be mimicked by gases with densities approaching that of the best vacuums achievable on the Earth [27].

In modern solar theory, sunspots are thought to be dark, as the magnetic fields they contain prevent hot gases from rising from the interior of the Sun (e.g. [75]). Conversely, the brightness of faculae are explained when magnetic fields dilute the solar material beneath them and causes the light to escape more easily. These explanations constitute stark contrasts with one another, while at the same time discounting much of what is known on the Earth relative to thermal emissivity. The fact remains that gases are unable to emit photons in a directionally dependent manner. Astrophysical explanations relative to the causes of directional emissivity, as related to photospheric limb darkening, solar granulations, sunspots, and faculae, with their reliance on "optical depth" and "solar opacities", remain at a serious disadvantage, relative to solar models based on condensed matter [27–30].

Irrespective of the mathematical elegance associated with modern solar models, there is no observational support that the body of the Sun is a gas. Given the nature of the solar spectrum, seismic activity, and the presence of structural entities such as sunspots, prominences, and faculae, modern theory must constantly resort to mathematical arguments, or the presence of magnetic fields, in order to endow a gaseous Sun with the properties of condensed matter [8–10]. In reality, while the corona displays features consistent with gaseous plasma, the photosphere, with its sunspots, faculae, and eruptive prominences, strongly manifests the condensed nature of the solar body. The idea that solar temperatures forbid the formation of condensed matter in the Sun ignores the reality that the phases of matter are not solely determined by temperature, but are a manifestation of many factors, including pressure of formation and the internal physical properties of materials [5–7].

Currently, numerous lines of evidence strongly support the condensed nature of the Sun. These include:

1) the continuous nature of the thermal spectrum [6, 27–30],
2) photospheric limb darkening [27, 28],
3) the absence of solar collapse [5, 6, 27],
4) a solar density (1.4 g/cm^3) consistent with a hydrogen lattice [6, 27],
5) the presence of seismic activity [6, 27],
6) the behavior of mass displacement on the solar surface [6, 27],
7) the chromosphere and critical opalescence [27],
8) the existence of solar oblateness [6, 27],
9) the extensive surface activity [6, 27, 28],
10) the orthogonal nature of photospheric/coronal flows [27],
11) the ability to image the solar surface [6, 27–29],
12) the presence of a powerful solar dynamo [27],
13) the nature and behavior of sunspots, including the Wilson effect [27, 28], and
14) the structure and dynamic evolution of solar granulation [28].

Each of these phenomena can be readily incorporated into a condensed model of the Sun. Conversely, gases can neither support nor act as structural entities. A striking example relative to thermal emission and the solar opacity problem in gaseous models has been addressed in detail [30].

In this work, a fifteenth line of evidence for the condensed nature of the Sun is presented:

15) the directional spectral emissivity of faculae. Emissivity fundamentally reflects a "Planckian proof" or a "thermal proof" for condensed matter. Along with 1) the thermal appearence of the solar spectrum, 2) the limb darkening of the photosphere, 3) the directional spectral emissivity of sunspots, and 4) the directional spectral emissivity of granulations [28], the emissivity of faculae constitutes one of the most powerful lines of evidence that the Sun is condensed matter. It therefore represents the fifth thermal proof for condensed matter on the surface of the Sun.

It remains highly likely that the Planckian proofs constitute direct physical evidence for a solar lattice [31]. Through the study of directional spectral emissivity, they argue for metallicity both within sunspots and faculae. Such metallicity represents a manifestation of the lattice and the conduction bands which it supports. The Planckian proofs also remind us of the need to properly address and understand complex emission mechanisms. Driven by a desire to better comprehend the solar spectrum, perhaps someday, the physics community, at last, will link thermal emission to a unique physical process as the author has suggested [31–33]. In so doing, condensed matter and theoretical physicists will finally conclude the work initiated, but left unfinished, by Max Planck [73].

Dedication

The work is dedicated to Professor Manuel Tzagournis, Senior Vice-President for Health Science and Dean of the College of Medicine (Emeritus) at The Ohio State University for the faith he placed in realizing the dreams and hopes of a young assistant professor.

Submitted on: November 01, 2013 / Accepted on: November 03, 2013
First published in online: November 04, 2012

References

1. Gamow G. The Birth and Death of the Sun. A Mentor Book: The New American Library, New York, N.Y., 1952.
2. Robitaille P.M. A thermodynamic history of the solar constitution — I: The journey to a gaseous sun. *Progr. Phys.*, 2011, v. 3, 3–25.
3. Robitaille P.M. A thermodynamic history of the solar constitution — II: The theory of a gaseous sun and Jeans' failed liquid alternative. *Progr. Phys.*, 2011, v. 3, 41–59.
4. Wigner E. and Huntington H.B. On the possibility of a metallic modification of hydrogen. *J. Chem. Phys.*, 1935, v.3, 764–770.
5. Robitaille P.M. Liquid metallic hydrogen: A building block for the liquid Sun. *Progr. Phys.*, 2011, v. 3, 60–74.
6. Robitaille P.M. A high temperature liquid plasma model of the Sun. *Progr. Phys.*, 2007, v. 1, 70–81 (also in arXiv: astro-ph/0410075).
7. Robitaille P.M. The Sun as a high energy/high density liquid metallic hydrogen plasma. *The 33rd IEEE International Conference on Plasma Science*, June 4–8, 2006, Traverse City, Michigan, p. 461, DOI:10.1109/PLASMA.2006.1707334.
8. Payne C.H. The relative abundances of the elements. Stellar Atmospheres. Harvard Observatory Monograph No. 1, Harvard University Press, Cambridge, MA, 1925, Chapter 13 (reprinted in part in Lang K.R. and Gingerich O. A source book in astronomy and astrophysics, 1900–1975, Harvard University Press, Cambridge, MA, 1979, p.245–248).
9. Unsöld A. Über die Struktur der Fraunhofersehen Linien und die quantitative Spektralanalyse der Sonnenatmosphäre. *Zeitschrift für Physik*, 1928, v. 46, 765–781.
10. Russell H.N. On the composition of the Sun's atmosphere. *Astrophys. J.*, 1929, v.70, 11–82.
11. Grevesse N. and Sauval A.J. Standard solar composition. *Space Science Reviews*, 1998, v. 85, 161–174.
12. Weir S.T., Mitchell A.C. and Nellis W.J. Metallization of fluid molecular hydrogen at 140 GPa (1.4 Mbar). *Phys. Rev. Letters*, 1996, v. 76(11), 1860–1863.
13. Mao H.K. and Hemley R.J. Optical studies of hydrogen above 200 Gigapascals: Evidence for metallization by band overlap. *Science*, 1989, v. 244, 1462–1464.
14. Silvera I.F. Evidence for band overlap metallization of hydrogen. *Science*, 1990, v. 247(4944), 863.
15. Mao H.K. and Hemley R.J. Evidence for band overlap metallization of hydrogen — Response. *Science*, 1990, v. 247(4944), 863–864.
16. Eggert J.H., Moshary F., Evans W.J., Lorenzana H.E., Goettel K.A. and Silvera I.F. Absorption and reflectance in hydrogen up to 230 GPa: Implications for metallization. *Phys. Rev. Letters*, 1991, v. 66, 193–196.
17. Besson J.M. Comment on "Metallization of fluid molecular hydrogen at 140 GPa (1.4 Mbar)". *Phys. Rev. Letters*, 1997, v. 78(26), 5026.
18. Holmlid L. Sub-nanometer distances and cluster shapes in dense hydrogen and in higher levels of hydrogen Rydberg matter by phase-delay spectroscopy. *J. Nanopart. Res.*, 2011, v. 13, 5535–5546.
19. Eremets M.I. and Troyan I.A. Conductive dense hydrogen. *Nature Materials*, 2011, v. 10, 927–931.
20. Research Highlights. Hydrogen made metallic. *Nature*, 2011, v. 479, 448.
21. Jephcoat A.P. High-pressure physics: Testing one's metal. *Nature Materials*, 2011, v. 10, 904–905.
22. Cartwright J. Chemists claim metallic hydrogen creation first. *Chemistry World*, November 14, 2011.
23. Howie R.T., Guillaume C.L., Scheler T., Goncharov A.F. and Gregoryanz E. Mixed molecular and atomic phase of dense hydrogen. *Phys. Rev. Letters*, 2012, v. 108(12), 125501 (5 pages).
24. Cartwright J. Hydrogen that mimics graphene. *Chemistry World*, April 2, 2012.
25. Milne E.A. Sir James Jeans — A Biography. Cambridge University Press, Cambridge, 1952.
26. http://royalsociety.org/about-us/governance/officers/ (accessed 10/15/2012)
27. Robitaille P.M. The solar photosphere: Evidence for condensed matter. *Progr. Phys.*, 2006, v. 2, 17–21.
28. Robitaille P.-M. On Solar granulations, limb darkening, and sunspots: Brief insights in remembrance of Father Angelo Secchi. *Progr. Phys.*, 2011, v. 3, 79–88.
29. Robitaille P.-M. On the presence of a distinct Solar surface: A reply to Hervé Faye. *Progr. Phys.*, 2011, v. 3, 75–78.

30. Robitaille P.M. Stellar opacity: The Achilles heel of the gaseous Sun. *Progr. Phys.*, 2011, v. 3, 93–99.
31. Robitaille P.M.L. On the validity of Kirchhoff's law of thermal emission. *IEEE Trans. Plasma Sci.*, 2003, v. 31(6), 1263–1267.
32. Robitaille P.-M. Blackbody radiation and the carbon particle. *Progr. Phys.*, 2008, v. 3, 36–55.
33. Robitaille P.-M. Kirchhoff's law of thermal emission: 150 years. *Progr. Phys.*, 2009, v. 4, 3–13.
34. Galilei G. and Scheiner C. On Sunspots. Translated by E. Reeves and A.V. Helden, University of Chicago Press, Chicago, 2010.
35. Wilson A. Observations on the solar spots. *Phil. Trans. Roy. Soc.*, 1774, v. 64, 1–30.
36. Tandberg-Hanssen E. Solar Activity. Blaisdell Publishing Co., Waltham, M.A., 1967.
37. Thomas J.H. and Weiss N.O. Sunspots and Starspots. Cambridge University Press, Cambridge, U.K., 2008.
38. Schwab H. Sonnenbeobachtungen im Jahre 1843. Von Herrn Hofrath Schwabe in Dessau. *Astronomische Nachrichten*, 1844, v. 21, 233–236.
39. Carrington R.C. Observations on the Spots of the Sun, from November, 9, 1853, to March 24, 1861, Made at Redhill. Williams and Norgate, London, U.K., 1863.
40. Hale G.E. On the probable existence of a magnetic field in Sun-spots. *Astrophys. J.*, 1908, v. 28, 315–343.
41. Sobotka M. Fine structure in sunspots. In: *Motions in the solar atmosphere* (A. Hanslmeier and M. Messerotti, eds.), Astrophysics and Space Science Library, v. 239, Kluwer Academic Publishers, Dordrecht, 1999, p.71–97.
42. Moradi H. and Cally P.S. Time-distance modeling in a simulated sunspot. *Solar Physics*, 2008, v. 251, 309–327.
43. Ilonidis S. and Zhao J. Determining absorption, emissivity reduction, and local suppression coeffcients inside sunspots. *Solar Physics*, 2011, v. 268, 377–388.
44. Langley S. Sur la température des diverses régions du soleil. Les noyaux noirs des taches. *Comptes Rendus*, 1875, v. 80, 746–749.
45. Frost E.B. Observations on the thermal absorption in the solar atmosphere made at Potsdam. *Astronnomische Nachrichten*, 1892, v. 130 (3105–3106), 129–146.
46. Modest M.F. Radiative heat transfer. McGraw-Hill, New York, 1993, p.92–108.
47. Thirumaleshwar M. Fundamentals of Heat and Mass Transfer. Dorling Kindersley, Dehli, 2009, p. 652.
48. Incropera F.P., DeWitt D.P., Bergman T.L., Lavine A.S. Fundamentals of Heat and Mass Transfer, 6th Edition. JohnWiley & Sons, Hoboken, NJ, 2007.
49. Hale G.E. The study of stellar evolution: An account of some recent methods of astrophysical research, The decennial publications of the University of Chicago — Second Series, Vol. X. University of Chicago Press, Chicago, 1908.
50. Rogerson J.B. On photospheric faculae. *Astrophys. J.*, 1961, v. 134, 331–338.
51. Chapman G.A. and Klabunde D.P. Measurements of the limb darkening of faculae near the solar limb. *Astrophys. J.*, 1982, v. 261, 387–395.
52. Libbrecht K.G., Kuhn J.R. On the facular contrast near the solar limb. *Astrophys. J.*, 1985, v. 299, 1047–1050.
53. Lawrence J.K. and Chapman G.A. Photometric observations of facular contrasts near the solar limb. *Astrophys. J.*, 1988, v. 335, 996–1004.
54. Berger T.E., van der Voort L.R., Löfdahl M. Contrast analysis of solar faculae and magnetic bright points. *Astrophys. J.*, 2007, v. 661, 1272–1288.
55. Wilson P.R. Solar and stellar activity cycles. Cambridge University Press, Cambridge, U.K., 1994.
56. Bray R.J. and Loughhead R.E. Sunspots. Chapman and Hall Ltd., London, U.K., 1964.
57. Chapman G.A. Facular line profiles and facular models. *Astrophys. J. Supp. Ser.*, 1977, v. 33, 35–54.
58. Tarbell T.D. and Title A.M. Measurements of magnetic fluxes and field strengths in the photospheric network. *Solar Physics*, 1977, v. 52, 13–25
59. Ortiz A., Solanki S.K., Domingo V., Fligge M. and Sanahuja B. On the intensity contrast of solar photospheric faculae and network elements. *Astron. & Astrophys.*, 2002, v. 388, 1036–1047.
60. de la Rue W., Stewart B. and Loewy B. Researches on solar physics — Series II: On the behaviour of sun-spots with regard to increase and diminution (abstract). *Proc. Roy. Soc. London*, 1865, v. 14, 59–63.
61. Wang H., Deng N. and Liu C. Rapid transition of uncombed penumbrae to faculae during large flares. *Astrophys. J.*, 2012, v. 748(2), 76.
62. Spruit H.C. Pressure equilibrium and energy balance of small photospheric fluxtubes. *Solar Physics*, 1976, v. 50, 269–295.
63. Walton S.R. Flux tube models of solar plages. *Astrophys. J.*, 1987, v. 312, 909–929.
64. Kononovich E.V. A unified interpretation of photospheric and facular granules. *Soviet Astronomy Letters*, 1979, v. 5, 50–52.
65. Schatten K.H., Mayr H.G., Omidvar K., Maier E. A hillock and cloud model for faculae. *Astrophys. J.*, 1986, v. 311, 460-473.
66. Unruh Y.C., Solanki S.K. and Fligge M. The spectral dependence o facular contrast and solar irradiance variations. *Astron. & Astrophys.*, 1999, v. 345, 635–642.
67. Keller C.U., Schüssler M., Vögler A. and Zakharov V. On the origin of solar faculae. *Astrophys. J. Letters*, 2004, v. 607, L59–L62.
68. Touloukian Y.S. and Ho C.Y. Thermophysical Properties of Matter (vols. 1). Plenum, New York, 1970.
69. Milne E.A. Selective radiation-pressure and the structure of a stellar atmosphere. *Mon. Not. Roy. Astron. Soc.*, 1927, v.87, 697–708.
70. Milne E.A. The effect of collisions on monochromatic radiative equilibrium. *Mon. Not. Roy. Astron. Soc.*, 1928, v. 88, 493–502.
71. Milne E.A. Bakerian Lecture: The structure and opacity of a stellar atmosphere. *Phil. Trans. Roy. Soc. London*, 1929, v. 228, 421–461.
72. Milne E.A. Thermodynamics of the stars. *Handbuch der Astrophysik*, 1930, v. 3, Part 1, 65–255.
73. Planck M. The Theory of Heat Radiation. P. Blakiston's Son & Co., Philadelphia, PA, 1914.
74. Robitaille P.M. On the temperature of the photosphere: Energy partition in the Sun. *Progr. Phys.*, 2011, v. 3, 89–92.
75. http://atst.nso.edu/files/press/ATST_book.pdf (accessed on 10/25/2012 — see Page 8).

Evolution of Stellar Objects According to J. Wheeler's Geometrodynamic Concept

Anatoly V. Belyakov
E-mail: belyakov.lih@gmail.com

The proposed model is based on J. Wheeler's geometrodynamic concept, in which space continuum is considered as a topologically non-unitary coherent surface admitting the existence of transitions of the input-output kind between distant regions of the space in an additional dimension. The existence of closed structures (macrocontours) formed at the expense of interbalance of gravitational, electric, magnetic and inertial forces has been substantiated. It is such macrocontours that have been demonstrated to form — independently of their material basis — the essential structure of stellar objects (SO) and to determine the position of these objects on the Hertzsprung-Russell diagram. Models of the characteristic types of stellar objects: stars and compact bodies emerging in the end of stellar evolution — have been presented, and their standard parameters at different stages of evolution have been calculated. The existence of the Hertzsprung-Russell diagram has been substantiated, and its computational analogue has been given. Parallels between stellar and microcosmic objects are drawn.

Recognizing the Seeker, Nature
itself will come to meet him.

Rockwell Kent

1 Introduction

Wheeler's geometrodynamic concept, in which microparticles are considered as vortical oscillating deformations on a non-unitary coherent surface, was earlier used by the author to construct model objects of the microcosm [1, 2]. Those works substantiated the existence of closed structures (contours), determining the properties of microparticles. At the same time, the idea about transitions between distant regions of space in the form of Wheeler's "wormholes" can be extended to the scale of macrocosm, and some contemporary astrophysical theories has already made use of it [4]. In this paper, the existence of closed contours is substantiated at the cosmological scale, and grounds are given that they make the basis of stellar objects (SO).

The work does not consider the nature of the cosmological medium that forms stellar bodies, nor it does the nature of mass/charge carriers, force interactions etc., or various physical *manifestations* of the evolutionary behavior of stellar objects. These tasks are a subject of specific disciplines.

The model presented in the paper has an outline, illustrative character and suggests a new look at the problem. For the model, the only important thing is the *existence* of the aforementioned *entities*, forming certain types of stellar structures and determining their evolution. The work does use specific SO terms, but only schematic SO models are considered, with their evolution depending only on a few parameters reflecting the most important features of the real objects.

The SO models used here are based on the balance between main interactions: electrical, magnetic, gravitational and inertial — with no additional coefficients introduced. The analysis gives good qualitative results and, in a number of cases, plausible quantitative parameters for the statistically averaged (typical) stellar objects.

2 Initial premises

As was shown earlier [1], from the purely mechanistic point of view the so-called *charge* only manifests the degree of the nonequilibrium state of physical vacuum; it is proportional to the momentum of physical vacuum in its motion along the contour of the vortical current tube. Respectively, the *spin* is proportional to the angular momentum of the physical vacuum with respect to the longitudinal axis of the contour, while the *magnetic interaction* of the conductors is analogous to the forces acting among the current tubes.

It is given that the elementary unit of such tubes is a unit with the radius and mass close to those of a classical electron (r_e and m_e).

It should be noted that in [1, 2] the expressions for the electrical and magnetic forces are written in a "Coulombless" form, with charge replaced by electron limiting momentum. In this case, the electrical and magnetic constants (ε_0 and μ_0) are expressed as follows:

$$\varepsilon_0 = \frac{m_e}{r_e} = 3.33 \times 10^{-16} \text{ kg/m}, \quad (1)$$

$$\mu_0 = \frac{1}{\varepsilon_0 c^2} = 0.0344 \text{ N}^{-1}. \quad (2)$$

The electrical constant here is, in fact, the linear density of the vortex tube, with the mass:

$$m = \varepsilon_0 l, \quad (3)$$

where l is the length of the vortex tube (thread) or contour.

To combine the interactions, let us express them in a dimensionless form with the common force dimension factor $\frac{1}{\mu_0}$. Taking into account (1) and (2),

$$F_e = \frac{1}{\mu_0}\left(\frac{r_e}{r_0}\right)^2 z_{e_1} z_{e_2}, \tag{4}$$

$$F_m = \frac{1}{\mu_0}\frac{l}{2\pi r_0}\frac{r_e^2}{(c\times[\mathrm{sec}])^2}\, z_{e_1} z_{e_2}, \tag{5}$$

$$F_g = \frac{1}{\mu_0}\frac{1}{f}\left(\frac{r_e}{r_0}\right)^2 z_{g_1} z_{g_2}, \tag{6}$$

$$F_i = \frac{1}{\mu_0}\frac{r_e}{r_0}\left(\frac{\mathrm{v}_0}{c}\right)^2 z_g, \tag{7}$$

where v_0, r_0, z_e, z_g, f are the rotary velocity and rotary radius or distance between the vortex tubes, the relative values of charge and mass in the parameters of electron charge and mass and the ratio of electrical-to-gravitational forces, which, under the given conditions, is expressed as follows:

$$f = \frac{c^2}{\varepsilon_0 \gamma} = 4.16\times 10^{42}, \tag{8}$$

where γ is the gravitational constant.

The *balance of electrical and magnetic forces* $F_e = F_m$ gives a geometrical mean, a characteristic linear parameter that is independent of the direction of the vortex tubes and the number of charges

$$R_\odot = \sqrt{r_0\, l} = \sqrt{2\pi}\, c\times[\mathrm{sec}] = 7.52\times 10^8 \text{ m}, \tag{9}$$

a magnitude close to the Sun radius and the sizes of typical stars.

The *balance of magnetic and gravitational forces* $F_m = F_g$ also results in a geometrical mean:

$$\sqrt{r_0\, l} = \sqrt{\frac{z_{g_1} z_{g_2}}{z_{e_1} z_{e_2}}}\sqrt{\frac{2\pi}{f}}\, c\times[\mathrm{sec}] = \sqrt{\frac{\varepsilon}{f}}\, R_\odot, \tag{10}$$

where the ratio of the products $\varepsilon = z_{g_1} z_{g_2}/z_{e_1} z_{e_2}$ is an *evolutionary parameter*, which characterizes the state of the medium and its changes, as the mass carriers become predominant over the electrical ones and, as a matter of fact, shows how the material medium differs from vacuum.

In the general case, expression (10) gives a family of lengthy contours, consisting of contra-directional closed vortex tubes (*m_g-contours*). The evolutionary parameter ε proportionally increases the mass of the vortex tube for the m_g-element:

$$m = \varepsilon\varepsilon_0\, l. \tag{11}$$

The vortex tubes can consist, in their turn, of a number of parallel vortex threads, whose stability is ensured by the *balance of magnetic and inertial forces* ($F_m = F_i$; *m_i-zones*). As follows from this balance,

$$\mathrm{v}_{0i} = \sqrt{\frac{z_{e_1} z_{e_2}}{z_g}}\sqrt{\frac{r_e\, l}{2\pi}}\times[\mathrm{sec}^{-1}]. \tag{12}$$

Unidirectional vortex threads of the length l rotate, with the rotary velocity v_{0i}, about the longitudinal axis along an orbit of indeterminate radius. When they are filled with the chains of single charges, having the mass of an electron, and their number $z_e = z_g = l/r_e$ (or when the tubes consist of single vortex threads in the quantity of l/r_e), we get the following equation:

$$\mathrm{v}_{0i} = \frac{l}{\sqrt{2\pi}}\times[\mathrm{sec}^{-1}]. \tag{13}$$

The *balance of gravitational and inertial (centrifugal) forces* $F_g = F_i$ gives a *virial*, from which one can derive the maximal gravitational mass of the object, satisfying condition (9):

$$M_m = \frac{R_\odot c^2}{\gamma} = f R_\odot \varepsilon_0 = 1.012\times 10^{36} \text{ kg}. \tag{14}$$

3 Structurizations of the primary medium and parameters of stellar objects

Now let us consider objects in which more than one pair of forces is balanced.

Let us assume that an initially unstructured maximal mass evolves and becomes more complex — through the emergence of m_i-zones, consisting of single elements of the length l_i and mass m_i. As follows from the constancy of μ_0 in the general case,

$$\frac{1}{\mu_0} = \varepsilon_0 c^2 = \frac{m_i \mathrm{v}_{i_0}^2}{r_i} \tag{15}$$

where $m_i = \varepsilon_0 l_i$ is the mass of a vortex m_i-element. From (13) and (15), one can obtain, having in mind (9), the ratio for its geometrical parameters:

$$\frac{l_i^3}{r_i} = R_\odot^2. \tag{16}$$

Driven by gravitation, the single tubes (threads) will combine into a local structure, the mass of which can also be calculated from the virial:

$$M_i = \frac{r_i \mathrm{v}_{i_0}^2}{\gamma}. \tag{17}$$

Let the object contain z_i local zones; then its mass will be $M_0 = z_i M_i$. Let us introduce a dimensionless parameter

$M = M_0/M_m$. Then, making some transformations, one can eventually obtain uniform equations for all the parameters of the evolving objects with an arbitrary relative mass M:

number of local zones

$$z_i = \frac{1}{M^{1/4}}\,, \tag{18}$$

zone radius

$$r_i = M^{3/4} R_\odot\,, \tag{19}$$

length of the vortex tube (thread)

$$l_i = M^{1/4} R_\odot\,, \tag{20}$$

rotary velocity in the zone

$$\mathrm{v}_{0i} = M^{1/4}\, c, \tag{21}$$

number of single vortex threads in the zone

$$n = \frac{M_i}{m_i} = f M\,, \tag{22}$$

and, having in mind (10), one can take $n = \varepsilon$.

Thus, as its mass decreases, the *object simultaneously becomes more and more complex*, getting subtly structured with m_i-zones.

Let us assume that the initial state of SO is a rotating disk, which can further develop into larger structures (m_g-contours) of the size $R_0 \times d_0$, where the contour length is $R_0 = l$ and diameter is $d_0 = r_0$. With these designations, equation (10) will look as follows:

$$\sqrt{d_0\, R_0} = \sqrt{\frac{\varepsilon}{f}}\, R_\odot\,. \tag{23}$$

Let us accept, quite schematically and roughly, that m_g-contours in the disk are oriented radially-spirally and are pulled in towards the center by the radial components of the gravitational forces. These forces are approximately equal to $(d_0/R_0)F_g$. Then, from the balance of centrifugal and gravitational forces,

$$\mathrm{v}_0 = \sqrt{\frac{d_0}{R_0}}\,\sqrt{\frac{\gamma m}{R_0}}\,, \tag{24}$$

where m and R_0 are the m_g-contour mass and the averaged disk radius respectively.

Let us define the number of m_g-contours as

$$z_0 = \frac{R_0}{d_0}\,. \tag{25}$$

With equation (11) in mind, the total mass of the object will amount to

$$M M_m = z_0\, m = z_0\, \varepsilon \varepsilon_0\, R_0. \tag{26}$$

Taking into account equations (8), (9), (23–26) and making some transformations, we can find parameters of the structured disk:

$$R_0 = M^{1/3}\, R_\odot\,, \tag{27}$$

$$z_0 = \frac{f M^{2/3}}{\varepsilon}\,, \tag{28}$$

$$\mathrm{v}_0 = \frac{\varepsilon c}{f M^{1/3}}\,. \tag{29}$$

The parameters found are averaged when the disk structural elements are tightly packed, and they determine the core of the object. Let us define the object boundaries — under the condition that, if the system of m_g-contours is rotating as a rigid disk, the rotary velocity of contours at the periphery must not exceed the speed of light. In this case, the maximal radius of the disk will be:

$$R_m = \frac{R_0\, c}{\mathrm{v}_0} = z_0\, R_\odot\,. \tag{30}$$

Let us further assume — within the framework of our simplified model — that the mass of the object is concentrated either in the center (the *state of core*) or at the periphery (the *state of outer layer*). Obeying the angular momentum conservation law, velocity at the periphery cannot be higher than:

$$\mathrm{v}_m = \frac{\mathrm{v}_0 R_0}{R_m} = \frac{\mathrm{v}_0^2}{c}\,. \tag{31}$$

Let the periods of core and outer layer rotation be expressed as $\tau_0 = R_0/\mathrm{v}_0$ and $\tau_m = R_m/\mathrm{v}_m$ respectively (the duration of the inner and outer cycles).

Having in mind (27–31) and taking into account that $\sqrt{2\pi} = 2.51$, we obtain

$$\tau_0 = 2.51 M^{2/3}\frac{f}{\varepsilon}, \tag{32}$$

$$\tau_m = 2.51 M^{4/3}\left(\frac{f}{\varepsilon}\right)^3\,. \tag{33}$$

Indeed, star cores rotate much faster that their outer layers [5]. As the medium condenses and becomes more and more different from vacuum, the evolutionary parameter ε grows. There are at least two characteristic values of this parameter satisfying the following conditions:

1. The number of m_g-elements z_0 is equal to the number of m_i-structures z_i, which should correspond to the most stable or *balanced* state of SO in the process of its evolution. In this case ($z_i = z_0$) — as it follows from (18) and (28),
$$\varepsilon = f\, M^{11/12}\,. \tag{34}$$
2. The number of m_g-elements is reduced to one, which will include all the m_i-structures. This state corresponds to the end of a certain period of object's evolution, i.e., to the *degenerate* state. Here, from (28),
$$\varepsilon = f M^{2/3}\,. \tag{35}$$

In the state of degeneration, when $z_0 = 1$, the period of core rotation will — as follows from (30), (32), (35) — be constant for any masses and amount to 2.51 sec, whereas the size of the outer layer will be equal to the standard radius $R_\odot$. In the general case, one can write, combining (34) and (35):

$$\varepsilon = fM^k, \tag{36}$$

where the parameter $k \geqslant 2/3$.

Visible dimensions of stars, i.e., radii of their photospheres, depend on many a specific factor; as a rule, they do not equal to the radius R_m and can be evaluated only roughly. The same can be said about star temperatures. Let us take the mass of the Sun as a standard (the validity of such a choice will be justified later) and consider the radius of the solar photosphere being close to $R_\odot$. Then, within the limits of the main sequence for the stable state and taking into account our disk model, the relative radius of the photosphere R_f for a star of arbitrary mass can be expressed via the mass of the Sun. It is evident that for a *two-dimensional* model,

$$R_f = \left(\frac{M}{M_\odot}\right)^{1/2} \tag{37}$$

and in the general case,

$$R_f = \left(\frac{M}{M_\odot}\right)^{i}, \tag{38}$$

where $i = 1 \ldots 1/3$ is a coefficient reflecting the density of packing of m_g-contours in the object.

To evaluate the model object temperature, let us consider its radiation as that of black body. Let the maximal temperature of radiation be achieved at the Compton wavelength of electron, $k = 2.426 \times 10^{-12}$ m, and let us assume that the radiation wavelength is inversely proportional to the rotary velocity of the contour vortex tubes at a given radius. Then, from Wien's formula,

$$T = \frac{b}{\lambda}, \tag{39}$$

where $b = 0.0029 \times 10^6$ m $\times\,^\circ$K. Having in mind this proportion, the radiation temperatures at the radii of core and photosphere (and an arbitrary radius as well) can be expressed as

$$T_0 = T_k\left(\frac{\mathrm{v}_0}{c}\right) \tag{40}$$

and

$$T_f = T_k\left(\frac{\mathrm{v}_0}{c}\right)\left(\frac{R_0}{R_f}\right), \tag{41}$$

whereas the energy of radiation (here and so forth, in keV) as

$$E = 511\frac{\mathrm{v}_0}{c}\ \text{keV}, \tag{42}$$

where T_k is the limiting temperature, corresponding to λ_k and equal to $1.19 \times 10^9\,^\circ$K.

Parameters	Balanced state	Degenerate state
ε	2.47×10^{37}	6.56×10^{38}
z	26.6	1
The core		
R_0	0.0126	0.0126
v_0	4.7×10^{-4}	0.0126
τ_0, sec	66.9	2.51
$T_0\,^\circ$K	5.6×10^5	1.5×10^7
The outer layer		
R_m	26.6	1
v_m	2.21×10^{-7}	1.57×10^{-4}
τ_m, sec	$3 \times 10^8 = 9.6$ years	$1.58 \times 10^4 = 4.4$ hours
$T_m\,^\circ$K	263	1.89×10^5
The photosphere		
R_f	1	1
$T_f\,^\circ$K	7050	1.89×10^5

Table 1: Note — radii and velocities are expressed as fractions of $R_\odot$ and c.

4 Model adequacy

It seems improbable that such a schematic and simple model would yield plausible results towards stellar objects. Yet it does. Let us calculate some parameters of a *solar-mass star*. The mass of the Sun equals to 2×10^{30} kg; in relative units, upon division by M_m, $M_\odot = 2 \times 10^{-6}$.

Table 1 shows the results of calculations according to the formulas given above.

In our notation, *angular momentum* of the Sun is equal to

$$0.4(2 \times 10^{30})\,\mathrm{v}_0\,R_0 = 0.4\,M_\odot^{23/12} M_m c\,R_\odot = \\ = 1.09 \times 10^{42}\ \text{kg m}^2/\text{sec}, \tag{43}$$

where the coefficient 0.4 takes account of the spherical shape of the body.

Comparing the calculated equilibrium-state parameters of this averaged standard object (a solar-type star) with the actual parameters of the Sun, one can see a close correspondence between their sizes, surface and core temperatures and periods of the solar cycle activity. The Sun's angular momentum is calculated with almost *perfect precision*.

By the end of evolution, upon reaching the degenerate state (at $z_0 = 1$), the periods of the inner (τ_0) and outer (τ_m) cycles diminish to their limits (Table 1). In this case, the single-thread spiral structure would flatten into a disk — thick as the size of the core (R_0) and radiating to the sector of the disk plane. The period of radiation will be $\tau_m = 4.4$ h; impulse duration, $\tau_0 = 2.5$ sec; and temperatures of the core and outer layer correspond to energies, 6.4 and 0.08 keV respectively.

The presence of m_i-zones in the m_g-contour will bring uncertainty into the period of radiation, which will be inversely proportional to the number of m_i-zones. For an object of the solar mass, the uncertainty in the period of impulses will amount to $\tau_m/z_i = 4.4\,h/26.6 = 598$ sec.

These parameters are typical and correspond well to the *x*-ray sources, *barsters*. For example, they perfectly fit the parameters of the X-ray source 3U 1820-30 in the globular cluster NGC6624 [5] etc.

Of course, the model presented here reflects only some essential features of stellar object structure. A stellar object can consist of toroids (balance of magnetic and gravitational forces), whose current-conducting elements rotate above the closed longitudinal axis of the tor (balance of magnetic and inertial forces), whereas the toroids themselves are oriented in the plane of the rotating disk (balance of gravitational and inertial forces). Such a system should hardly be stable. The core would rotate faster than the periphery, and the m_g-contours would coil up, with their kinetic energy transforming into other forms (and then, probably, transforming back). Describing such a system as a multiturn plane-spiral mechanical pendulum might be nave, yet in any case, there should take place an *oscillatory process of the object's gravimagnitodynamical structure*. Indeed, the paired dark spots in the equatorial zone of the Sun seem to be the outlet of m_g-contours — undergoing magnetic reversal and changing their intensity and polarity with the period of 11 years. Their registered quantity (from several to a hundred) does not contradict the calculated mean $z_0 = 26.6$.

Now let us calculate the *density of the SO core*. In the atoms of stellar matter (hydrogen, for the most part), substance circulates, according to our model, within $p^+ - e^-$ — contours with the mass $\varepsilon_0\, r_0$, and circulation speed cannot be higher than that of light [1].

At the same time, the magnitude of the charge e_0 is constant at any quantum number and equals to the momentum of the contour mass $\varepsilon_0\, r_0\, \mathrm{v}_0$. At $\mathrm{v}_0 \to c$, $r_0 \to r_{0\,min}$, therefore

$$r_{0\,min} = \frac{e_0}{\varepsilon_0\, c} = 1.65 \times 10^{-12}\ \mathrm{m}\,. \qquad (44)$$

The density of maximally condensed hydrogen atoms will amount (for a spherical volume) to

$$\rho_{max} = \frac{3m_H}{4\pi r_{0\,min}^3} = 8.82 \times 10^7\ \mathrm{kg/m^3}\,, \qquad (45)$$

where m_H is the mass of a hydrogen atom.

Now let us represent the mean density of the core matter as a ratio of the core mass to its cubic radius. Having in mind the corresponding expressions, one can see that the density is invariable and depends only on the gravitational constant:

$$\rho_0 = \frac{MM_m}{R_0^3} = \frac{M_m}{R_\odot^3} = \frac{1}{2\pi\gamma \times [\mathrm{sec}]^2} = \\ = 2.38 \times 10^9\ \mathrm{kg/m^3}\,. \qquad (46)$$

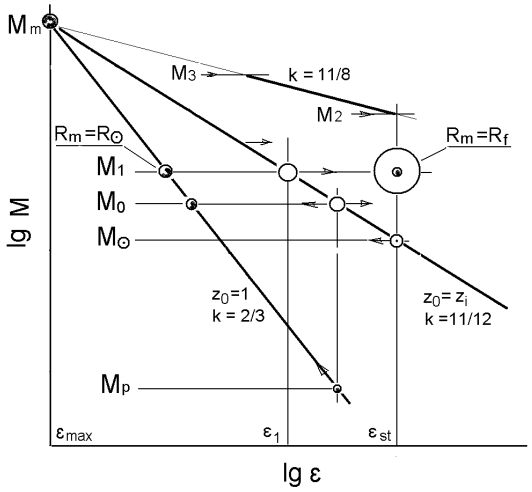

Fig. 1: The diagram "evolutionary parameter — mass".

As follows from the density ratio, a volume equal to that of a single hydrogen atom should contain 27 atoms of the initial matter, which corresponds, by the number of protons, to atoms of the iron group. The density is typical for white dwarfs, such as the famous Kuiper star.

It is interesting that the parameters obtained: $R_\odot$, ρ_0 and $\tau_0 = 2.51$ sec — practically indistinguishable from the values that should characterize the neck of a hypothetical magnetic "wormhole" of the mass M_m [4].

5 Analogues of the Hertzsprung-Russell (H-R) diagram and their applications

The Hertzsprung-Russell (H-R) diagram shows the evolutionary position of stellar objects on the "spectral class (temperature) — luminosity" coordinate plane. Let us consider its analogues: diagrams "evolutionary parameter — mass", and "temperature — mass".

5.1 The diagram "evolutionary parameter — mass"

On such a diagram (Fig. 1), $\varepsilon(M)$ dependencies would better be plotted on a logarithmic scale. At any k, the diagram rays converge on a point corresponding to the limiting mass M_m and limiting evolutionary parameter $\varepsilon_{max} = f$.

Specific parameters of SO will depend on the position of the object on the diagram. In general, with the converging point M_m approached then, as follows from (27–33), (40), (41), the number of m_g-contours will tend to 1; the rotary velocity, to the speed of light; the core and outer layer radii, to $R_\odot$; the periods of the inner and outer cycles, to 2.51 sec; and the core and outer layer temperatures, to T_k.

Evidently, for any given SO, the course of evolution may go both towards larger ε values (condensation of medium), up to $z = 1$, and smaller ε values (depression of medium), up to the shedding of the envelope at the end of the evolutionary process. ***Using the microcosm analogies, one can compare***

these states to the Bohr and ionized atoms respectively.

Let consider a stellar object which is in the main sequence and has a value of the evolutionary parameter corresponding to the line of equilibrium at $k = 11/12$. At $\varepsilon = const$, the equilibrium mass M_0 will correspond to a smaller mass M_p on the line of degeneration, for which $k = 2/3$ and $z_0 = 1$ (Fig. 1). In this case, one can obtain a mass ratio from (34) and (35):

$$M_p = M_0^{11/8} . \tag{47}$$

Since the mass of the Sun is considered standard, we shall take the evolutionary parameter value on the line of equilibrium for the solar mass ε_{st} as standard too.

5.2 Collapsing red giants

At the end of their evolution, stars become red giants and then shed their envelope (transfer to the state of the core), turning to white dwarfs, neutron stars or, in the case of the largest masses, "black holes".

Let us consider a star of chosen characteristic mass, for which every m_g-contour on the line of equilibrium has the mass of the Sun, i.e., satisfying the condition $M_0 = z_0 M_\odot$. Taking into account (28) and (34), we obtain $M_0 = M_\odot^{4/5} = 2.76 \times 10^{-5} = 13.8$ s.m. (masses of the Sun). Let us calculate the typical mass of a white dwarf forming from the core of such a star. Let us assume that on the line of star equilibrium, its core (and, therefore, the mass M_p as well) are on the line of degeneration (Fig. 1). Then, having in mind (47),

$$M_p = M_0^{11/8} = M_\odot^{11/10} = 5.38 \times 10^{-7} , \tag{48}$$

which corresponds to 0.27 s.m.

After the envelope and core are separated, they can be considered discretely. Let the envelope evolve to a standard parameter ε_{st}, and the core delay at the critical stage of the transformation process. Combining these states, let take the white dwarf mass M_p be proportional to the number of m_g-contours z_p — of the total number of m_g-contours z_0 of the mass M_0 at ε_{st}:

$$M_p = \frac{M_0 z_p}{z_0} . \tag{49}$$

Having in mind (28), (34) and (48), one can find the number of m_g-contours in the core:

$$z_p = \frac{f M_0^{25/24}}{\varepsilon_{st}} = M_\odot^{-1/12} = 2.98. \tag{50}$$

Therefore, the total mass of the star will be equivalent to $M_0/M_p = M_0^{-3/8} = M_\odot^{-3/10} = 51.2$ white dwarf masses, which corresponds to the number of nucleons in the nucleus of iron (more precisely, if $z_p = 3$, then $M_\odot = 1.9 \times 10^{-6}$ and the number of "nucleons" is equal to 52). Here we see another analogy with the microcosm: ***a standard red giant, containing 52 white dwarf masses, and a white dwarf, containing three***

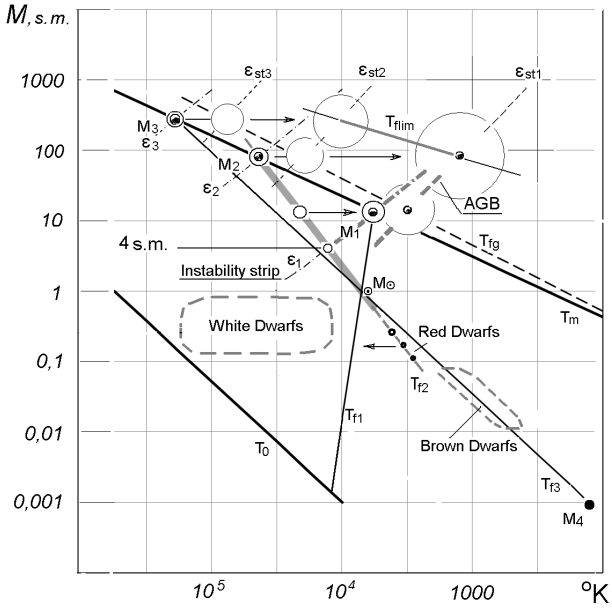

Fig. 2: The diagram "temperature-mass".

m_g-contours, will match an atom of iron, containing 52 nucleons, and a nucleon, consisting of three quarks. Later, other analogies with the microcosm will come into view.

Thus, it seems that the mass of the Sun and its evolutional parameter ε_{st} on the line of equilibrium are, indeed, standard. At $z_0 = 3$, the parameter $k \approx 0.75$, and it changes slightly in a wide range of masses. One can, therefore, expect that the condition (50) is optimal for other masses as well. Then, from (50),

$$\varepsilon_{st} = \frac{f M_0^{25/24}}{3} . \tag{51}$$

5.3 The diagram "temperature-mass"

Since logarithms of luminosity and mass are approximately proportional within the limits of the main sequence, it would be convenient to draw the H-R diagram analog in the coordinates of "temperature — mass".

From (27–30), (34), (40) and (41), one can obtain expressions of the $T(M)$ form, corresponding to the equilibrium temperatures at the radii of the outer layer R_m and core R_0 at $k = 11/12$. On a logarithmic scale (Fig. 2), they are straight lines, converging on the point M_m (outside the diagram):

$$T_m = T_k M^{7/6} , \tag{52}$$

$$T_0 = T_k M^{7/12} . \tag{53}$$

Stars of the main sequence have photospheres whose radii are usually smaller than R_m. To construct dependencies $T(M)$ for the photosphere, let us use formula (37). Taking into account (38), one can obtain, in the general case:

$$T_f = T_k M_\odot^i M^{k-i} . \tag{54}$$

For the equilibrium state at $k = 11/12$, we obtain three lines corresponding to three possible variants of packing of m_g-contours: into one-, two- and three-dimensional structures — i.e., at $i = 1, 1/2, 1/3$ (Fig. 2):

$$T_{f_1} = T_k\, M_\odot\, M^{-1/12}\,, \tag{55}$$

$$T_{f_2} = T_k\, M_\odot^{1/2} M^{5/12}\,, \tag{56}$$

$$T_{f_3} = T_k\, M_\odot^{1/3} M^{7/12}\,. \tag{57}$$

These lines converge on the point with coordinates close to the real parameters of the Sun, and their crossing with the outer-layer equilibrium line gives three characteristic masses: M_1, M_2 and M_3. The mass $M_1 = M_\odot^{4/5} = 13.8$ s.m., i.e., this mass also satisfies the condition $M_1 = z_0\, M_\odot$ and is equal to the mass of a red giant, which was calculated in the previous section. The mass $M_2 = 79.4$ s.m. is the largest possible mass for a main-sequence star. According to (47), this mass can give rise to an object whose mass will be 3 s.m., which corresponds to the maximal mass of a neutron star. The mass $M_3 = 277$ s.m. is the largest possible mass for a star with the most condense packing. According to our model, the structure of SO is two-dimensional; hence, stars of the main sequence are on the line T_{f_2} (bold line). Here, on the diagram *T-M*, one can also see isolines of the parameter ε, which, following (27–30), (41) and combining the constants, will look as

$$T_f = 6.86 \times 10^{-77}\, \frac{\varepsilon^2}{M^{2/3}}\,. \tag{58}$$

It should be noted that specific sequences of the globular-cluster stars formed from a medium with the same evolutionary parameter are also located along their own ε isolines.

When stars leave the main sequence and evolve towards lesser ε and T (to the right on the diagram), SO parameters change; particularly increasing is the envelope radius. Let us assume that beyond the line of equilibrium, $R_f = R_m$ (actually, the visible sizes of a star depend on many specific factors but we shall abstract from them in our model).

When calculating temperatures of the star envelopes (41), we implied that a part of the core radiation energy is transformed into other forms or spent in the star inner processes. But for the envelopes of giant stars, which are located to the right of the equilibrium line on the *T-M* diagram, formula (41) gives underrated results. The average density of giant stars is extremely low, and the energy of hot core radiation will insignificantly be absorbed by the rarefied atmosphere of these stars. In this case, to determine temperature of the photosphere, one can use the well-known formula for thermal radiation power, considering core as a radiation source:

$$N = \sigma T^4 S\,, \tag{59}$$

where σ is the Stefan-Boltzmann constant equal to $5.67{\times}10^{-8}$ W m^{-2}(°K)$^{-4}$. Having in mind the evident dependence of temperature on the linear size, the temperature of the photosphere can be expressed via the temperature of the core:

$$T_f = T_0 \left(\frac{R_0}{R_f}\right)^{1/2}. \tag{60}$$

Taking into account (27–30), (40) and accepting $R_f = R_m$, one can obtain, by analogy to (58),

$$T_f = 1.4 \times 10^{-55}\, \frac{\varepsilon^{3/2}}{M^{1/2}}\,. \tag{61}$$

This formula should be used when the star evolves beyond the equilibrium line and the radius of its envelope greatly increases. It is evident that the formula gives a bit overrated values of T_f. In Fig. 2, isolines plotted according to (61) are indicated as ε_{st}.

Taking into account (51) and substituting the ε_{st} expression in (61), one can obtain the line $T(M)$, along which stars turning into red giants are lined up:

$$T_{fg} = 0.192\, T_k\, M_0^{17/16}\,. \tag{62}$$

The parameters of stars with the masses M_1 and M_2 calculated for different ε values are shown in Table 2.

As for the "superstar" object, with the calculated mass $M_3 = 277$ s.m., its existence has been verified. The recently discovered star R136a1 has the following parameters: $M_0 = 265$ s.m., $R_f = 63R_\odot$ and $T_f \geqslant 40000$°K [7]. The calculated parameters of such a star — assuming it to be on the extension of the main sequence — are as follows: T_{f_2}, according to (56), is equal to 72500°K; ε from (61) is equal to 4.8×10^{38}; $R_f = R_m$ and, according to (30), is equal to $57R_\odot$. In other words, the object should be somewhere to the right of the main sequence line.

Located in the bottom part of the diagram are red dwarfs. Their typical parameters are the following: mass, $0.1, \ldots, 0.8$ s.m.; radius, $0.1 \ldots 0.85R_\odot$; temperature, below 3800°K [8, 9]. Since their radii are approximately proportional to their masses, they are on the line T_{f_1}, but their temperatures are lower, so it looks like they are on the extension of the main sequence. It is supposed that they evolve towards more condensed states, i.e., towards higher ε and T.

Lying on the lower segment of the T_{f_3} line are brown dwarfs. Their typical parameters are: mass, $0.012 \ldots 0.08$ s.m.; temperature, $3000 \ldots 300$ °K. Their radii change insignificantly over the range of masses and are approximately equal to that of Jupiter [10, 11].

At the very bottom of the diagram is the mass $M_4 = 1.95 \times 10^{-9}$ — the giant planet Jupiter. The temperature of its outer layer on the line T_{f_3} is equal, according to (57), to 123°K, i.e., it is close to the temperature of the outer atmosphere layers. The densities of Jupiter, brown dwarfs and the Sun are approximately equal; all these objects are near the line T_{f_3}.

Thus, all the types of SO are arranged logically on the *T-M* diagram.

Parameters	M_1 = 13.8 s.m		M_2 = 79.4 s.m		
	ε_1	ε_{st_1}	ε_2	ε_{st_2}	ε_{st_1}
ε	2.76×10^{38}	2.47×10^{37}	1.37×10^{39}	1.53×10^{38}	2.47×10^{37}
v_0	0.00219	0.000197	0.0061	0.00068	0.00011
R_0	0.0302	0.0302	0.0542	0.0542	0.0542
R_m	13.8	153.4	8.9	80	495
R_f	3.7	153.4	8.9	80	495
τ_0, sec	34.5	388	22.3	200	1242
τ_m, days	83	1.15×10^5	7	5037	1.2×10^6
τ_{mz}, days	6	752	0.78	63	2409
T_0, °K	2.6×10^6	2.34×10^5	7.2×10^6	8.07×10^5	1.3×10^5
T_m, °K	5710	3290	44000	21000	1370
T_f, °K	21200	3290	44000	21000	1370

Table 2: Note — radii and velocities are expressed as fractions of $R_\odot$ and c.

5.4 Variability of stellar objects

The types of variability of SO radiation are very diverse, and variability is intrinsic, to some degree, to all SO including the Sun. The most common type of variability is optical alternating variability (pulsations). According to our model, such pulsations are a natural result of the existence of oscillatory processes in the complex SO structure.

The most stable, in terms of amplitude and period of brilliancy oscillations, are pulsating stars of high luminosity — *Cepheids*, yellow giant stars [12, 13]. On the diagram *T-M*, their position would correspond to the mass M_1 on the equilibrium line T_m, where $R_f = R_m$.

Leaving the main sequence, stars become variable upon crossing the isoline ε_1 (*instability strip*), corresponding to the equilibrium parameter ε for the characteristic mass M_1. As follows from the diagram $T-\varepsilon$, the parameter ε decreases for masses larger than M_1 and increases for masses smaller than M_1 — until it reaches the isoline ε_1.

The masses of Cepheids are in the range 4 . . . 20 s.m. The minimal Cepheids mass is defined by the intersection of the isoline ε_1 and the line T_{f_2}, giving $M = 4.1$ s.m. which agrees with the value indicated in [14]. One should bear in mind that this intersection *point* on the diagram *T-M* corresponds to a *segment* on the diagram *ε-M* — from the line of equilibrium to ε_1. This segment corresponds to the initial period when the star begins to descend the main sequence. During this process, $R_f \to R_m$, which results in the star luminosity to grow. The growth is not reflected on the *T-M* diagram; on the diagram $H-R$, it corresponds to the initial segment of the star's evolutionary track.

Going on, stars evolve in the direction of lower ε values and reach the isoline ε_{st_1} (*asymptotic branch of giants, ABG*). The isoline corresponds to the equilibrium parameter ε_{st} for the standard solar mass (Fig. 1), under which the sizes of the star envelopes and the periods of their outer cycles reach their maxima. Located on ABG are *long-period variable stars* (with the period of brilliancy oscillations up to 1000 days), *semi-regular variable stars* (with the period of brilliancy oscillations up to 2000 days) and so on. Within the framework of our model, their variability can be explained not only by the existence of the outer layer period, τ_m, but also by a heterogeneity of their outer layer radiance [15, 16]. The heterogeneity results from the passage — along the star disk perimeter with the intervals of τ_{mz} — of hot (cold) zones, containing m_g-contours.

The calculated parameters R_m, T_m and τ_{mz} for M_1 (Table 2) are in a reasonable agreement with the averaged observation data for Cepheids at ε_1 and for long-period variables at ε_{st_1} [12, 17].

The parameters of SO of the mass M_2 on the line of equilibrium at ε_2 approximately correspond to those of hot supergiants PV Tel-type, with the period of pulsations from 0.1 to 1 day. On the line T_{fg} at ε_{st_2}, they correspond to the parameters of α Cyg-type super-giants, with the periods from several days to several weeks [12]. Further evolution of such stars in the direction of smaller ε values results in the formation of red super-giants.

6 Compact stellar objects

This group of SO includes white dwarfs, having the maximally compact packing of atoms, with the density ρ_0, and stellar bodies based on neutron stars, whose matter is compressed to the nuclear density ρ_j. Such objects are formed in the extreme cases, when SO evolve in the direction of either the largest ε values (when $R_f \to R_\odot$; "outer-layer state") or the smallest ones (when the envelope is shed; "core state"). In both cases, the initial oscillatory process is replaced with the rotation of the final compact object, of the mass M_p, with

the rate v_p.

At the final stage of evolution, there is, as indicated in [18], the possibility of a physical "coupling" of the star envelope with the core. Let us assume that there exists a ***process analogous to the absorption of an electron by the proton; i.e., the final compact object acquires the momentum of the outer layer, with the transition to an "excited" state***. We cannot consider the mechanism of this phenomenon within the framework of our model (moreover, the envelope and the core are considered here as different states of the same single object), so let us restrict ourselves to a formal application of the momentum conservation law:

$$M_0 v_m = M_p v_p. \tag{63}$$

6.1 White dwarfs

A white dwarf resulting from the star evolution towards lesser ε values, should inherit the parameters of the star core by the moment of the envelope shedding. For a star of the mass M_1 the parameters will be as follows: core temperature, 234000°K; period of rotation, 388 sec (Table 2). According to (47), (27) and (46), the mass, radius and mean density of white dwarfs are 0.27 s.m., 0.0082 $R_\odot$ and 2.38×10^9 kg/m^3 respectively. Indeed, very young white dwarfs can be observed in the X-ray range; the periods of their pulsations are in the range of tens to thousands of seconds, and they have typical sizes and densities being in agreement with the calculated parameters [12, 19, 20].

A white dwarf resulting from the evolution of a low-mass star towards larger ε values (without shedding of the envelope) should have the mass $M_p \approx M_0$. Then, its $v_p \approx v_m$.

Having in mind (29), (31) and (36), let us represent v_m as

$$v_m = cM_0^{2k-2/3} \tag{64}$$

and the period of rotation as

$$\tau_m = \frac{R_0}{v_m} = 2.51 M_0^{1-2k}. \tag{65}$$

At $z = 1$ and $k = 2/3$, an object of the mass 0.27 s.m. will have the following parameters: $v_m/c = 6.7\times10^{-5}$; $\tau_m = 308$ sec; and the energy of radiation, according to (42), equal to 0.034 keV ($T = 79000$°K). Here, the calculated parameters are, too, typical for a young white dwarf. As the object on the *T-M* diagram shifts to the right, the parameter k grows, which corresponds to the decline of the rotary velocity and temperature of the white dwarf.

On the diagram "*spectrum-luminosity*", the zone of white dwarfs seems much narrower than that on the diagram *T-M*, since their luminosity is determined by the radius, which, according to (27), is proportional to cubic root of the object mass.

6.2 Neutronization

In the context of our model, the process of neutronization can be represented as a loss of stability of the structure of m_g-contours and the transition of the structure (through its inversion along the vertical axis) from the plain two-dimensional into a one-dimensional configuration, which is energetically more favorable. Let us assume that the result will be a single m_g-contour or just a single vortical tube (neutron object).

Roughly, the parameters of such a primitive object can be defined as in Chapter 3. Placing the parameter R along the vertical axis and considering $z = 1$, one can obtain:

$$v_n = \frac{fM_n c}{\varepsilon}, \tag{66}$$

$$d_n = \frac{\varepsilon^2 R_\odot}{f^2 M_n}, \tag{67}$$

$$R_n = \frac{fM_n R_\odot}{\varepsilon}, \tag{68}$$

$$\tau_n = 2.51\frac{(\varepsilon/f)^3}{M_n^2}. \tag{69}$$

Rotary velocity cannot exceed the speed of light. Therefore, at $v_n \leqslant c$, $\varepsilon \geqslant fM_n$. Thus, for compact objects, the parameter k in (36) should be $\leqslant 1$ (in any event, as follows from the comparison of the calculated and actual data, k cannot be much larger than 1). Let us limit ourselves to defining parameters at $v_n = c$. Expressing ε from (66), one can obtain:

$$d_n = M_n R_\odot, \tag{70}$$

$$R_n = R_\odot, \tag{71}$$

$$\tau_n = 2.51 M_n. \tag{72}$$

It should be noted that a high-frequency modulation with τ_n up to 10^{-6} sec is present on the radiation diagrams of some neutron stars — pulsars [6].

As the evolutionary parameter grows, the sizes of a neutron object shrink along the axes, and on the line of degeneration, at $z = 1$, one can rewrite expressions (67–69), having in mind (35), in the following form:

$$d_n = R_n = M_n^{1/3} R_\odot, \tag{73}$$

$$\tau_n = \frac{R_\odot}{c} = 2.51 \text{ sec}. \tag{74}$$

Of course, this scheme is ideal. In reality, the objects based on neutron stars are in some intermediate state, and in the general case,

$$d_n = M_n^j R_\odot, \tag{75}$$

where $j = 1/3, \ldots, 1$ is a coefficient taking account of the object packing (shape).

It seems that the neutron state should be realized, to some extent, in the core of any star — and this can be proved. Let

represent the mass of a single vortex tube as that of a cylinder of the length R_n and radius d_n. Taking into account (70) and (71),

$$M_n\, M_m = \rho_n\, (M_n R_\odot)^2\, R_\odot, \tag{76}$$

where ρ_n is the vortex tube averaged density. Let us assume that ρ_n cannot exceed the nuclear density ρ_j, which shall be considered equal to $m_p/r_e^3 = 7.47 \times 10^{16}$ kg/m^3, where m_p is the mass of a proton. Then, as follows from (76),

$$M_{min} \geqslant \frac{M_m}{\rho_j R_\odot^3}\,, \tag{77}$$

which, upon substitution of values, gives $3.19{\times}10^{-8} M_m$. This mass corresponds to 0.016 solar masses or 17 Jupiter masses — exactly what the smallest cosmological mass, which is still considered a star, should be.

6.3 Masses of "black holes"

The diagrams ε-M and T-M show the boundary of a critical mode, where the rotary velocity of a vortex tube reaches that of light. On the diagram ε-M, the ray indicating the critical situation looks — taking into account that M_n is the mass of the compact object to be raised — as

$$\varepsilon = f M_n = f M^{11/8}\,. \tag{78}$$

On the diagram T-M, the same ray has — upon substitution of ε in (61) — the following form:

$$T_{f\,lim} = T_k\, M^{25/16}. \tag{79}$$

As follows from this construction, a ray segment is limited by the ordinates of the masses M_2 and M_3 and intersection with the isolines ε_{st_1} and ε_{st_2} — there are almost perfect ternary points of intersection. It is these masses that give rise to neutron objects with the masses, according to (47), $3, \ldots, 16$ s.m., which are the sources of hard X-ray radiation and *candidates for the star mass "black holes"* [18].

Indeed, for giant stars of a mass $M_2{-}M_3$, the critical mode begins before the moment they reach the asymptotic branch of giants (super-giants). With further decrease of the parameter ε, a star should release the excess of angular momentum — probably, by means of dropping the excess mass, which can be interpreted as shedding of the envelope with the formation of *supernova*. Next, the star core of a mass $M_n < \varepsilon/f$ transforms to an object which presently is classified as the "black hole" candidate. If neutronization of SO occurs far beyond the critical boundary (at low ε values), the mass of the emerging object will be very small. The latter might be one of the causes of the supernova remnants to contain few compact objects.

6.4 Radio pulsars

In our model, the simplest radio pulsar is a vortex tube which, by definition, is in the region Y ("boson"). The vortex tube is a macro-oscillator or radiator, with oscillations forming as longitudinal vibrations along the entire tube, while propagating to the X region as a cross wave from their source (the entrance of the vortex tube to the Y region; orifice) [2]. Presumably, radiation in the observable region X has a wavelength λ_p commensurable with the characteristic size of a single element of the vortex tube. A vortex tube, according to (22), consists of $n = \varepsilon$ single vortex threads — therefore, the characteristic linear size of a single element (region of radiation) will amount, under the condition of maximally compact packing of vortex threads in three dimensions, to

$$d_p = \varepsilon^{1/3} r_e\,. \tag{80}$$

The speed of vortex tube rotation can be expressed as a proportion of light speed — using the analogies described in Chapter 3:

$$\mathrm{v}_p = c\,\frac{\lambda_k}{d_p}\,. \tag{81}$$

Taking into account (36) and combining the constants, one can find the period of a pulsar:

$$\tau_p = \frac{d_p}{\mathrm{v}_p} = \frac{\varepsilon^{2/3} r_e^2}{c\lambda_k} = 282.5\, M_p^{2k/3}\ \mathrm{sec}\,. \tag{82}$$

Along the vortex tube of the pulsar, radiation is formed by m_i-zones, the number of which is determined by the pulsar mass. The averaged profile of the radiation pulse is a result of random superposition of many single pulses. Therefore the duration of the generalized pulsar pulse τ_{p_i} can be in the range from the duration of a single m_i-zone pulse to the total duration of pulses of all the zones, i.e. from r_i/v_{0i} to $z_i\, r_i/\mathrm{v}_{0i}$. Having in mind (18), (19) and (21),

$$\tau_{pi} = 2.51 M_p^{1/2\ldots1/4}\,. \tag{83}$$

For a pulsar, the standard mass is taken as 1.4 of that of the Sun. Then the pulsar period at $k = 2/3 \ldots 1$ will be, according to (82), in the range from 0.97 to 0.045 sec; and the duration of the generalized pulse will be, according to (83), in the range from 0.1 to 0.0042 sec, this corresponding to the temporal parameters of the majority of radio pulsars [21–23].

Radio radiation of pulsars covers a broad range and is extremely heterogeneous in time, intensity and frequency. Nevertheless, there are stable averaged spectra of energy distribution over frequency obtained by multiple instant measurements of radiation at different frequencies over large periods of time.

Let $\lambda_p = 2\pi d_p$, then the *frequency of radiation*, taking into account (80–82), will be as follows:

$$\nu_p = \frac{c}{2\pi d_p} = \frac{c}{2\pi\varepsilon^{1/3} r_e}\ \mathrm{Hz}, \tag{84}$$

which, having in mind (82), can be reduced to

$$\nu_p = 1.77\tau_p^{-1/2}\ \text{GHz}. \tag{85}$$

Since d_p is the minimal parameter provided that m_i-zone are packed most compactly, expression (84) will give *maximal* frequencies. However, the averaged spectrum extends far in the region of low frequencies and has an energy maximum. On the basis of our model, this fact can be accounted for by pulsation of the vortex tube in the limits of d_n, formula (75), and the existence of its optimal packing, less than 3, which the pulsar assumes most of the time. As indicated in [3], it may be the fractal dimension $e = 2.72$. In this case, the power of the parameter ε will be equal to $1/e$, and, as follows from (84), $\nu_p/\nu_m = \varepsilon^{0.0345}$. Having in mind (82), one can obtain, for the frequency of the maximum:

$$\nu_m = 0.0804\tau_p^{-0.55}\ \text{GHz}. \tag{86}$$

Formulas (85) and (86) are virtually identical to the interpolation formulas given in [23].

Although radiation of pulsars is not thermal, the *power of radiation* N_p can be determined on the basis of a formal use of the Boltzmann formula for thermal radiation of black body under the following conditions:

- taken as the area of the radiating surface is the cross-section of the vortex tube, $S = d_p^2$;
- taken as the effective temperature T_{ef} is the temperature corresponding to the radio frequency T_ν increased proportionally to the relative length of the vortex tube (i.e. proportionally to the ratio of the initial-object* radius to the diameter of the vortex tube, $T_{ef} = T_\nu R_0/d_p$).

Since, having in mind (39, 40), $T_\nu = T_k\lambda_k/d_p$, one can obtain, taking into account (36) and (80) and combining the constants,

$$T_{ef} = 1.06\times 10^7 M_p^{1/3-2k/3}. \tag{87}$$

Finally, after calculating the constants, we get an expression for N_p:

$$N_p = \sigma T_{ef}^4\, S = 1.45\times 10^{20} M_p^{4/3-2k}\ \text{W}. \tag{88}$$

Thus, our model predicts that at $k \to 2/3$, a radio pulsar should have a *lower* limit for radiation power (N_{min}), which the pulsar will be approaching as its rotation is getting slower. The limit N_{min} is equal to 1.45×10^{20} W and does not depend on the pulsar mass. At $k = 1$, expression (88) will give an upper limit N_p, which is dependent on the pulsar mass. The limits do exist [23], and no pulsars has been found at the luminosity below N_{min}.

On the basis of (82) and (88), a dependence $N(\tau_p)$ can be constructed (Fig. 3), which corresponds to the correlation given in [23]. To cover the zone of millisecond pulsars, the dependence is plotted in the range of masses $3\ldots 0.016$ s.m. — i.e. up to the minimal masses still able to neutronize (see Chapter 6.2). (The question on the range of radio pulsar masses is still open, since they can be determined only in rare cases).

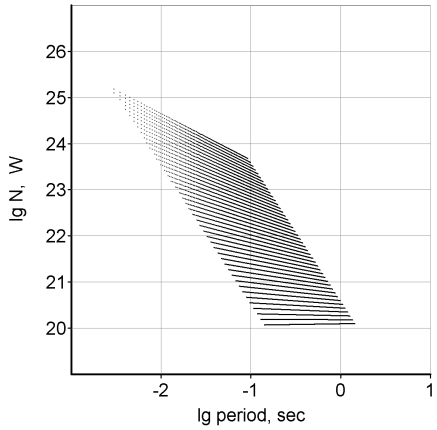

Fig. 3: Dependence of the radio pulsar radiation power on its period. $M_p = 3\ldots 0.016$ s.m., $k = 0.66\ldots 1$.

6.5 Excited states. Gamma-pulsar

Essentially, pulsar or vortex tube is a lengthy solenoid. In our model, the full length of a thread $z_i\, l_i$ does not depend, according to (18) and (20), from the mass and is equal to $R_\odot$; the length of a turn is, in general case, $\pi M_p^j R_\odot$, and the number of turns in the initial state is $\mathrm{N} = M^{-j}/\pi$.

Let us assume that the configuration of the vortex tube can change — e.g., upon the formation of a secondary spiral structure. In this case, the initial radius can diminish to the minimal radius of the vortex tube d_p, and the number of turns can grow to the number $\mathrm{N}_m = R_\odot/\pi d_p$. Then, taking into account (36) and (80),

$$\frac{\mathrm{N}_m}{\mathrm{N}} = 1.66\times 10^9 M_p^{j-k/3} = 10^5\ldots 10^9, \tag{89}$$

which will result in the correspondingly increased magnetic power and activity of the pulsar.

This state can be considered as an "excited" state of the radio pulsar. If the effective temperature grows proportionally as well, the energy corresponding to this increase will be transferred into the gamma range. Multiplying (87) by (89) and taking into account that for the vortex tube $j = 1$, one can obtain

$$T_{ef} = 1.76\times 10^{16} M_p^{4/3-k}. \tag{90}$$

Thus, at certain combinations of the parameters, formula (90) will give (upon conversion into electron-volts) values up to $10^{13}\ldots 10^{14}$ eV. This explains, for example, the observed gamma radiation of the famous pulsar in the Crab Nebula (more than 10^{12} eV). Ratio (89) serves estimation purposes, yet it can be used in other cases as well.

*The object of the initial mass (before neutronization).

6.6 X-ray pulsars

Massive stars give rise to neutron objects. Let us assume that such an object can be formed at any stage of star evolution, with the envelope momentum transferred to this newly formed object. Let us also assume that further evolution of this system as a whole can go both to the right (up to the state of outer layer) and left (up to the state of core) of the equilibrium line with the eventual formation of an *x*-ray pulsar of the mass M_p.

As a rule, X-ray pulsars do not radiate in the radio range. According to the model considered, we can assume this residual compact object to be already in the neutron state, while its vortex tube (or a part of the tube) excited at the expense of an additionally absorbed momentum to be still in the X region and to radiate in the X-ray range.

Let us determine the pulsar's parameters. Having in mind (63) and (64) and substituting, according to (47), $M_p^{8/11}$ for M_0, one can obtain for the pulsar:

$$\mathrm{v}_p = cM_p^{1.454k-0.7575}, \tag{91}$$

$$E_p = 511M_p^{1.454k-0.7575}\ \mathrm{keV}. \tag{92}$$

The pulsar period d_n/v_p, in the case of arbitrary pulsar form, will be equal to

$$\tau_p = \frac{M_p^j R_\odot}{\mathrm{v}_p} = 2.51\, M_p^{0.7575-1.454k+j}. \tag{93}$$

It should be noted that at $k = 0.75$ and $j = 1/3$, the M_p factor in (93) will be zero and $\tau_p = 2.51$ sec — the same period for any mass.

Let us consider the pulsar radiation to be mainly thermal. Then, one can calculate its power according to the Boltzmann formula, taking as the *radiating surface* that of the vortex tube of the length R_0 (i.e. $S = \pi d_p R_0$). In this case — analogously to (88), taking into account (27), having in mind $T_p = (T_k E_p)/511$ and after transformations — one can obtain, for an X-ray pulsar:

$$N_p = 1.22 \times 10^{38} M_p^{6.15k-2.7}\ \mathrm{W}. \tag{94}$$

The parameters of most of the known X-ray pulsars fit into the intervals calculated according to (92–94) for the standard mass 1.4 s.m. at $k = 2/3 \ldots 1$ and $j = 1/3 \ldots 1$: $\tau_p = 0.002 \ldots 260$ sec, $E_p = 0.07 \ldots 35$ keV, $N_p = 10^{20} \ldots 10^{30}$ W. Periods of more than 1000 sec are characteristic for small masses or for the cases when momentum is not fully transferred from the outer layer to the emerging compact object. Thus, there exist restrictions on the magnitudes of periods, energy and radiation power; and it is them that explain, to a certain degree, the partially non-thermal form of the pulsars energy spectrum (a cut-off in its high-energy region) [18, 24].

Radiating in the X-ray region are also some radio pulsars. Let us demonstrate the adequacy of our model on these objects — on the example of correlation between *x*-ray luminosity and the parameter $(d\tau/dt)/\tau^{3.5}$, given in [23]. The period derivative $d\tau/dt$, the rate of deceleration of pulsar rotation, is determined from observations. In our model, rotation slowdown is determined by the general process of evolution of the object's medium, i.e., by the parameter k. So let us use a derivative of the period in respect to k, considering the parameter j constant and replace the aforementioned expression by corresponding equivalent. In the end, differentiating (93) and combining the constants, one can obtain

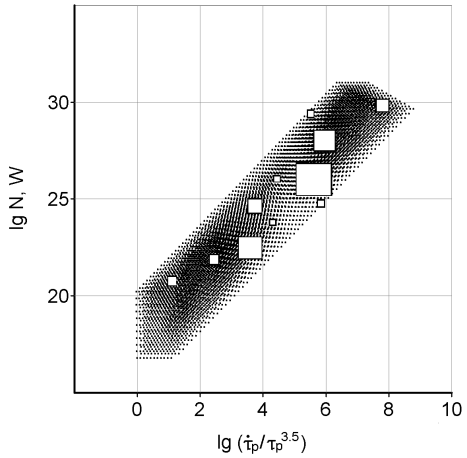

Fig. 4: Dependence of the radio pulsar *x*-ray luminosity on the parameter $(d\tau_p/dk)/\tau_p^{3.5}$. $M_p = 3 \ldots 0.3$ s.m., $k = 0.66 \ldots 1$, $j = 0.68 \ldots 0.73$. Observation data are taken from [23].

$$\frac{d\tau_p/dk}{\tau_p^{3.5}} = -3.35 \lg M_p\, \tau_p^{-2.5}. \tag{95}$$

Fig. 4 shows the dependence of X-ray luminosity of a radio pulsar on the parameter $(d\tau_p/dk)/\tau_p^{3.5}$ in the range of masses $3 \ldots 0.3$ s.m. The dependence fits the observation data at the values of the parameter $j = 0.68 \ldots 0.73$. In Fig. 4, the size of squares is approximately proportional to the number of observation points (41 points in total according to [23]). In our case, the derivative does not require a scale coefficient to satisfy the initial conditions.

It is known that during *outbursts*, the power of radiation (luminosity) reaches a magnitude of the order of 10^{32} W and higher [25]. According to our model, such an increase in luminosity can be explained by periodical excitation of the vortex tube (see Section 6.5). In this case, multiplying (94) by (89), one can obtain

$$N_{pm} = 2.03 \times 10^{47} M_p^{5.82k+j-2.7}. \tag{96}$$

Formula (96) gives rational results. For the mass $M = 1.4$ s.m., N_p will reach, depending on the parameters, magnitudes of $10^{38} \ldots 10^{39}$ W, which agrees with the power of the giant gamma-ray outburst from the source SGR 1900-14, which was registered in August 1998 (about 10^{38} W) [27].

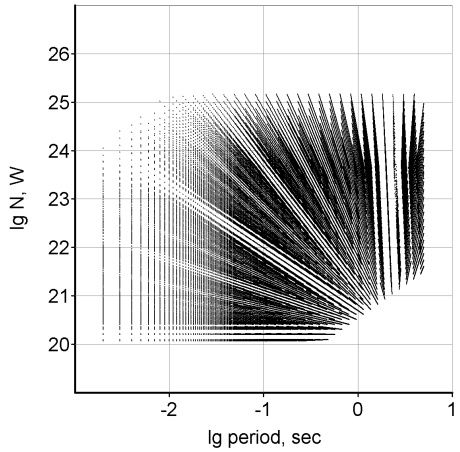

Fig. 5: The solution region: dependence of the radio pulsar radiation power on its period. $M_p = 3 \ldots 0.016$ s.m., $k = 0.66 \ldots 1$, $j = 0.33 \ldots 1$.

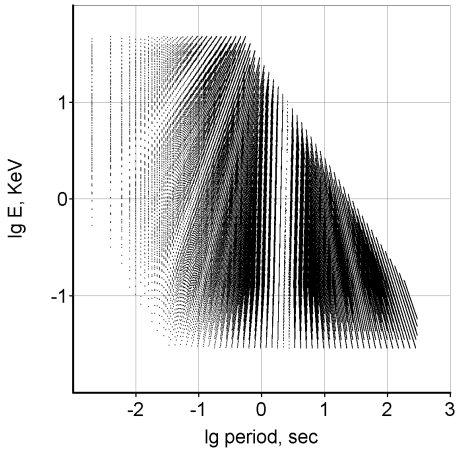

Fig. 6: The solution region: dependence of the X-ray pulsar radiation energy on its period. $M_p = 3 \ldots 0.3$ s.m., $k = 0.66 \ldots 1$, $j = 0.33 \ldots 1$.

It would be interesting to get independent estimates of the mass of compact objects, which, as one can see, have a similar origin. Let us assume that in the process of their possible inter-transformations, their masses and periods change insignificantly. Let the X-ray and radio pulsar periods are equal in the marginal cases — when the initial SO, giving rise to a compact object, evolves towards the largest or smallest ε values.

Let us consider the case when evolution goes towards larger ε. With ε increasing, the mass M_p should grow and at $z \to 1$ become equal to the original mass M_0 (Fig. 1). Perhaps, such a process should be associated with *accretion in binary star systems*. Proceeding to the mass M_0, let us substitute $M_0^{11/8}$ for M_p in (91). Then $d_n = M_0^j R_\odot$ and (93) will take a form of

$$\tau_p = 2.51 M_0^{1.042-2k+j}. \tag{97}$$

Equating (82) to (97) for the periods, combining the constants and making transformations, one can obtain in the end:

$$\lg M_0 = \frac{2.052}{1.042 - 2.667k + j}. \tag{98}$$

In the limit, $k = 2/3$ and $j = 1/3$ (sphere), then $M_0 = 8{\times}10^{-6}$ or 4 s.m. This mass can be considered as the total one of a *low-mass binary star system* containing an X-ray pulsar, this being in agreement with the accepted estimate (2.5 s.m. + 1.4 s.m.) [18]. Such a pulsar will have a relatively hard X-ray radiation [25], and, with the growth of the parameters j, its period will decrease.

The obtained mass value is, in fact, coincides with the minimal mass of a Cepheids (see Section 5.4). Thus, an SO with the mass 4 s.m. can evolve both to the right of the equilibrium line (shedding the envelope) and to the left (forming a binary star system). In both cases, a compact object will be formed at the end of evolution, and one can suppose that the stellar mass of 4 s.m. is the *minimal mass* able to give rise to neutron stars.

Let an X-ray pulsar evolve towards lesser ε values. Equating expressions (82) and (93), one can obtain

$$\lg M_p = \frac{2.052}{0.7575 - 2.121k + j}. \tag{99}$$

In the limit, $k = 1$ and $j = 1$ (vortex tube), then $M_p = 2.3 \times 10^{-6}$ or 1.15 s.m. Here, we have got a typical pulsar mass. Such a pulsar will have a relatively soft X-ray radiation, and with the parameter j growing, the pulsar period will increase. Such objects can correspond to *single neutron stars* [26]. Indeed, as follows from the observation data, pulsars of binary systems will mainly speed up their rotation, whereas single objects will slow down.

The properties of SO are determined by the totality of their parameters; that is why two-parameter diagrams always have a wide scatter of experimental points. Let us represent the solution region of the dependence $N(\tau_p)$ for radio pulsars more extensively — expressing its period according to (93), which contains the parameter j, and considering some radio pulsars evolved from the X-ray ones, with their periods being approximately the same (Fig. 5). The region of observation values [23] fits well the solution region.

Analogously, using formulas (92) and (93), one can plot a solution region of the dependence $E(\tau_p)$ for the X-ray pulsars (Fig. 6). Clusters on the images may indicate regions where pulsars have preferable parameters — e.g., the right bottom part in Fig. 6 may indicate, by the combination of parameters, a region of single neutron stars.

There appears a question: can slow X-ray pulsars transform into radio pulsars, whose period will not exceed several seconds? One can suppose that comparatively to radio pulsars, X-ray ones have an excessive angular momentum (since their radius in the region X is much larger than that of ra-

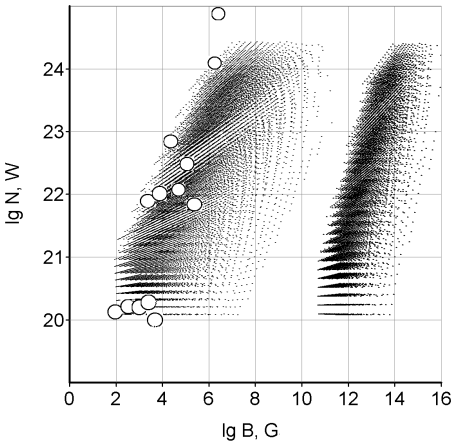

Fig. 7: The solution region: dependence of the radio pulsar radiation power on its magnetic field — $N(B)$ to the left; $N(B_m)$ to the right. $M_p = 2 \dots 0.2$ s.m., $\tau_p = 0.003 \dots 3$ sec, $k = 0.66 \dots 1$, $j = 0.33 \dots 1$. Observation data are taken from [23].

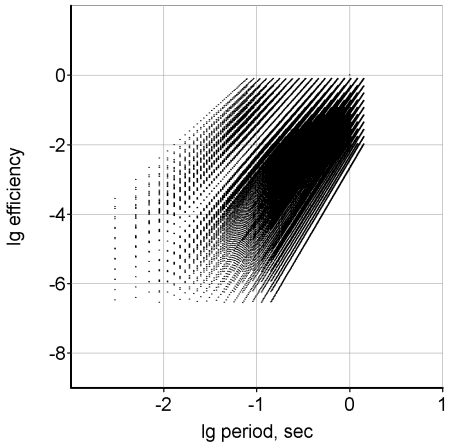

Fig. 8: The solution region: dependence of the efficiency of transformation of rotation energy in-to radio radiation on the pulsar period (initial state). $M_p = 3 \dots 0.016$ s.m., $k = 0.66 \dots 1$, $j = 0.33 \dots 0.55$.

dio pulsars in the region Y, and as they "submerge" into the region Y, their period shortens).

Thus, ***it can be supposed that gamma, X-ray and radio pulsars are different forms of excited vortex tube or, using another analogy with the microcosm, three species of neutrino. The primary state — radio pulsar — possesses only the initial angular momentum of the vortex tube or spin***.

6.7 Magnetic properties of pulsars

Our model explains the correlation between the magnitude of the magnetic field B and other pulsar parameters. According to SI definition, for a lengthy solenoid, $B = \mu\mu_0\, nI$, where n is the number of turns per unit of length, I is the current strength and μ is the relative magnetic permeability.

The initial solenoid length is equal to R_0. Let $n = \mathrm{N}/R_0$. Let us define the coefficient μ as the compactness of the solenoid coil in the initial state $\mathrm{N}d_p/R_0$. The current strength I in the "Coulombless" form is $z_e m_e\, c(R_\odot/r_e) \times 1/[\mathrm{sec}]$ (see Section 2), where z_e is the number of single charges per coulomb, equal to $1/e_0$.

In our model, SI units for B are m^{-1}. To switch from SI to the Gaussian system of units, introduction of an additional factor of 10^{-4} is needed. Opening the expressions for μ_0, ε_0 and $R_\odot$, taking into account that $\mathrm{N} = M^{-j}/\pi$, as well as (27), (36) and (80), and making transformations, one can finally obtain

$$B = 1.27 \times 10^{-4} M_p^{k/3-2j-2/3}\ \mathrm{G}. \qquad (100)$$

Many radio pulsars have larger B values. For the excited state, multiplying (100) by (89), we will have

$$B_m = 2.1 \times 10^{5} M_p^{-j-2/3}\ \mathrm{G}. \qquad (101)$$

Fig. 7 shows the solution regions for the dependences $N(B)$ (to the left) and $N(B_m)$ (to the right) calculated according to formulas (88), (100) and (101) in the range of masses $2 \dots 0.2$ s.m. and periods $0.003 \dots 3$ sec. The figure also represents the observation data for the pulsars with small B values taken from [23]. Masses and periods are connected using formula (93), which contains the parameter j. It is known that according to the strength of their magnetic field, pulsars are clustered near values of the order of 10^9 and 10^{13} G [18], which agrees, in general, with the distributions obtained.

To analyze pulsar parameters, the function $\eta(\tau_p)$ is also used, which includes the magnetic force B [23]:

$$\eta = \frac{3N_p\, c^3 \tau_p^4}{8\pi^4 B^2 R_*^6}, \qquad (102)$$

where η is the pulsar efficiency, i.e., the effectiveness of transformation of the pulsar rotation energy into radio radiation.

According to [23], formula (102) takes $R_* = 10^6$ cm. For more objectiveness, let us replace this constant with the diameter of the vortex tube according to (75). Having in mind (82), (88) and (100), let us transform (102) to the form (in the Gaussian system):

$$\lg \eta = 8.5 + (2.667 - 2j) \lg M_p\,. \qquad (103)$$

Together with formula (82), this gives the region of $\eta(\tau)$ solutions for radio pulsars (Fig. 8). Since $\eta < 1$, there are limitations for some combinations of the parameters. In the accepted, according to [23], range of η values, the parameter j is limited by the range $0.33 \dots 0.55$, which is characteristic for pulsars with small B values. The orientation of clusters on the diagram indicates the increase of η with the growth of the period.

Analogously, substituting the parameter B_m into (102), one can obtain

$$\lg \eta = -11.9 + (0.667k - 4j + 2.667) \lg M_p. \qquad (104)$$

In this case (Fig. 9), in the accepted range of η values, the parameter j is limited by a narrow range of large values,

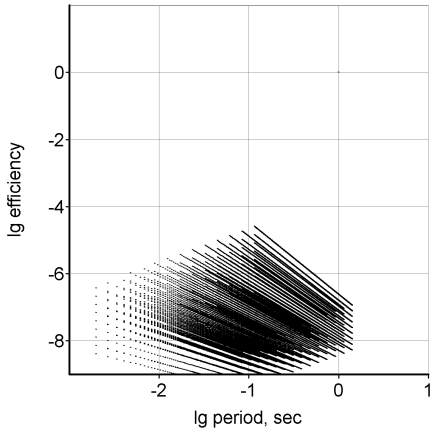

Fig. 9: The solution region: dependence of the efficiency of transformation of rotation energy in-to radio radiation on the pulsar period (excited state). $M_p = 3 \ldots 0.016$ s.m., $k = 0.66 \ldots 1$, $j = 0.94 \ldots 1$.

$0.94 \ldots 1$, which corresponds to pulsars with a strong magnetic field. In this range of parameters, η will grow as the period decreases. These solution ranges complement each other and agree with the body of the observation data of the diagram $\eta(\tau)$ given in [23]. Thus, there are at least two pulsar populations, with different magnitudes of their magnetic field and different form factors (parameter j), which was also indicated in [23].

From (101), one can find that the magnitude of the pulsar magnetic field can reach $10^{14} \ldots 10^{15}$ G. Such a growth of the magnetic field also explains the phenomenon of *magnetars* [27, 28].

As follows from our model — and it is getting evidence now — there are no essential differences between magnetars and X-ray pulsars. For example, the sources SWIFT J1822.31606 [29] and PSR J18460258 [30] possess features of both objects.

7 Conclusion

Thus, our model, which is built exclusively on the balances of basic interactions, describes different kinds of stellar objects. It is shown that SO features are mainly determined by their masses and the state of the evolving medium that they are made of. Together with the basic constants, these parameters (M and ε) determine the evolutionary behavior of stellar objects and the very existence of the well-known Hertzsprung-Russell diagram. In a number of cases, they are sufficient for the calculation of basic SO parameters: the mass of the final compact objects, radiation energy, radiation power and periods or rotation.

The model reveals analogies between the macro- and microlevels of matter: cosmological masses and elementary particles.

Indeed, the ***general range of stellar masses can be roughly divided into three subranges — by the analogy with the three families of elementary particles***:

- stars with masses less than 4 s.m., which in the end of evolution will become white dwarfs;
- giant stars with masses $4 \ldots 79$ s.m., which in the end of evolution will give raise to neutron stars;
- super-giant stars with masses $79 \ldots 277$ s.m., which in the end of evolution will give raise to X-ray sources — candidates for black holes.

It is the ***stars of small masses and their final states (cold white dwarfs, "protons") that are the "first family" of stellar population***. They make the majority of it and are stable on the cosmological scale, since their lifetimes are immeasurably longer than the lifetimes of other stellar objects.

Hopefully, the results obtained and the presented model can be useful for further theoretical studies in the field.

Submitted on: June 26, 2012 / Accepted on: October 10, 2012

References

1. Belyakov A.V. Charge of the electron, and the constants of radiation according to J. A. Wheeler's geometrodynamic model. *Progress in Physics*, 2010, v.4, 90–94.
2. Belyakov A.V. Macro-analogies and gravitation in the micro-world: further elaboration of Wheeler's model of geometrodynamics. *Progress in Physics*, 2012, v.2, 47–57.
3. Belyakov A.V. On the independent determination of the ultimate density of physical vacuum. *Progress in Physics*, 2011, v.2, 27–29.
4. Novikov I.D., Kardashev N.S., Shatskiy A.A. Multicomponent Universe and astrophysic of the "wormhole". *Uspekhi-Physics*, 2007, v.177(9), 1017–1023.
5. Beck P.G., Montalban J. et al. Fast core rotation in red-giant stars as revealed by gravity-dominated mixed modes. *Nature*, January 2012, v.481, 55–57.
6. Narlikar J. Violent Phenomena in the Universe. Oxford University Press, Oxford, 1984.
7. Crowther P.A. The R136 star cluster hosts several stars whose individual masses greatly exceed the accepted 150 $M_\odot$ stellar mass limit. *Monthly Notices of the Royal Astronomical Society*, 2010, v.408(2), 731–751.
8. Burrows A., Hubbard W.B., Saumon D., Lunine, J.I. An expanded set of brown dwarf and very low mass star models. *The Astrophysical Journal*, 1993, v.406, no.1, 158–171.
9. Kaltenegger L., Wesley A. Transits of earth-like planets. *The Astrophysical Journal*, 10 June 2009, v.698, 519–527.
10. Spiegel D.S., Burrows A., Milsom J.A. The Deuterium-burning mass limit for brown dwarfs and giant planets. ariv: astro-ph/1008.5150.
11. Michael C.L. et al. CFBDSIR J1458+1013B: a very cold (>T10) brown dwarf in a binary system. ariv: astro-ph/1103.0014.
12. Kholopov P.N., Samus N.N., Goranskiy V.P. et al. Main catalog of the variable stars. v. I-III. Nauka, Moscow, 1985–1987 (in Russian).
13. Berdnikov L.N., Samus N.N. Studies of classical cepheids. *Astronomical & Astrophysical Transactions*, 1999, v.18(2), 373–384.
14. Berdnikov L.N., Dambis A.K. Cepheids and RR Lyr variables. Present star astronomy. Sternberg Astron. Inst., Moscow, 16 June 2011 (in Russian).
15. Mennessier M.O., Mowlavi N., Alvarez R., Luri X. Long period variable stars: galactic populations and infrared luminosity calibrations. *Astronomy & Astrophysics*, 2001, v.374, 968–979.

16. Hampton M., Gregory W.H. et al. HD 12545, a study in spottedness. *Publication of the Astronomical Society of the Pacific*, January 1996, v.108, 68–72.

17. Le Bertre T., Lebre A., Waelkens C. (Eds.). Asymptotic Giant Branch Stars. *Proc. 191st Symp. IAU*, 1999.

18. Svertilov S.I. Cosmic X-ray and gamma-ray radiation. Skobeltzin Inst. Nucl. Research, Moscow, April 2006 (in Russian).

19. Shapiro S.L., Teukolcky S.A. Black holes, white dwarfs and neutron stars. v.1–2. Nauka, Moscow, 1985.

20. Kepler S.O., Vauclair G., Nather R.E., Winget D.E., Robinson E.L. G117-B15A — how is it evolving? *White dwarfs; Proceedings of IAU Colloquium 114th*, August 1988, (A90-32719 13-90).

21. Manchester R., Talor D. Pulsars. Nauka, Moscow, 1980.

22. Matveenko L.I., Usov V.V. Physics of the Cosmos. Nauka, Moscow, 1986 (in Russian).

23. Malov I.F. Radio pulsars. Nauka, Moscow, 2004 (in Russian).

24. Tsygankov S.S., Lutovinov A.A. Studies of x-ray pulsars with space observatories. *Proceedings of the VIII-th Young Scientist Conference*, 2005, 226–228 (in Russian).

25. Aleksandrovich N.A., Borozdin K.N., Arefjev V.A., Sunyaev R.A., Skinner D.K. Observations of the X-ray transit pulsar-burster GRO J1744-28 with the telescope TTM of the orbital observatory "MIR-KVANT". *Soviet Astron. Journal Letters*, 1998, v.24, no.1.

26. Popov S.B., Prohorov M.E. Astrophysics of the isolated neutron stars: radio-quiet neutron stars and magnetars. Sternberg Astron. Inst., Moscow, 2002 (in Russian).

27. Kouveliotou C., Duncan R.C., Thompson C. Magnetars. *Scientific American Russian Edition*, 2003, no.6 (in Russian).

28. Tsygankov S.S., Lutovinov A.A. Universe magnetic heart. *Priroda*, 2011, no.1, 10–18 (in Russian).

29. Scholz P., Ng C.-Y., Livingstone M.A., Kaspi V.M., Cumming A., Archibald R. SWIFT J1822.31606: post-outburst evolution of a nearby magnetar. arXiv: astro-ph/1204.1034.

30. Gavriil F.P., Gonzalez M.E., Gotthelf E.V., Kaspi V.M., Livingstone M.A., Woods P.M. Magnetar-like emission from the young pulsar in Kes 75. *Science*, 28 March 2008, v.319, no.5871, 1802–1805.

Sampling the Hydrogen Atom

Norman Graves

192 Old Woosehill Lane, Wokingham, UK. E-mail: normangraves@btinternet.com

A model is proposed for the hydrogen atom in which the electron is an objectively real particle orbiting at very near to light speed. The model is based on the postulate that certain velocity terms associated with orbiting bodies can be considered as being affected by relativity. This leads to a model for the atom in which the stable electron orbits are associated with orbital velocities where Gamma is n/α, leading to the idea that it is Gamma that is quantized and not angular momentum as in the Bohr and other models. The model provides a mechanism which leads to quantization of energy levels within the atom and also provides a simple mechanical explanation for the Fine Structure Constant. The mechanism is closely associated with the Sampling theorem and the related phenomenon of aliasing developed in the mid-20th century by engineers at Bell labs.

Since the emergence of quantum theory just over a century ago every model that has been developed for the hydrogen atom incorporates the same basic assumption. From Niels Bohr through de Broglie and Schrödinger up to and including the Standard Model all such theories are based on an assumption first put forward by John Nicholson.

Nicholson recognised that the units of Planck's constant are the same as those of angular momentum and so he reasoned that perhaps Planck's constant was a measure of the angular momentum of the orbiting electron. But Nicholson went one step further and argued that Planck's constant was the fundamental unit or quantum of angular momentum and therefore the angular momentum of the orbiting electron could only take on values which were an integer multiple of Planck's constant. This allowed Bohr to develop a model in which the energy levels of the hydrogen atom matched those of the empirically developed Rydberg formula [1]. When the Bohr model was superseded Nicholson's assumption was simply carried forward unchallenged into these later models.

Nicholson's assumption however lacks any mathematical rigour. It simply takes one variable, angular momentum, and asserts that if we allow it to have this characteristic quantization then we get energy levels which appear to be correct. In so doing it fails to provide any sort of explanation as to just why such a quantization should take place.

In the mid-20th century a branch of mathematics emerged which straddles the boundary between continuous functions and discrete solutions. It was developed by engineers at Bell Labs to address problems of capacity in the telephone network. While at first site there appears to be little to connect problems of network capacity with electrons orbiting atomic nuclei it is the application of these mathematical ideas which holds the key to explaining quantization inside the atom.

In the 1930's and 40's telecommunications engineers were concerned to increase the capacity of the telephone network. One of the ideas that surfaced was called Time Division Multiplexing. In this each of a number of incoming telephone lines is sampled by means of a switch, the resulting samples are sent over a trunk line and are decoded by a similar switch at the receiving end before being sent on their way. This allowed the trunk line to carry more telephone traffic without the expense of increasing the number of cables or individual lines. The question facing the engineers at the time was to determine the minimum frequency at which the incoming lines needed to be sampled in order that the telephone signal can be correctly reconstructed at the receiving end.

The solution to this problem was arrived at independently by a number of investigators, but is now largely credited to two engineers. The so called Nyquist-Shannon sampling theorem is named after Harry Nyquist [2] and Claude Shannon [3] who were both working at Bell Labs at the time. The theorem states that in order to reproduce a signal with no loss of information, then the sampling frequency must be at least twice the highest frequency of interest in the signal itself. The theorem forms the basis of modern information theory and its range of applications extends well beyond transmission of analogue telephone calls, it underpins much of the digital revolution that has taken place in recent years.

What concerned Shannon and Nyquist was to sample a signal and then to be able to reproduce that signal at some remote location without any distortion, but a corollary to their work is to ask what happens if the frequency of interest extends beyond this Shannon limit? In this condition, sometimes called under sampling, there are frequency components in the sampled signal that extend beyond the Shannon limit and maybe even beyond the sampling frequency itself.

A simple example can be used to illustrate the phenomenon. Suppose there is a cannon on top of a hill, some distance away is an observer equipped with a stopwatch. The job of the observer is to calculate the distance from his current location to the cannon. Sound travels in air at roughly 340 m/s. So it is simply a matter of the observer looking for the flash as the cannon fires and timing the interval until he

hears the bang. Multiplying the result by 340 will give the distance to the cannon in metres, let's call this distance D.

This is fine if the cannon just fires a single shot, but suppose the cannon is rigged to fire at regular intervals, say T seconds apart. For the sake of argument and to simplify things, let's make T equal to 1. If the observer knows he is less than 340 m from the cannon there is no problem. He just makes the measurement as before and calculates the distance D. If on the other hand he is free to move anywhere with no restriction placed on his distance to the cannon then there is a problem. There is no way that the observer knows which bang is associated with which flash, so he might be located at any one of a number of different discrete distances from the cannon. Not just any old distance will do however. The observer must be at a distance of D or $D + 340$ or $D + 680$ and so on, in general $D + 340n$. The distance calculated as a result of measuring the time interval between bang and flash is ambiguous. In fact there are an infinite number of discrete distances which could be the result of any particular measured value. This phenomenon is known as aliasing. The term comes about because each actual distance is an alias for the measured distance.

Restricting the observer to be within 340 m of the cannon is simply a way of imposing Shannon's sampling limit and by removing this restriction we open up the possibility of ambiguity in determining the position of the observer due to aliasing.

Let's turn the problem around a little. If instead of measuring the distance to the cannon the position of the observer is fixed. Once again to make things simpler, let's choose a distance of 340m. This time however we are able to adjust the rate of fire of the cannon until the observer hears the bang and sees the flash as occurring simultaneously. If the rate of fire is one shot per second then the time taken for the slower bang to reach the observer exactly matches the interval between shots and so the two events, the bang and the flash are seen as being synchronous. Notice that the bang relates, not to the current flash, but to the previous flash.

If the rate of fire is increased then at first, for a small increment, the bang and the flash are no longer in sync. They come back into sync however when the rate of fire is exactly two shots per second, and again when the rate is three shots per second. If we had a fast enough machine gun this sequence would extend to infinity for a rate of fire which is an integer number of shots per second. Notice that now the bang no longer relates to the previous flash, but to a previous flash. It is interesting to note also that if the rate of fire is reduced from once per second then the observer will never hear and see the bang and the flash in sync with one another and so once per second represents the minimum rate of fire which will lead to a synchronous bang and flash. In fact what we have here is a system that has as its solutions a base frequency and an infinite set of harmonic frequencies.

Suppose now that there is some mechanism which feeds back from the observer to the cannon to drive the rate of fire such that bang and flash are in sync, and suppose that this feedback mechanism is such as to always force the condition to apply to the nearest rate of fire which produces synchronisation.

We now have a system which can cause a variable, in this case the rate of fire of the gun, to take on a series of discrete values even though, in theory at least, the rate of fire can vary continuously. Equally important is that if the feedback mechanism is capable of syncing the system to the lowest such frequency then all the multiples of this frequency are also solutions, in other words if the base frequency is a solution then so are harmonics of the base frequency.

This idea that there are multiple discrete solutions which are harmonics of a base frequency is an interesting one since it couples the domains of the continuous and the discrete. Furthermore what the example of the cannon shows us is that any system which produces results which are a harmonic sequence must involve some sort of sampling process. This becomes clear if we consider the Fourier representation of a harmonic sequence. A harmonic sequence of the type described consists of a number of discrete frequencies, spreading up the spectrum and spaced equally in the frequency domain with each discrete frequency represented by a so called Dirac function. Taken together they form what is described as a Dirac comb, in this case in the frequency domain. The inverse Fourier transform of such a Dirac comb is itself another Dirac comb, only this time in the time domain, and a Dirac comb in the time domain is a sampling signal [4].

This link between a Dirac comb in the frequency domain and a corresponding Dirac comb in the time domain means that if ever we observe a set of harmonics in some natural process there must inevitably be some form of sampling process taking place in the time domain and vice versa.

One such example, in which this relationship has seemingly been overlooked, is found in the structure of the hydrogen atom.

By the beginning of the 20th century it was becoming evident that the universe was composed of elements which were not smooth and continuous but were somehow lumpy or granular in nature. Matter was made up of atoms, atoms themselves contained electrons and later it emerged that the atomic nucleus was itself composed of protons and neutrons.

Perhaps even more surprising was that atoms could only absorb or emit energy at certain discrete levels. These energy levels are characteristic of the atom species and form the basis of modern spectroscopy. The issue facing the scientists of the day was that this discrete behaviour is not associated with the discrete nature of the structure of the atom; that can easily be explained by asserting that any atom contains an integer number of constituent particles. Where energy levels are concerned, the quantization effects involve some sort of process that is taking place inside the atom.

The atom with the simplest structure is that of hydrogen,

comprising a single proton surrounded by an orbiting electron and work began to investigate its structure and to understand the mechanisms which gave it its characteristic properties.

The first such theoretical model was proposed by Niels Bohr [5]. Bohr used simple classical mechanics to balance the centrifugal force of the orbiting electron against the electrostatic force pulling it towards the atomic nucleus. He needed a second equation in order to solve for the radius and velocity of the orbiting electron and came upon the idea proposed by John Nicholson [6]. Nicholson reasoned that the units of Planck's constant matched those of angular momentum and so he proposed that the angular momentum of the orbiting electron could only take on values which were an integer multiple of was Planck's constant.

Bohr's equations worked, but they threw up a strange anomaly. In Bohr's model each energy level is represented by the orbiting electron having a specific orbit with its own particular orbital velocity and orbital radius. The really strange thing was that in order to fit with the conservation laws, transitions from one energy state to another had to take place instantly and in such a way that the electron moved from one orbit to another without ever occupying anywhere in between, a sort of discontinuity of position. This ability to jump instantaneously across space was quickly dubbed the Quantum Leap in the popular media, a phrase which still has resonance today.

Bohr reasoned that

$$l = mv_n r_n = n\hbar \tag{1}$$

$$\frac{Kq^2}{\hbar c} = \frac{mv_n^2}{r_n} \tag{2}$$

which means

$$v_n = \frac{Kq^2}{n\hbar} \tag{3}$$

$$r_n = \frac{n^2\hbar^2}{mKq^2}\,. \tag{4}$$

where m is the rest mass of the electron, q is the charge on the electron, r_n is the orbital radius for the nth energy level, v_n is the orbital velocity for the nth energy level, l is the angular momentum, K is the Coulomb force constant, $\hbar$ is Planck's constant.

Equation 1 represents Nicholson's assumption that angular momentum can only take on values which are integer multiples of Planck's constant.

Equation 2 balances the centrifugal force against the electrostatic force.

Equation 3 shows that the orbital velocity decreases with increasing energy level.

Equation 4 shows that the orbital radius increases as the square of the energy level and leads directly to the idea of the Quantum Leap.

It was widely accepted that the Bohr model contained substantial flaws. Not only did it throw up the quirky quantum leap, but it took no account of special relativity, it failed to explain why the electron orbit did not decay due to synchrotron radiation but most important of all it failed to explain the nature of the quantization of angular momentum*. The fact is that the assumption that angular momentum is quantized lacks any mathematical rigour, the assumption is arbitrary and expedient and fails to address the underlying question as to why and how such quantization occurs but merely asserts that if we make the assumption then the numbers seem to fit. Nevertheless, and despite this, the Bohr assumption has continued to be accepted and forms an integral part of every theory which has come along since.

In a paper published in 1905 Einstein had shown that light, which had hitherto been considered a wave, was in fact a particle [7]. In an effort to explain quantization the French mathematician Louis de Broglie turned this idea on its head and suggested that perhaps the electron was not a particle but should be considered as a wave instead. He calculated the wavelength of the electron, dividing Planck's constant by the electron's linear momentum and found that when he did so the orbital path of base energy state contained one wavelength; that of the second energy state contained two wavelengths and so on, in what appeared at first site to be a series of harmonics†.

On any other scale the wavelength of an object in orbit is associated with the orbital path length or circumference of the orbit and can be derived as a result of dividing the angular momentum of the orbiting object by its linear momentum. De Broglie instead chooses to associate the wavelength of the particle with the value of Planck's constant divided by the linear momentum, while at the same time assuming that the angular momentum of the particle was an integer multiple of Planck's constant. In choosing to substitute Planck's constant in this way instead of the angular momentum when calculating the wavelength, what de Broglie is doing is to coerce the wavelength of the electron to be an integer fraction of the orbital path length. Viewed in this light de Broglie's contribution can be seen as less of an insight and more of a contrivance.

If you were to observe an object in orbit, say a moon orbiting Jupiter or the proverbial conker‡ whirling on the end of a string, what you see is a sine wave. The orbiting object

*At first site it appears that the energy of the electron in the Bohr atom decreases with increasing energy level. However since the radius changes with energy level, the potential energy does also. When these two effects are combined, the energy levels increase with increasing energy level.

†In fact they are not harmonics of a single fundamental frequency, but instead each harmonic relates to a different base frequency and these two effects combine in such a way that they form a sub harmonic or inverse harmonic sequence

‡A conker is a horse chestnut on a string often used in a children's game

subtends a wave to an external observer of the form:

$$d = R\sin(\omega t) \tag{5}$$

or

$$d = R\sin(2\pi F t)\,. \tag{6}$$

where d is the displacement about some mean

For such a body we can easily calculate the orbital radius if we know the angular momentum and the linear momentum.

$$R = \frac{l}{p} = \frac{mvr}{mv}\,. \tag{7}$$

Furthermore we can identify the wavelength of such a wave with the orbital circumference which is simply.

$$\lambda = 2\pi R\,. \tag{8}$$

This is true for all orbiting objects no matter whether they are the size of a planet or the size of a conker.

By what rational then does de Broglie identify the wavelength of the orbiting electron, not with the angular momentum in this way, but with Planck's constant, which he believes, according to Bohr's assumption, to be an integer fraction of the angular momentum?

The alignment of wavelength with Planck's constant in this way cannot be justified either mathematically or mechanically. It is a contrivance which leads to the idea that there is some sort of wavelength which is an integer fraction of the orbital circumference. This is no miraculous discovery, not an insight into the workings of the atom, but an artificial device which reinforces and sustains the Bohr assumption without any basis in mechanics.

Other later models, such as that of Schrödinger, are based directly on the work of de Broglie and therefore inherently follow Bohr's assumption, up to and including the currently proposed Standard Model. Having been adopted by Bohr, later theorists simply continued with this working assumption and incorporated it into all subsequent models for the atom, without ever bothering to go back and justify it, until now it has become an item of received wisdom and an article of faith.

The trouble with all of these models is that the assumption proposed by Nicholson and adopted by Bohr is not based on finding any mechanism that leads to angular momentum being quantized in this way. The assumption was simply expedient — it just happens to give the values for the absorption and emission spectra of the hydrogen atom which match those of the Rydberg formula.

The year 1905 was an eventful one for Albert Einstein. In that year, he not only published his paper on the discrete nature of the photon but he also published two further seminal works as well as submitting his Ph.D. thesis. The most famous of his other papers concerned the dynamics of moving bodies [8]. This is the paper whose later editions contained the equation $e = mc^2$. The paper was based on a thought experiment and concerned the perception of time, distance and mass as experienced by two observers, one a stationary observer and one moving relative to the stationary observer at speeds approaching that of light.

What Einstein showed is that time elapses more slowly for a moving observer, that distances measured by a moving observer are foreshortened relative to those same distances measured by a stationary observer and that a stationary observer's perception of the mass of a moving object is that it has increased. All three effects occur to the same extent and are governed by a factor γ (Gamma). The time between two events observed by the stationary observer as time t is seen by the moving observer as time $T = t/\gamma$. Similarly the distance between two point measured by the stationary observer as distance d is seen by the moving observer as distance $D = d/\gamma$. As far as the stationary observer is concerned the mass of the moving object is seen to increase by this same factor γ.

Gamma is referred to as the Lorentz factor and is given by the formula:

$$\gamma = \frac{c}{\sqrt{c^2 - v^2}} = \frac{1}{\sqrt{1 - \frac{v^2}{c^2}}}\,. \tag{9}$$

Both observers agree on their relative velocity but go about calculating it in different ways. For the stationary observer the velocity of the moving observer is the distance travelled divided by the time taken as measured in his stationary domain. For the stationary observer the velocity is:-

$$v = \frac{d}{t}\,. \tag{10}$$

For the moving observer the distance as measured in his own domain is foreshortened by the factor Gamma, but the time taken to cover that distance reduced by the same factor Gamma.

$$v = \frac{D}{T} = \frac{\frac{d}{\gamma}}{\frac{t}{\gamma}} = \frac{d}{t}\,. \tag{11}$$

There is a great deal of experimental evidence to support Einstein's Special Theory. One of the more convincing experiments was carried out at CERN in 1977 and involved measuring the lifetimes of particles called muons in an apparatus called the muon storage ring [9]. The muon is an atomic particle which carries an electric charge, much like an electron, only more massive. It has a short lifetime of around 2.2 microseconds before it decays into an electron and two neutrinos.

In the experiment muons are injected into a 14m diameter ring at a speed close to that of light, in fact at 99.94% of the speed of light where Gamma has a value of around 29.33. The muons, which should normally live for 2.2 microseconds, were seen to have an average lifetime of 64.5 microseconds; that is the lifetime of the muon was increased

by a factor Gamma. This comes about because the processes which take place inside the muon and which eventually lead to its decay are taking place in an environment which is moving relative to us at 99.94% of the speed of light and in which time, relative to us, is running 29.33 times slower. Hence the muon, in its own domain, still has a lifetime of 2.2 microseconds, it's just that to us, who are not moving, this appears as 64.5 microseconds.

Travelling at almost the speed of light a muon would normally be expected to cover a distance of 660 metres or roughly 7.5 times around the CERN ring during its 2.2 microsecond lifetime, but in fact the muons travelled almost 20,000 metres or 220 times around the ring. This is because distance in the domain of the muon is compressed so what we stationary observers see as being 20,000 metres the muon sees as being just 660 metres.

Both parties agree that during its lifetime the muon completes some 220 turns around the ring. We stationary observers see this as having taken place in some 64.5 microseconds, corresponding to a frequency of 3.4 MHz, while the muon sees these 220 turns as having been completed in just 2.2 microseconds, corresponding to a frequency of 100 Mhz. Hence for the muon and indeed all objects orbiting at close to light speed orbital frequency is multiplied by a factor Gamma relative to that of a stationary observer and it is this multiplication of orbital frequency which holds the key to the discrete energy levels of the atom.

As well as this effect on orbital frequency the muon ring experiment serves to show that considerations of special relativity can be applied to objects in orbit, this despite the fact that object in orbit are subject to a constant acceleration towards the orbital centre. However where the orbital velocity is constant, it is reasonable and correct to apply considerations of special relativity around the orbital path. In effect what we are doing is to resolve the orbital velocity into two components, one tangential component which has a constant velocity and one radial where there is a constant acceleration.

We have seen that speed is invariant with respect to relativity. Both the moving object and the stationary observer agree on their relative speed. This invariance of speed is central to the derivation of special relativity and so is deemed to be axiomatic. There is however one circumstance where it is reasonable to suggest that this need not be the case. For a stationary observer we normally require the use of two clocks in order to measure velocity; one at the point of departure and one at the point of arrival (at least conceptually). An object which is in orbit however returns once per cycle to its point of departure and so we can measure the orbital period of such an object with a single clock provided we do so over a complete orbit.

Thus for an object in orbit it is possible to define two velocity terms relating to the tangential or orbital velocity*. The first of these I have called the Actual Velocity and is simply the distance around the orbit divided by the orbital period as measured by the stationary observer. The second velocity term is the distance around the orbit as measured by the moving observer divided by the orbital period as measured by the stationary observer. Such a velocity term straddles or couples the two domains, that of the orbiting object and that of the stationary observer and so could sensibly be called the "Coupling Velocity" or possibly the "Relativistic Velocity". A simple calculation shows that the Relativistic Velocity is related to the Actual Velocity by the same factor Gamma an hence:

$$v_R = \frac{D}{t} = \frac{d}{t\gamma} = \frac{v}{\gamma} . \tag{12}$$

Thus far Relativistic Velocity is only a definition. However there is one set of circumstances where such a velocity term can indeed be justified and that is when dealing with the equations of motion relating to objects in orbit. It is considered here to be meaningful to use this Relativistic Velocity term when dealing with orbital velocities such as occur when calculating angular momentum, centripetal and centrifugal force and acceleration.

Nicholson had suggested that because Planck's constant has the units of angular momentum that it was somehow associated with the angular momentum of the orbiting electron. Here we take up that idea and suggest that the angular momentum of the orbiting electron is equal to Planck's constant, but reject his other idea that angular momentum is quantized. Instead we assume that orbital velocity is affected by relativity and use this to derive the equations of motion of the orbiting electron.

Planck's constant is then seen, not as a fundamental quantum of angular momentum but instead as providing a limiting value for angular momentum. The effect would not be significant at low velocities, but if the electron orbiting the hydrogen atom were to do so at close to light speed then:

$$l = \hbar = (m\gamma)\, r \left(\frac{c'}{\gamma} \right) . \tag{13}$$

where l is the angular momentum, $\hbar$ is Planck's constant, m is the mass of the electron, r is the orbital radius of the electron, c' is the orbital velocity of the electron and is very close to c, the speed of light.

Both the mass term and the velocity term are affected by relativity. The mass term because mass increases by factor Gamma as the object's velocity approaches the speed of light and in this case the velocity term is affected because we are dealing with an object in orbit and it is therefore appropriate

*In fact it is possible to define a further two velocity terms, the relativistic distance divided by the relativistic time and the actual distance divided by the relativistic time. The first of these is the invariant velocity discussed earlier. As a stationary observer we do not have any direct access to the moving clock and so these velocities can only be described mathematically and appear to have no physical significance.

to use Relativistic Velocity which is the Actual Velocity divided by Gamma. However since we are concerned here with an orbital velocity very close to the speed of light, to a first approximation we can substitute c for c' in Equation 13.

$$l = \hbar = (m\gamma)\, r \left(\frac{c}{\gamma}\right). \tag{14}$$

The two Gamma terms will cancel. The terms for rest mass, Planck's constant and the speed of light are all constants, which must therefore mean that the orbital radius is also a constant

$$R = \frac{\hbar}{mc}. \tag{15}$$

This not unfamiliar term is known as the Reduced Compton Wavelength although here it takes on a new and special significance as the characteristic radius at which an electron will orbit at or near light speed. This serves to explain why the orbiting electron does not emit synchrotron radiation. It does not do so because it is not driven to orbit the atomic nucleus by virtue of being accelerated by forces towards the orbital centre in the normal way, instead it is constrained to orbit at this radius by the limiting effect of Planck's constant. It is as if the electron is orbiting on a very hard surface from which it cannot depart and which it cannot penetrate. Equation 15 also means that there is no need to introduce the idea of a quantum leap or later equivalents. If the electron is constrained to always orbit at a fixed radius, then changes in energy level have to take place as a result of changes in orbital velocity, with no accompanying change of radius. Indeed this idea that the electron orbits at constant radius is a necessary condition for the electron to be considered objectively real.

Substituting Relativistic Velocity into the force balance equation that Bohr himself used, but at an orbital velocity very close to that of light yields another interesting result*

$$\frac{Kq^2}{\hbar c} = \frac{(m\gamma)}{r}\left(\frac{c}{\gamma}\right)^2. \tag{16}$$

Which combines with Equation 15 and simplifies to give:

$$\frac{Kq^2}{\hbar c} = \frac{1}{\gamma}. \tag{17}$$

Readers may be familiar with the term on the left of this equation which is known as the Fine Structure Constant often written as α (Alpha). So for the base energy state of the atom

$$\gamma = \frac{1}{\alpha}. \tag{18}$$

α has a value of $7.2973525698 \times 10^{-3}$

From this and Equation 9 we can easily calculate the corresponding orbital velocity and frequency as measured by the stationary observer.

$$\frac{v}{c} = \sqrt{1-\alpha^2} = 0.999973371. \tag{19}$$

The orbital velocity turns out to be 99.9973% of the speed of light c, thus vindicating the first approximation made in Equation 14 and the frequency (in the domain of the stationary observer)

$$\omega_1 = \frac{v}{R} = 7.76324511 \times 10^{20}. \tag{20}$$

The physicist Richard Feynman [10] once said of Alpha that:

"It has been a mystery ever since it was discovered more than fifty years ago, and all good theoretical physicists put this number up on their wall and worry about it. Immediately you would like to know where this number for a ***coupling***† *comes from: is it related to pi or perhaps to the base of natural logarithms? Nobody knows. It's one of the greatest damn mysteries of physics: a magic number that comes to us with no understanding by man. You might say the "hand of God" wrote that number, and "we don't know how He pushed his pencil." We know what kind of a dance to do experimentally to measure this number very accurately, but we don't know what kind of dance to do on the computer to make this number come out, without putting it in secretly!"*

Equation 18 effectively solves the mystery, providing an explanation for the physical significance of the Fine Structure Constant. It is seen simply as the ratio of two velocities, the Relativistic Velocity and the Actual Velocity of the orbiting electron. Since these two velocities share the same orbital period, it can also be seen as the ratio of two orbital path lengths, the one traversed at non-relativistic speeds to that traversed by the orbiting electron at near light speed. The Fine Structure Constant is seen to be dynamic in nature. Its value relies on the fact that the electron is in motion, orbiting at near light speed; it does so at a speed that is necessary to maintain structural equilibrium within the hydrogen atom, since it is only by travelling at this speed that the structural integrity of the atom can be maintained. In the world of the atom, where there is no friction and in the absence of any sort of external input, the atom remains stable and, unless disturbed in some way, the electron will continue in this state indefinitely. In this sense it defines the speed at which the electron has to travel in order to achieve a stable orbit.

So far we have only considered the lowest or base energy state of the atom. We have seen that one of the effects of relativity is to multiply frequency in the domain of a moving object by Gamma. The frequency in the domain of the

*Once again since the orbital velocity is very close to the speed of light we can, to a first approximation, substitute c as the Actual Velocity

†My emphasis — the term Coupling Velocity resonates with the idea of Alpha as a coupling constant.

electron which corresponds to this stable state is simply calculated by multiplying by Gamma — equivalent to dividing by Alpha – to give.

$$\Omega = \frac{\omega_1}{\gamma} = 1.06378925 \times 10^{23} . \quad (21)$$

But just as was the case with the observer and the cannon if there is a frequency Ω at which the atom is stable then frequencies of $n\Omega$ must also be stable for all n = integer which in turn means that there are stable states for all

$$\gamma_n = \frac{n}{\alpha} \quad (22)$$

and so

$$r_n = R = \frac{\hbar}{mc} \quad (23)$$

and

$$\frac{v_n}{c} = \sqrt{\frac{n^2 - \alpha^2}{n^2}} . \quad (24)$$

Equation 23 shows that the orbital radius remains the same for all energy levels, while Equation 24 describes the orbital velocity for the nth energy state*. Table 1 shows the resulting orbital velocities for the first 13 energy states and the theoretically infinite state of the hydrogen atom and as you might expect they match the absorption and emission spectra of the hydrogen atom perfectly.

During the 1930's and 40's Einstein and Bohr disagreed over the nature of reality, with Bohr arguing that the laws of physics were different on the scale of the atom and that as a consequence reality becomes subjective in nature. Particles are not considered to discrete point particles in the classical sense, but instead are considered to be nebulous wave-particles which manifest themselves as either particles or as waves when subjected to some sort of observing process. Einstein on the other hand took the view that reality had to be objective and that particles must therefore be discrete point particles having deterministic position and velocity.

In the end the debate was largely resolved by default. Bohr simply outlived Einstein and so his ideas prevailed and form the basis of today's Standard Model. Einstein is nowadays often described as being an old man, set in his ways and unable to accept the new ways of thinking. But this is to misconstrue Einstein's position, which was one of principle.

Einstein had argued that the laws of physics are the same for all reference frames, while Bohr reasoned that the laws of physics are different on the scale of the atom. Einstein was concerned with reference frames of comparable scale that were in motion with respect to one another but it is logical to extend his idea to reference frames of differing scales. If we start from this position and pursue the idea that particles are objectively real and that the laws of physics are the same independent of scale then it is necessary to question our current understanding of the laws of physics. They must be deficient in some way and it is necessary to find a way in which the laws must be modified to describe the atom but which does not affect our understanding on all other scales.

The idea of relativistic velocity postulated here does just that. It provides a model for the structure and dynamics of the hydrogen atom which is consistent with particles which are objectively real. At the same time it does what all previous models have failed to do and provides a mechanism to explain exactly why the energy levels of the atom are quantized without the need of resorting to arbitrary assumptions. The idea of a Relativistic Velocity or Coupling Velocity, a velocity term which is affected by relativity, solves all of the problems that faced Niels Bohr with his model and produces a model for the hydrogen atom which matches the emission and absorption spectra of the atom.

Here quantization takes place with respect to the variable Gamma as the orbital velocity of the electron gets ever closer to the speed of light with increasing energy level, and not with respect to angular momentum as postulated by Bohr. Angular momentum for the orbiting electron remains substantially constant and equal to Planck's constant over all of its energy levels as the orbital velocity varies from 99.99733% of c for the base energy state upwards as energy levels increase, although never quite achieving the theoretical limit of 100%, while Gamma is constrained to take on values which are integer multiples of a base value, that value being the reciprocal of the Fine Structure Constant. Planck's constant takes on a new and special significance, not as the quantum of angular momentum of the existing models, but as a lower limit for angular momentum below which it cannot exist.

The orbital radius of the electron remains substantially constant irrespective of the energy level of the atom, a necessary condition for an objectively real electron, and so transitions from one energy state to another take place without the need to introduce the idea of discontinuity of position, inherent in the Bohr model, or its equivalent probability density functions and wave particle duality found in other more recent models. Such transitions are easily explained as simple changes in the orbital velocity of the electron over a dynamic range which lies very close to the speed of light. With no changes in orbital radius, changes in energy level involve no change in potential energy, only the kinetic energy of the orbiting electron changes between energy states.

Thus the morphology of the atom remains substantially unaltered for all energy levels. This is consistent with the atom having the same physical and chemical properties irrespective of energy level. The Bohr model, and indeed the standard model, would have us believe that the morphology of the atom changes substantially with energy level, with the orbital radius increasing as the square of the energy level with no theoretical upper limit. Such changes are difficult to rec-

*Notice that since the orbital radius remains substantially the same for all energy levels, there is no change in potential energy between the various different energy levels, only a change in kinetic energy.

n	v_n/c	$1/\gamma_n$	Energy eV	ΔEnergy	eV
1	0.999973371	0.007297559	7.76324511E+20	255485.925	13.607
2	0.999993343	0.003648853	7.76340016E+20	255496.130	3.402
3	0.999997041	0.002432577	7.76342887E+20	255498.020	1.512
4	0.999998336	0.001824435	7.76343892E+20	255498.682	0.850
5	0.999998935	0.001459549	7.76344357E+20	255498.988	0.544
6	0.999999260	0.001216291	7.76344610E+20	255499.154	0.378
7	0.999999457	0.001042536	7.76344762E+20	255499.255	0.278
8	0.999999584	0.000912219	7.76344861E+20	255499.320	0.213
9	0.999999671	0.000810861	7.76344929E+20	255499.364	0.168
10	0.999999734	0.000729775	7.76344977E+20	255499.396	0.136
11	0.999999780	0.000663432	7.76345013E+20	255499.420	0.112
12	0.999999815	0.000608146	7.76345040E+20	255499.438	0.094
13	0.999999842	0.000561366	7.76345061E+20	255499.452	0.081
∞	1.000000000	0.000000000	7.76345184E+20	255499.532	0.000

Table 1:

oncile with an atom who's physical and chemical properties remain the same for all energy levels.

The model explains all of the shortcomings found in the Bohr model, the absence of orbital decay due to synchrotron radiation and the need for a quantum leap. Bohr had ignored the effects of special relativity on the energy levels of the atom, even though they should have been small but significant at the velocities predicted by his model. Here they are fully integrated into the model.

The model sheds a new light on the nature of the wave particle duality. The electron is seen as a point particle in the classical sense, having deterministic position and velocity*. Electrons are thus objectively real. The electron has wavelike properties, but these derive from the orbital motion of an objectively real particle. The waves are seen as the projection of the circular orbit of the objectively real electron onto an external observer, in much the same way that we can describe the orbit of the moons of distant planets as having a wavelike nature. There is no need to invent the ether or what has more recently passed for the ether, the so called fabric of space time, as a medium in which these waves exist. In the final analysis where vacuum contains absolutely nothing, there is nothing to wave except the particle and that is precisely what the model provides.

The introduction of Relativistic Velocity has another major implication. It extends the laws of physics down to the scale of the atom and possibly beyond. With its introduction the same set of physical laws extends from a scale of approximately 10^{-20} m to 10^{20} m thus doing away with the notion that a different set of physical law applies on the scale of the atom. It is quite likely therefore that a single set of physical laws exists for all scales and throughout the universe.

Finally it provides a simple mechanical explanation for the existence and the value of the hitherto mysterious Fine Structure Constant.

Appendix 1 Derivation of Centripetal Acceleration under relativistic conditions

The idea that orbital velocity is affected by relativity is central to the theory presented here, so it is perhaps worthwhile examining this idea in a little more detail. Before doing so however it is necessary to restate that the use of Special Relativity in dealing with objects which have constant orbital velocity is entirely appropriate, this despite the fact that such objects are subject to acceleration. The velocity of an object which is in orbit can be considered as having two components, a tangential component and a radial component. For constant orbital velocity, the tangential component is itself constant and therefore can be dealt with using Special Relativity which affects the time and distance measured along the orbital path. Direct evidence to support this comes in the form of the Muon ring experiment described earlier.

Such an orbiting object is subject to constant acceleration towards the orbital centre and it is this acceleration which in effect maintains the circular path. Conventional wisdom has it that this centripetal acceleration is not affected by relativity, since it acts in a direction which is normal to the velocity of the object. Here it is argued that this cannot be the case since the distances involved in calculating centripetal acceleration derive directly from the distances travelled around the orbital path and that these distances are themselves affected by relativity. It can then be shown that this is equivalent to substituting Relativistic Velocity in place of Actual Velocity in the standard formula for calculating centripetal acceleration.

Einstein showed that objects which are travelling at close

*This is not to say that uncertainty does not exist, it does, but it is seen as a practical issue of measurement when the scale of the measurement tools is similar to that of the measured object and not as being an intrinsic property of the particle.

to light speed are affected in three ways, time in the domain of the moving observer advances at a slower rate than it does for a stationary observer, distance for the moving object is foreshortened in the direction of travel relative to that same distance as measured by the stationary observer. The mass of a moving object appears increased as far as the stationary observer is concerned. All three effects occur to the same extent by the factor Gamma (γ). Gamma is named after the Dutch physicist Hendrik Antoon Lorentz (1853 — 1928). Gamma is given by the formula

$$\gamma = \frac{1}{\sqrt{1 - \frac{v^2}{c^2}}} . \tag{25}$$

Examination of the effect of relativity on an object moving at close to the speed of light however reveals that both time and distance are scaled by a factor $1/\gamma$ and so from Equation 25

$$\frac{1}{\gamma} = \sqrt{1 - \frac{v^2}{c^2}} . \tag{26}$$

It can be seen that this is the equation of a circle, more specifically a quadrant of a unit circle, since v is constrained to lie between 0 and c as shown in Figure 1.

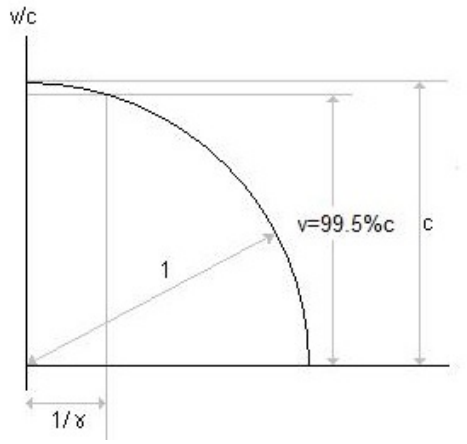

Fig. 1:

If the object under consideration is in circular orbit, then this quadrant can be superimposed on the orbital path to form a hemisphere. Objects orbiting at non-relativistic speeds see the path length around the orbit as being equal in length to the equator, while objects orbiting at higher speeds follow a path length described by a line of latitude on the hemisphere. An object orbiting at the theoretical maximum speed of light would then be pirouetting at the pole. We can consider the length of the orbital path as being represented by the line of latitude formed by a slicing plane which cuts through the hemisphere parallel to the equatorial plane. In Figure this is at approximately 15% of the speed of light c and so the orbital path length is just a little less than the equatorial path length, around 99%.

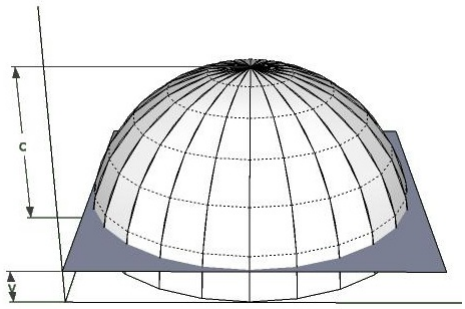

Fig. 2:

In Figure 3 the orbital velocity is approximately 80% of the speed of light and so the orbital path length as seen by the moving object is approximately 60% that for an object moving at non-relativistic speed

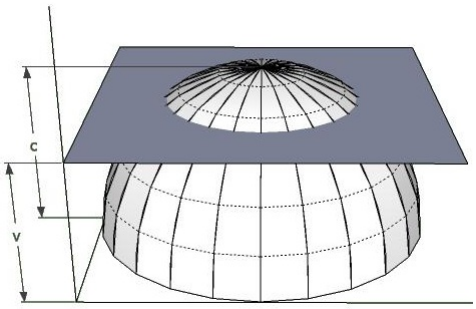

Fig. 3:

In Figure 4 the orbital velocity is around 98% of the speed of light and the corresponding orbital path length is approximately 20% of that for non-relativistic motion.

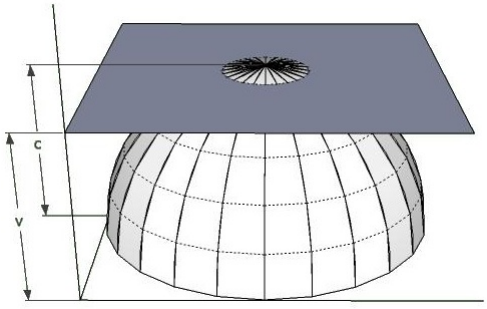

Fig. 4:

This hemispheric model of the motion of an orbiting object is useful because it allows us to visualise the orbital path

length as being foreshortened by relativity while at the same time the radius of the orbit is unaffected by relativity. The orbital geometry is non-Euclidean and in reality all takes place in just one plane. The introduction of this third dimension is just a device to allow us to visualise what is going on. The orbiting object sees the distance it travels around one orbit as being reduced by a factor Gamma, but nevertheless sees the orbital radius as being unaffected by relativity since this is at right angles to the direction of travel. Thus we can represent the radius of the orbit as being the distance from a point on the relativistic orbit to the centre of the hemisphere.

The term Actual Velocity has been adopted to describe the velocity of the orbiting object as seen by a stationary observer. This is easily calculated as the circumference of the orbital path, the equator of the hemisphere (d), divided by the orbital period (t), both measured by the stationary observer.

The theory postulates that there is a velocity term which is affected by Gamma. This is termed the Relativistic Velocity, but only becomes significant when the Actual Velocity is close to the speed of light. This velocity term can be calculated by taking the foreshortened distance around the line of latitude, which represents the orbital path as seen by the moving observer, divided by the orbital period as measured by a stationary observer. The foreshortened distance around the orbit is calculated as d/γ and the orbital period remains the same as for Actual Velocity (t) and hence this Relativistic Velocity is then easily calculated as $v_R = d/t\gamma$.

We can use this term directly in calculating the angular momentum of the orbiting object. This is simply a restatement of the argument used earlier. Angular momentum is the product of the mass, the velocity and the radius of an orbiting point object. However the mass of the object is affected by relativity, appearing to increase the mass by a factor Gamma (γ) and so:

$$l = (m\gamma)\, r \left(\frac{v_R}{\gamma} \right) . \tag{27}$$

However since for Gamma to take on a significant value v_R must be very close to c, the speed of light and so we can substitute c for v_R. Also since the angular momentum of an electron in orbit around an atomic nucleus is given by Planck's constant we can substitute this for l in Equation 27 to give:

$$l = \hbar = mcr . \tag{28}$$

In effect we are simply substituting Relativistic Velocity for Actual Velocity in the standard textbook formula for calculating angular momentum. This is recognising that the orbital velocity is the distance around the orbit as measured by the moving object divided by the orbital period as measured by a stationary observer.

We can of course use this same argument to substitute Relativistic Velocity for Actual Velocity in the formula for centripetal acceleration and hence derive expressions for centripetal and centrifugal forces. However in the case of centripetal acceleration it is also useful to derive an expression for the relativistic case from first principles.

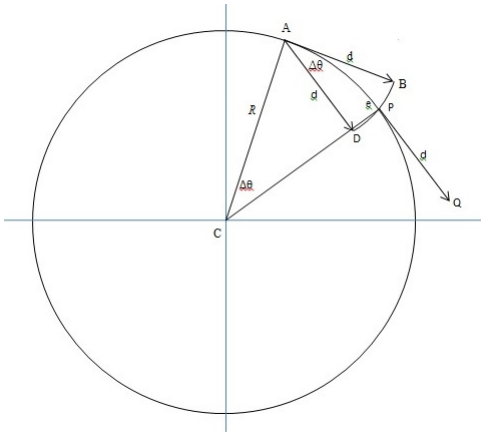

Fig. 5:

The formula for centripetal force was first derived by Christian Huygens in 1659 and describes a constant force acting on a body in circular motion towards the centre of the circle. When combined with Newton's second law this leads to the idea that a body in circular motion is subject to a constant acceleration towards the centre called centripetal acceleration.

It is customary when deriving the formula for centripetal acceleration to use velocity vectors directly. Here we take a slightly different approach and use the distance vectors instead. This is because in the proposed theory only the distance component of velocity is affected by relativity and not the time component. In other respects the derivation is the same as that found in many standard texts.

Consider an object in orbit around a point C at radius R. At a particular instant t the object is at point A and some short interval of time later Δt it is at point P, having moved through an angle subtended at the centre of the circle of $\Delta\theta$.

The vector representing the distance moved in time Δt is AB and has length d and is tangential to the circle, hence CAB is a right angle. At $t + \Delta t$ the object is at P and has a distance vector PQ, also of length d. We can translate the vector PQ to A forming AD. The vector BD then represents the distance moved towards the centre of the circle in time Δt. Note that for as $\Delta\theta$ tends to 0 the line BD tends to a straight line.

Then

$$d = R\Delta\theta . \tag{29}$$

Since APC and ABD are similar triangles (for small $\Delta\theta$)

$$e = d\Delta\theta \tag{30}$$

and the acceleration towards the centre of the circle is

$$a = \frac{e}{\Delta t^2} . \tag{31}$$

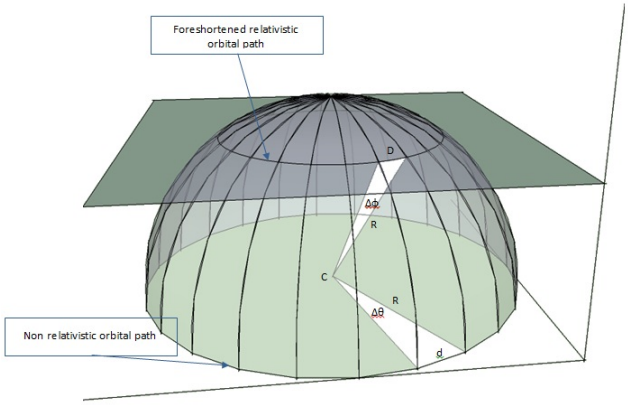

Fig. 6:

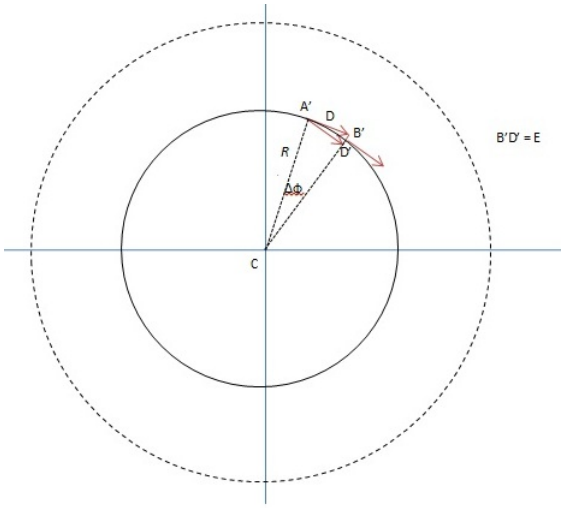

Fig. 7:

Therefore

$$a = \frac{R\Delta\theta^2}{\Delta t^2} . \tag{32}$$

Multiplying both top and bottom by R gives

$$a = \frac{R^2\Delta\theta^2}{R\Delta t^2} . \tag{33}$$

But since

$$v = \frac{d}{\Delta t} = \frac{R\Delta\theta}{\Delta t} . \tag{34}$$

Then

$$a = \frac{v^2}{R} . \tag{35}$$

When we take into consideration the effects of special relativity, the situation becomes a little more complicated. Although the orbital path is foreshortened, as represented by the line of latitude in Figure 6, and hence the circumference of this circle is reduced by a factor Gamma, the radius of the circle is not affected and remains the same as that for the equatorial orbital path.

Figure 6 attempts to show this by introducing a third dimension and using the hemispherical representation developed above. In reality however the radius and the orbital path are co-planar. It can be seen from Figure 6 that the angle subtended by a short segment of the circumference is less for the relativistic path than for the non-relativistic path. From Figure 6 it is evident that

$$\Delta\phi = \frac{\Delta\theta}{\gamma} \tag{36}$$

and

$$R\Delta\phi = \frac{R\Delta\theta}{\gamma} . \tag{37}$$

Figure 7 shows the foreshortened orbital path in plan view. The dashed circle represents the non-relativistic orbital path while the radii are shown dotted to indicate that they are not to scale in this representation.

The distance travelled during time Δt is foreshortened by relativity, instead of travelling a distance AB the object only travels a distance A'B'=D in Figure 7.

$$D = R\Delta\phi . \tag{38}$$

Once again the triangles CA'B' and A'B'D' are similar and so the distance travelled towards the centre of the orbit E is

$$E = D\Delta\phi . \tag{39}$$

Once again the triangles CA'B' and A'B'D' are similar and so the distance travelled towards the centre of the orbit E is

$$A = \frac{E}{\Delta t^2} . \tag{40}$$

Which is also

$$A = \frac{R\Delta\phi^2}{\Delta t^2} \tag{41}$$

Again we can multiply both denominator and numerator by R to give

$$A = \frac{R^2\Delta\phi^2}{R\Delta t^2} . \tag{42}$$

Which gives

$$A = \frac{R^2\Delta\theta^2}{R\Delta t^2\gamma^2} \tag{43}$$

and so

$$A = \frac{v^2}{R\gamma^2} . \tag{44}$$

Equation 44 represents a more general case for calculating centripetal acceleration. When the orbital velocity is low, under non-relativistic conditions, the value of Gamma is unity

and the formula can be simplified to the more familiar one shown in Equation 35. Effectively therefore the formula for centripetal acceleration under relativity substitutes Relativistic Velocity for Actual Velocity in the standard textbook formula.

It is the geometry of the triangle AB'D' which lies at the heart of the argument. Here it is argued that the length B'D' is affected by relativity even though it is measured in a direction at right angles to the direction of travel. This comes about because the lengths of the two sides AB' and AD' are both themselves affected by relativity and the triangle must have geometric integrity and so B'D' must also be scaled by relativity. If it was not then the triangle AB'D' would be a very strange triangle indeed. It would have to be an isosceles triangle in which the third side could be longer than the sum of the two other sides. The direction of the vectors AB' and AD' could not be preserved. Even in non-Euclidian geometry such a triangle would not be possible and so B'D' must be scaled by Gamma.

The measurement of time on the other hand can only take place in the domain of the observer, so the moving observer sees his time in his own domain and the stationary observer sees time in his domain. The two domains are related by a factor Gamma, but from the point of view of direct measurement this is a theoretical connection. In other words the stationary observer has no direct access to the moving clock and, vice versa, the moving observer has no direct access to the stationary clock.

Appendix 2 An Analytical Method for calculating Actual Velocity

A more analytical approach for calculating the value for c' can be found without the first approximation used above:

The equation for the value of gamma

$$\gamma = \frac{1}{\sqrt{1 - \frac{v^2}{c^2}}} . \tag{45}$$

From which

$$v = c\sqrt{\frac{\gamma^2 - 1}{\gamma^2}} . \tag{46}$$

Substituting this into the force balance equation gives

$$\frac{m_0 c^2(\gamma^2 - 1)}{R\gamma^3} = \frac{Kq^2}{R^2} . \tag{47}$$

Recognising that $\hbar = m_0 Rc$ and simplifying gives

$$\frac{\gamma^2 - 1}{\gamma^3} = \frac{Kq^2}{\hbar c} . \tag{48}$$

The term on the right hand side is the Fine Structure Constant which is denoted by α. Substituting and rearranging gives the following equation for γ.

$$\alpha\gamma^3 - \gamma^2 + 1 = 0 . \tag{49}$$

The numerical value for α^* is $7.2973525698 \times 10^{-3}$. Substituting this and calculating the three roots gives:

$\gamma = 137.028700944403$

$\gamma = -0.996384222264$

$\gamma = 1.0036823521665$

Only the first of these three values is significant. This cubic equation gives a more precise value for Gamma. By recognizing that v is very close to c in the force balance equation the value of Gamma can be calculated as:

Substituting in the equation for γ gives a value for v:

$$v = c\sqrt{\frac{\gamma^2 - 1}{\gamma^2}} = 0.999973371c . \tag{50}$$

v is the Actual Velocity of the electron around its orbit and as can be seen it is very close to c, the velocity of light, being some 99.9973371% of c, which is in agreement with the method of first approximation to the first 8 significant figures.

Appendix 3 The Rydberg Formula

Joseph Jakob Balmer (1825–1898) was a Swiss mathematician and numerologist who, after his studies in Germany, took up a post teaching mathematics at a girls' school in Basel. A colleague in Basel suggested that he take a look at the spectral lines of hydrogen to see if he could find a mathematical relationship between them. Eventually Balmer did find a common factor† $h = 3.6456 \times 10^{-7}$ which led him to a formula for the wavelength of the various spectral lines.

$$\lambda = \frac{hm^2}{m^2 - 4} , \tag{51}$$

where m is an integer with value 3 or higher.

Balmer originally matched his formula for $m = 3, 4, 5, 6$ and based on this he predicted an absorption line for $m = 7$. Balmer's seventh line was subsequently found to match a new line in the hydrogen spectrum that had been discovered by Ångström.

Balmer's formula dealt with a particular set of spectral lines in the hydrogen atom and was later found to be a special case of a more general result which was formulated by the Swedish physicist Johannes Rydberg.

$$\frac{1}{\lambda} = R_H\left(\frac{1}{n_1^2} - \frac{1}{n_2^2}\right) , \tag{52}$$

where λ is the wavelength of the spectral line, R_H is the Rydberg constant for hydrogen, n_1 and n_2 are integers and $n_1 < n_2$.

By setting n_1 to 1 and allowing n_2 to take on values of $2, 3, 4 \ldots \infty$ the lines take in a series of values known as the Lyman series. Balmer's series is obtained by setting $n_1 = 2$ and allowing n_2 to take on values of $3, 4, 5 \ldots \infty$. Similarly for other values of n_1 series of spectral lines have been named according to the person who first discovered them and so:

*CODATA - http://physics.nist.gov/cgi-bin/cuu/Value?alph

†h here is not to be confused with Planck's constant.

n_1	n_2	Series
1	$2 \ldots \infty$	Lyman series
2	$3 \ldots \infty$	Balmer series
3	$4 \ldots \infty$	Paschen series
4	$5 \ldots \infty$	Brackett series
5	$6 \ldots \infty$	Pfund series
6	$7 \ldots \infty$	Humfreys series

Other series beyond these do exist, but they are not named.

By substituting different values for R, it was found that Rydberg's formula worked for all so called *hydrogenic*[*] atoms.

The value of R_H can be found by considering the case where $n_1 = 1$ and $n_2 = \infty$, a condition which represents the maximum possible change in energy level within the hydrogen atom. R_H is then the wavelength of the absorption line associated with such an energy change and was calculated to have a value of 1.097×10^7

This was subsequently found to be given by the formula:

$$R_H = \frac{1}{4\pi} \frac{m_0 c \alpha^2}{\hbar} . \tag{53}$$

The highest possible energy level for the atom occurs when n, the energy level, equals the theoretical value of infinity. The corresponding value for the Actual Velocity would then be c, the speed of light.

The equation for the energy of an orbiting body of mass m with velocity v is easily obtained in any standard text and is given by:

$$e = \frac{1}{2} m v^2 . \tag{54}$$

If we assume that the electron is orbiting at near light speed then the maximum possible energy[†] of an electron orbiting the hydrogen nucleus where the orbital velocity has a theoretical value of c, the speed of light and the mass of the electron is m_0 is

$$e = \frac{1}{2} m_0 c^2 . \tag{55}$$

The energy potential for a hydrogen atom in any arbitrary energy state n is the difference between this maximum energy value and the energy of the nth state

$$e_n = \frac{1}{2} m_0 c^2 - \frac{1}{2} m_0 v_n^2 = \frac{1}{2} m_0 (c^2 - v_n^2) . \tag{56}$$

We saw earlier that gamma could be expressed in terms of c, the velocity of light and v, the Actual Velocity using Einstein's equation for special relativity and that $\gamma_n = n\gamma_0$

$$\gamma_n = \frac{c}{\sqrt{c^2 - v_n^2}} . \tag{57}$$

This is easily rearranged to give an expression for $c^2 - v^2$

$$c^2 - v_n^2 = \frac{c^2}{\gamma_n^2} \tag{58}$$

In the base energy state $n = 0$ and $\gamma_0 = 1/\alpha$

$$c^2 - v_0^2 = c^2 \alpha^2 \tag{59}$$

Hence the maximum energy potential for the atom is

$$e_p = \frac{1}{2} m_0 c^2 \alpha^2 . \tag{60}$$

Substituting numerical values for m_0, c and α gives the maximum energy potential of the atom as
$e_p = 2.18009839 \times 10^1 8$ Joules
or
$e_p = 13.6071$ eV.

The energy potential for any arbitrary energy level n is given by

$$e_{pn} = \frac{1}{2} \frac{m_0 c^2 \alpha^2}{n^2} . \tag{61}$$

Hence the difference between any two energy levels n and m is

$$e_{n,m} = \frac{1}{2} m_0 c^2 \alpha^2 \left(\frac{1}{n^2} - \frac{1}{m^2} \right) . \tag{62}$$

and the difference in orbital frequency is

$$\omega_{n,m} = \frac{1}{2} \frac{m_0 c \alpha^2}{\hbar} \left(\frac{1}{n^2} - \frac{1}{m^2} \right) \tag{63}$$

This can be expressed in terms of wavelength, similar to the Rydberg formula, by dividing both sides by 2π to give

$$\frac{1}{\lambda_{n,m}} = \frac{1}{4\pi} \frac{m_0 c \alpha^2}{\hbar} \left(\frac{1}{n^2} - \frac{1}{m^2} \right) \tag{64}$$

and

$$R_H = \frac{1}{4\pi} \frac{m_0 c \alpha^2}{\hbar} . \tag{65}$$

Submitted on: October 8, 2012 / Accepted on: October 11, 2012

[*]A hydrogenic atom is one which is ionized such that it has only one orbiting electron. In theory, at least, any atom can be ionized so as to become hydrogenic.

[†]Note that the electron is orbiting at the same radius for all energy levels, the potential energy of the electron therefore remains the same and all changes in energy level which are then associated with changes in kinetic energy and hence with the velocity of the electron.

References

1. Heilbron J.L. Historical Studies in the Theory of Atomic Structure. *Arno Press*, 1981.
2. Nyquist H. Certain Topics in Telegraph Transmission Theory. *Trans. AIEE*, Apr 1928, v.47, 617–644, .
3. Shannon C.E. Communication in the Presence of Noise. *Proc. Institute of Radio Engineers*, Jan 1949, v.37, no.1, 10–21.

4. Bracewell R.N. The Fourier Transform and Its Applications (revised ed.). *McGraw-Hill*, 1st ed., 1965, 2nd ed. 1978.
5. Bohr N. On the Constitution of Atoms and Molecules. Part I. *Philosophical Magazine*, 1913, v.26, 1–24.
6. Nicholson J.W. A structural Theory of the Chemical Elements. *Philosophical Magazine*, 1911, v.22, 864–889.
7. Einstein A. Über einen die Erzeugung und Verwandlung des Lichtes betreffenden heuristischen Gesichtspunkt (On a Heuristic Viewpoint Concerning the Production and Transformation of Light). *Annalen der Physik*, 1905, Bd.17(6), 132–134.
8. Einstein A. Zur Elektrodynamik bewegter Körper (On the Electrodynamics of Moving Bodies). *Annalen der Physik*, 1905, Bd.17(10), 891–921.
9. Bailey H., Borer K., Combley F., Drumm H., Krienen F., Lange F., Picasso E., von Ruden W., Farley F.J.M., Field J.H., Flegel W. & Hattersley P.M. Measurements of relativistic time dilatation for positive and negative muons in a circular orbit. *Nature*, 1977, v.268(5618), 301–305.
10. Feynman R.P. QED: The Strange Theory of Light and Matter. Princeton University Press, 1985, p.129.

The Elastodynamics of the Spacetime Continuum as a Framework for Strained Spacetime

Pierre A. Millette

University of Ottawa (alumnus), K4A 2C3 747, Ottawa, Canada. E-mail: PierreAMillette@alumni.uottawa.ca

We derive the elastodynamics of the spacetime continuum by applying continuum mechanical results to strained spacetime. Based on this model, a stress-strain relation is derived for the spacetime continuum. From the kinematic relations and the equilibrium dynamic equation of the spacetime continuum, we derive a series of wave equations: the displacement, dilatational, rotational and strain wave equations. Hence energy propagates in the spacetime continuum as wave-like deformations which can be decomposed into dilatations and distortions. Dilatations involve an invariant change in volume of the spacetime continuum which is the source of the associated rest-mass energy density of the deformation, while distortions correspond to a change of shape of the spacetime continuum without a change in volume and are thus massless. The deformations propagate in the continuum by longitudinal and transverse wave displacements. This is somewhat reminiscent of wave-particle duality, with the transverse mode corresponding to the wave aspects and the longitudinal mode corresponding to the particle aspects. A continuity equation for deformations of the spacetime continuum is derived, where the gradient of the massive volume dilatation acts as a source term. The nature of the spacetime continuum volume force and the inhomogeneous wave equations need further investigation.

1 Introduction

Strained spacetime has been explored recently by Millette [1] from a continuum mechanical and general relativistic perspective, and by Tartaglia *et al* in the cosmological context, as an extension of the spacetime Lagrangian, to obtain a generalized Einstein equation [2, 3].

As shown in [1], the applied stresses from the energy-momentum stress tensor result in strains in the spacetime continuum. The presence of strains as a result of applied stresses is an expected continuum mechanical result. The strains result in a deformation of the continuum which can be modeled as a change in the underlying geometry of the continuum. The geometry of the spacetime continuum of General Relativity resulting from the energy-momentum stress tensor can thus be seen as a representation of the deformation of the spacetime continuum resulting from the strains generated by the energy-momentum stress tensor.

In this paper, we examine in greater details the elastodynamics of the spacetime continuum as a framework for describing strained spacetime.

2 Elastodynamics of the Spacetime Continuum

2.1 Model of the Elastodynamics of the Spacetime Continuum

The spacetime continuum (*STC*) is modelled as a four-dimensional differentiable manifold endowed with a metric $g_{\mu\nu}$. It is a continuum that can undergo deformations and support the propagation of such deformations. A continuum that is deformed is strained.

An infinitesimal element of the unstrained continuum is characterized by a four-vector x^μ, where $\mu = 0, 1, 2, 3$. The time coordinate is $x^0 \equiv ct$.

A *deformation* of the spacetime continuum corresponds to a state of the *STC* in which its infinitesimal elements are displaced from their unstrained position. Under deformation, the infinitesimal element x^μ is displaced to a new position $x^\mu + u^\mu$, where u^μ is the displacement of the infinitesimal element from its unstrained position x^μ.

The spacetime continuum is approximated by a deformable linear elastic medium that obeys Hooke's law. For a general anisotropic continuum in four dimensions [4, see pp. 50–53],

$$E^{\mu\nu\alpha\beta}\varepsilon_{\alpha\beta} = T^{\mu\nu} \tag{1}$$

where $\varepsilon_{\alpha\beta}$ is the strain tensor, $T^{\mu\nu}$ is the energy-momentum stress tensor, and $E^{\mu\nu\alpha\beta}$ is the elastic moduli tensor.

The spacetime continuum is further assumed to be isotropic and homogeneous. This assumption is in agreement with the conservation laws of energy-momentum and angular momentum as expressed by Noether's theorem [5, see pp. 23–30]. For an isotropic medium, the elastic moduli tensor simplifies to [4]:

$$E^{\mu\nu\alpha\beta} = \lambda_0(g^{\mu\nu}g^{\alpha\beta}) + \mu_0(g^{\mu\alpha}g^{\nu\beta} + g^{\mu\beta}g^{\nu\alpha}) \tag{2}$$

where λ_0 and μ_0 are the Lamé elastic constants of the spacetime continuum. μ_0 is the shear modulus (the resistance of the continuum to *distortions*) and λ_0 is expressed in terms of κ_0, the bulk modulus (the resistance of the continuum to *dilatations*) according to

$$\lambda_0 = \kappa_0 - \mu_0/2 \tag{3}$$

in a four-dimensional continuum. A *dilatation* corresponds to a change of volume of the spacetime continuum without a change of shape while a *distortion* corresponds to a change of shape of the spacetime continuum without a change in volume.

2.2 Stress-Strain Relation of the Spacetime Continuum

Substituting Eq.(2) into Eq.(1), we obtain the stress-strain relation for an isotropic and homogeneous spacetime continuum

$$2\mu_0\varepsilon^{\mu\nu} + \lambda_0 g^{\mu\nu}\varepsilon = T^{\mu\nu} \tag{4}$$

where

$$\varepsilon = \varepsilon^{\alpha}{}_{\alpha} \tag{5}$$

is the trace of the strain tensor obtained by contraction. The volume dilatation ε is defined as the change in volume per original volume [6, see pp. 149–152] and is an invariant of the strain tensor.

It is interesting to note that the structure of Eq.(4) is similar to that of the field equations of General Relativity, viz.

$$R^{\mu\nu} - \frac{1}{2}g^{\mu\nu}R = -KT^{\mu\nu} \tag{6}$$

where $K = 8\pi G/c^4$ and G is the gravitational constant. This strengthens our conjecture that the geometry of the spacetime continuum can be seen as a representation of the deformation of the spacetime continuum resulting from the strains generated by the energy-momentum stress tensor.

Rest-Mass Energy Relation

As shown in [1], the contraction of Eq.(4) yields the relation

$$2(\mu_0 + 2\lambda_0)\varepsilon = T^{\alpha}{}_{\alpha} \equiv T \tag{7}$$

where $T^{\alpha}{}_{\alpha}$ corresponds to the invariant rest-mass energy density

$$T^{\alpha}{}_{\alpha} = T = \rho c^2 \tag{8}$$

where ρ is the rest-mass density. The relation between the invariant volume dilatation ε and the invariant rest-mass energy density is thus given by

$$2(\mu_0 + 2\lambda_0)\varepsilon = \rho c^2 \tag{9}$$

or, in terms of the bulk modulus κ_0,

$$4\kappa_0\varepsilon = \rho c^2. \tag{10}$$

As we noted in [1], this equation demonstrates that rest-mass energy density arises from the volume dilatation of the spacetime continuum. The rest-mass energy is equivalent to the energy required to dilate the volume of the spacetime continuum, and is a measure of the energy stored in the spacetime continuum as volume dilatation. The volume dilatation is an invariant, as is the rest-mass energy density.

Decomposition into Distortions and Dilatations

As also shown in [1], when the strain tensor $\varepsilon^{\mu\nu}$ and the energy-momentum stress tensor $T^{\mu\nu}$ are decomposed into a deviation tensor (the *distortion*) and a scalar (the *dilatation*), the strain-stress relation then becomes separated into dilatation and distortion relations:

$$\begin{aligned} &\text{dilatation} : t = 2(\mu_0 + 2\lambda_0)e = 4\kappa_0 e = \kappa_0\varepsilon \\ &\text{distortion} : t^{\mu\nu} = 2\mu_0 e^{\mu\nu} \end{aligned} \tag{11}$$

where

$$\varepsilon^{\mu\nu} = e^{\mu\nu} + e g^{\mu\nu} \tag{12}$$

with

$$e^{\mu}{}_{\nu} = \varepsilon^{\mu}{}_{\nu} - e\delta^{\mu}{}_{\nu} \tag{13}$$

$$e = \frac{1}{4}\varepsilon^{\alpha}{}_{\alpha} = \frac{1}{4}\varepsilon \tag{14}$$

and similarly

$$T^{\mu\nu} = t^{\mu\nu} + t g^{\mu\nu} \tag{15}$$

with

$$t^{\mu}{}_{\nu} = T^{\mu}{}_{\nu} - t\delta^{\mu}{}_{\nu} \tag{16}$$

$$t = \frac{1}{4}T^{\alpha}{}_{\alpha}. \tag{17}$$

The distortion-dilatation decomposition is evident in the dependence of the dilatation relation on the bulk modulus κ_0 and of the distortion relation on the shear modulus μ_0. The dilatation relation of Eq.(11) corresponds to rest-mass energy, while the distortion relation is traceless and thus massless, and corresponds to shear transverse waves. We also noted in [1] that this decomposition of spacetime continuum deformations into a massive dilatation and a massless transverse wave distortion is somewhat reminiscent of wave-particle duality.

3 Kinematic Relations

The strain $\varepsilon^{\mu\nu}$ can be expressed in terms of the displacement u^{μ} through the kinematic relation [6, see pp. 149–152]:

$$\varepsilon^{\mu\nu} = \frac{1}{2}(u^{\mu;\nu} + u^{\nu;\mu} + u^{\alpha;\mu}u_{\alpha}{}^{;\nu}) \tag{18}$$

where the semicolon (;) denotes covariant differentiation. For small displacements, this expression can be linearized to give the symmetric tensor

$$\varepsilon^{\mu\nu} = \frac{1}{2}(u^{\mu;\nu} + u^{\nu;\mu}) = u^{(\mu;\nu)}. \tag{19}$$

We use the small displacement approximation in this analysis.

An antisymmetric tensor $\omega^{\mu\nu}$ can also be defined from the displacement u^{μ}. This tensor is called the rotation tensor and is defined as [6]:

$$\omega^{\mu\nu} = \frac{1}{2}(u^{\mu;\nu} - u^{\nu;\mu}) = u^{[\mu;\nu]}. \tag{20}$$

Where needed, displacements in expressions derived from Eq.(19) will be written as $u_{\parallel}$ while displacements in expressions derived from Eq.(20) will be written as $u_{\perp}$. Using different symbolic subscripts for these displacements provides a reminder that symmetric displacements are along the direction of motion (longitudinal), while antisymmetric displacements are perpendicular to the direction of motion (transverse).

In general, we have [6]

$$u^{\mu;\nu} = \varepsilon^{\mu\nu} + \omega^{\mu\nu} \tag{21}$$

where the tensor $u^{\mu;\nu}$ is a combination of symmetric and antisymmetric tensors. Lowering index ν and contracting, we get the volume dilatation of the spacetime continuum

$$u^{\mu}{}_{;\mu} = \varepsilon^{\mu}{}_{\mu} = u_{\parallel}{}^{\mu}{}_{;\mu} = \varepsilon \tag{22}$$

where the relation

$$\omega^{\mu}{}_{\mu} = u_{\perp}{}^{\mu}{}_{;\mu} = 0 \tag{23}$$

has been used.

4 Dynamic Equation

4.1 Equilibrium Condition

Under equilibrium conditions, the dynamics of the spacetime continuum is described by the equation [4, see pp. 88–89],

$$T^{\mu\nu}{}_{;\mu} = -X^{\nu} \tag{24}$$

where X^{ν} is the volume (or body) force. As Wald [7, see p. 286] points out, in General Relativity the local energy density of matter as measured by a given observer is well-defined, and the relation

$$T^{\mu\nu}{}_{;\mu} = 0 \tag{25}$$

can be taken as expressing local conservation of the energy-momentum of matter. However, it does not in general lead to a global conservation law. The value $X^{\nu} = 0$ is thus taken to represent the macroscopic local case, while Eq.(24) provides a more general expression.

At the microscopic level, energy is conserved within the limits of the Heisenberg Uncertainty Principle. The volume force may thus be very small, but not exactly zero. It again makes sense to retain the volume force in the equation, and use Eq.(24) in the general case, while Eq.(25) can be used at the macroscopic local level, obtained by setting the volume force X^{ν} equal to zero.

4.2 Displacement Wave Equation

Substituting for $T^{\mu\nu}$ from Eq.(4), Eq.(24) becomes

$$2\mu_0\varepsilon^{\mu\nu}{}_{;\mu} + \lambda_0 g^{\mu\nu}\varepsilon_{;\mu} = -X^{\nu} \tag{26}$$

and, using Eq.(19),

$$\mu_0(u^{\mu;\nu}{}_{\mu} + u^{\nu;\mu}{}_{\mu}) + \lambda_0\varepsilon^{;\nu} = -X^{\nu}. \tag{27}$$

Interchanging the order of differentiation in the first term and using Eq.(22) to express ε in terms of u, this equation simplifies to

$$\mu_0 u^{\nu;\mu}{}_{\mu} + (\mu_0 + \lambda_0)u^{\mu}{}_{;\mu}{}^{\nu} = -X^{\nu} \tag{28}$$

which can also be written as

$$\mu_0\nabla^2 u^{\nu} + (\mu_0 + \lambda_0)\varepsilon^{;\nu} = -X^{\nu}. \tag{29}$$

This is the *displacement wave equation*.

Setting X^{ν} equal to zero, we obtain the macroscopic displacement wave equation

$$\nabla^2 u^{\nu} = -\frac{\mu_0 + \lambda_0}{\mu_0}\varepsilon^{;\nu}. \tag{30}$$

4.3 Continuity Equation

Taking the divergence of Eq.(21), we obtain

$$u^{\mu;\nu}{}_{\mu} = \varepsilon^{\mu\nu}{}_{;\mu} + \omega^{\mu\nu}{}_{;\mu}. \tag{31}$$

Interchanging the order of partial differentiation in the first term, and using Eq.(22) to express u in terms of ε, this equation simplifies to

$$\varepsilon^{\mu\nu}{}_{;\mu} + \omega^{\mu\nu}{}_{;\mu} = \varepsilon^{;\nu}. \tag{32}$$

Hence the divergence of the strain and rotation tensors equals the gradient of the massive volume dilatation, which acts as a source term. This is the continuity equation for deformations of the spacetime continuum.

5 Wave Equations

5.1 Dilatational (Longitudinal) Wave Equation

Taking the divergence of Eq.(28) and interchanging the order of partial differentiation in the first term, we obtain

$$(2\mu_0 + \lambda_0)u^{\mu}{}_{;\mu}{}^{\nu}{}_{\nu} = -X^{\nu}{}_{;\nu}. \tag{33}$$

Using Eq.(22) to express u in terms of ε, this equation simplifies to

$$(2\mu_0 + \lambda_0)\varepsilon^{;\nu}{}_{\nu} = -X^{\nu}{}_{;\nu} \tag{34}$$

or

$$(2\mu_0 + \lambda_0)\nabla^2\varepsilon = -X^{\nu}{}_{;\nu}. \tag{35}$$

Setting X^{ν} equal to zero, we obtain the macroscopic longitudinal wave equation

$$(2\mu_0 + \lambda_0)\nabla^2\varepsilon = 0. \tag{36}$$

The volume dilatation ε satisfies a wave equation known as the dilatational wave equation [6, see p. 260]. The solutions of the homogeneous equation are dilatational waves which are longitudinal waves, propagating along the direction of motion. Dilatations thus propagate in the spacetime continuum as longitudinal waves.

5.2 Rotational (Transverse) Wave Equation

Differentiating Eq.(28) with respect to x^α, we obtain

$$\mu_0 u^{\nu;\mu}{}_{\mu}{}^{\alpha} + (\mu_0 + \lambda_0) u^{\mu}{}_{;\mu}{}^{\nu\alpha} = -X^{\nu;\alpha}. \tag{37}$$

Interchanging the dummy indices ν and α, and subtracting the resulting equation from Eq.(37), we obtain the relation

$$\mu_0 (u^{\nu;\mu}{}_{\mu}{}^{\alpha} - u^{\alpha;\mu}{}_{\mu}{}^{\nu}) = -(X^{\nu;\alpha} - X^{\alpha;\nu}). \tag{38}$$

Interchanging the order of partial differentiations and using the definition of the rotation tensor $\omega^{\nu\alpha}$ of Eq.(20), the following wave equation is obtained:

$$\mu_0 \nabla^2 \omega^{\mu\nu} = -X^{[\mu;\nu]} \tag{39}$$

where $X^{[\mu;\nu]}$ is the antisymmetrical component of the gradient of the volume force defined as

$$X^{[\mu;\nu]} = \frac{1}{2}(X^{\mu;\nu} - X^{\nu;\mu}). \tag{40}$$

Setting X^ν equal to zero, we obtain the macroscopic transverse wave equation

$$\mu_0 \nabla^2 \omega^{\mu\nu} = 0. \tag{41}$$

The rotation tensor $\omega^{\mu\nu}$ satisfies a wave equation known as the rotational wave equation [6, see p. 260]. The solutions of the homogeneous equation are rotational waves which are transverse waves, propagating perpendicular to the direction of motion. Massless waves thus propagate in the spacetime continuum as transverse waves.

5.3 Strain (Symmetric) Wave Equation

A corresponding symmetric wave equation can also be derived for the strain $\varepsilon^{\mu\nu}$. Starting from Eq.(37), interchanging the dummy indices ν and α, adding the resulting equation to Eq.(37), and interchanging the order of partial differentiation, the following wave equation is obtained:

$$\mu_0 \nabla^2 \varepsilon^{\mu\nu} + (\mu_0 + \lambda_0) \varepsilon^{;\mu\nu} = -X^{(\mu;\nu)} \tag{42}$$

where $X^{(\mu;\nu)}$ is the symmetrical component of the gradient of the volume force defined as

$$X^{(\mu;\nu)} = \frac{1}{2}(X^{\mu;\nu} + X^{\nu;\mu}). \tag{43}$$

Setting X^ν equal to zero, we obtain the macroscopic symmetric wave equation

$$\nabla^2 \varepsilon^{\mu\nu} = -\frac{\mu_0 + \lambda_0}{\mu_0} \varepsilon^{;\mu\nu}. \tag{44}$$

This strain wave equation is similar to the displacement wave equation Eq.(30).

6 Discussion and Conclusion

In this paper, we have proposed a framework for the analysis of strained spacetime based on the elastodynamics of the spacetime continuum (*STCED*). In this model, the emphasis is on the displacements of the spacetime continuum infinitesimal elements from their unstrained configuration as a result of the strains applied on the *STC* by the energy-momentum stress tensor, rather than on the geometry of the *STC* due to the energy-momentum stress tensor.

We postulate that this description based on the deformation of the continuum is a description complementary to that of General Relativity which is concerned with modeling the resulting geometry of the spacetime continuum. Interestingly, the structure of the resulting stress-strain relation is similar to that of the field equations of General Relativity. This strengthens our conjecture that the geometry of the spacetime continuum can be seen as a representation of the deformation of the spacetime continuum resulting from the strains generated by the energy-momentum stress tensor. The equivalency of the strain description and of the geometrical description still remains to be demonstrated.

The equilibrium dynamic equation of the spacetime continuum is described by $T^{\mu\nu}{}_{;\mu} = -X^\nu$. In General Relativity, the relation $T^{\mu\nu}{}_{;\mu} = 0$ is taken as expressing local conservation of the energy-momentum of matter. The value $X^\nu = 0$ is thus taken to represent the macroscopic local case, while in the general case, the volume force X^ν is retained in the equation. This dynamic equation leads to a series of wave equations as derived in this paper: the displacement (u^ν), dilatational (ε), rotational ($\omega^{\mu\nu}$) and strain ($\varepsilon^{\mu\nu}$) wave equations.

Hence energy is seen to propagate in the spacetime continuum as deformations of the *STC* that satisfy wave equations of propagation. Deformations can be decomposed into dilatations and distortions. *Dilatations* involve an invariant change in volume of the spacetime continuum which is the source of the associated rest-mass energy density of the deformation. *Distortions* correspond to a change of shape of the spacetime continuum without a change in volume and are thus massless. Dilatations correspond to longitudinal displacements and distortions correspond to transverse displacements of the spacetime continuum.

Hence, every excitation of the spacetime continuum can be decomposed into a transverse and a longitudinal mode of propagation. We have noted that this decomposition into a dilatation with rest-mass energy density and a massless transverse wave distortion, is somewhat reminiscent of wave-particle duality, with the transverse mode corresponding to the wave aspects and the longitudinal mode corresponding to the particle aspects.

A continuity equation for deformations of the spacetime continuum is derived; we find that the divergence of the strain and rotation tensors equals the gradient of the massive volume dilatation, which acts as a source term.

The nature of the spacetime continuum volume force remains to be investigated. In addition, the displacement, dilatational, rotational and strain inhomogeneous wave equations need further investigation.

Submitted on: November 2, 2012 / Accepted on: November 8, 2012

References

1. Millette P.A. On the Decomposition of the Spacetime Metric Tensor and of Tensor Fields in Strained Spacetime. *Progress in Physics*, 2012, v. 4, 5–8.
2. Tartaglia A. A Strained Space-time to Explain the large Scale Properties of the Universe. *International Journal of Modern Physics: Conference Series*, 2011, v. 3, 303–311.
3. Tartaglia A., Radicella N., Sereno M. Lensing in an elastically strained space-time. *Journal of Physics: Conference Series*, 2011, v. 283, 012037.
4. Flügge W. Tensor Analysis and Continuum Mechanics. Springer-Verlag, New York, 1972.
5. Kaku M. Quantum Field Theory; A Modern Introduction. Oxford University Press, Oxford, 1993.
6. Segel L.A. Mathematics Applied to Continuum Mechanics. Dover Publications, New York, 1987.
7. Wald R.M. General Relativity. The University of Chicago Press, Chicago, 1984.

Oblique-Length Contraction Factor in the Special Theory of Relativity

Florentin Smarandache
University of New Mexico 705 Gurley Ave. Gallup, NM 87301, USA. E-mail: smarand@unm.edu

In this paper one generalizes the Lorentz Contraction Factor for the case when the lengths are moving at an oblique angle with respect to the motion direction. One shows that the angles of the moving relativistic objects are distorted.

1 Introduction

According to the Special Theory of Relativity, the Lorentz Contraction Factor is referred to the lengths moving along the motion direction. The lengths which are perpendicular on the direction motion do not contract at all [1].

In this paper one investigates the lengths that are oblique to the motion direction and one finds their Oblique-Length Contraction Factor [3], which is a generalization of the Lorentz Contraction Factor (for $\theta = 0$) and of the perpendicular lengths (for $\theta = \pi/2$). We also calculate the distorted angles of lengths of the moving object.

2 Length-Contraction Factor

Length-Contraction Factor $C(v)$ is just Lorentz Factor:

$$C(v) = \sqrt{1 - \frac{v^2}{c^2}} \in [0, 1] \quad for\ v \in [0, 1] \tag{1}$$

$$L = L' \cdot C(v) \tag{2}$$

where L = non-proper length (length contracted), L' = proper length. $C(0) = 1$, meaning no space contraction [as in Absolute Theory of Relativity (ATR)].

$C(c) = 0$, which means according to the Special Theory of Relativity (STR) that if the rocket moves at speed 'c' then the rocket length and laying down astronaut shrink to zero! This is unrealistic.

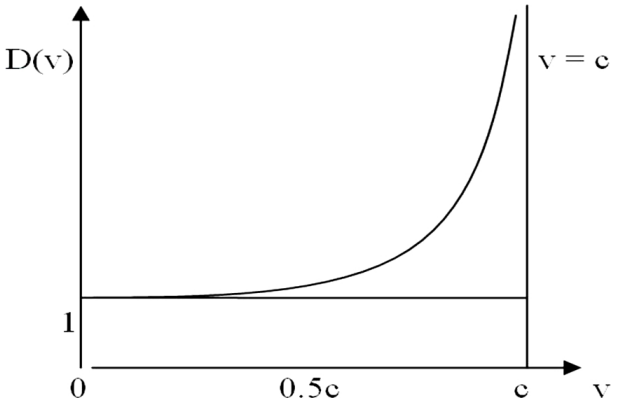

Fig. 1: The graph of the Time-Dilation Factor

3 Time-Dilation Factor

Time-Dilation Factor D(v) is the inverse of Lorentz Factor:

$$D(v) = \frac{1}{\sqrt{1 - \frac{v^2}{c^2}}} \in [1, +\infty] \quad for\ v \in [0, c] \tag{3}$$

$$\Delta t = \Delta t' \cdot D(v) \tag{4}$$

where Δt = non-proper time and, $\Delta t'$ = proper time. $D(0) = 1$, meaning no time dilation [as in Absolute Theory of Relativity (ATR)]; $D(c) = \lim_{v \to c} D(v) = +\infty$, which means according to the Special Theory of Relativity (STR) that if the rocket moves at speed 'c' then the observer on earth measures the elapsed non-proper time as infinite, which is unrealistic. $v = c$ is the equation of the vertical asymptote to the curve of $D(v)$.

4 Oblique-Length Contraction Factor

The Special Theory of Relativity asserts that all lengths in the direction of motion are contracted, while the lengths at right angles to the motion are unaffected. But it didn't say anything about lengths at oblique angle to the motion (i.e. neither perpendicular to, nor along the motion direction), how would they behave? This is a generalization of Galilean Relativity, i.e. we consider the oblique lengths. The length contraction factor in the motion direction is:

$$C(v) = \sqrt{1 - \frac{v^2}{c^2}}. \tag{5}$$

Suppose we have a rectangular object with width W and length L that travels at a constant speed v with respect to an observer on Earth.

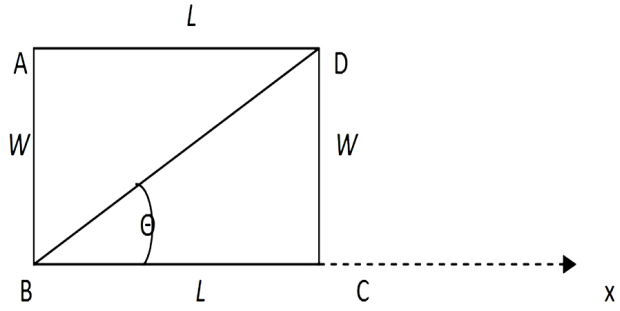

Fig. 2: A rectangular object moving along the x-axis

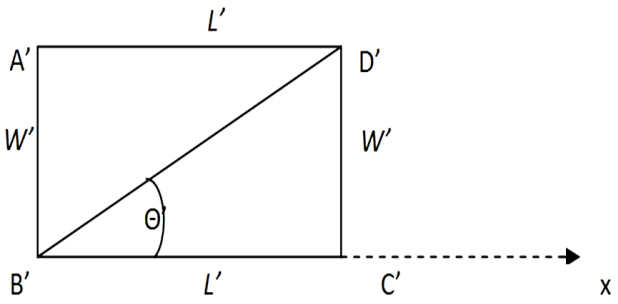

Fig. 3: Contracted lengths of the rectangular object moving along the x-axis

Then its lengths contract and its new dimensions will be L' and W': where $L' = L \cdot C(v)$ and $W' = W$. The initial diagonal of the rectangle ABCD is:

$$\begin{aligned} \delta &= |AC| = |BD| = \sqrt{L^2 + W^2} \\ &= \sqrt{L^2 + L^2 \tan^2\theta} = L\sqrt{1 + \tan^2\theta} \end{aligned} \tag{6}$$

while the contracted diagonal of the rectangle $A'B'C'D'$ is:

$$\begin{aligned} \delta' &= |A'C'| = |B'D'| \\ &= \sqrt{(L')^2 + (W')^2} = \sqrt{L^2 \cdot C(v)^2 + W^2} \\ &= \sqrt{L^2 C(v)^2 + L^2 \tan^2\theta} = L\sqrt{C(v)^2 + \tan^2\theta}. \end{aligned} \tag{7}$$

Therefore the lengths at oblique angle to the motion are contracted with the oblique factor

$$\begin{aligned} OC(v,\theta) &= \frac{\delta'}{\delta} = \frac{L\sqrt{C(v)^2 + \tan^2\theta}}{L\sqrt{1 + \tan^2\theta}} \\ &= \sqrt{\frac{C(v)^2 + \tan^2\theta}{1 + \tan^2\theta}} = \sqrt{C(v)^2\cos^2\theta + \sin^2\theta} \end{aligned} \tag{8}$$

which is different from C(v).

$$\delta' = \delta \cdot OC(v,\theta) \tag{9}$$

where $0 \le OC(v,\theta) \le 1$.

For unchanged constant speed v, the greater is θ in $\left(0, \frac{\pi}{2}\right)$ the larger gets the oblique-length contradiction factor, and reciprocally. By oblique length contraction, the angle

$$\theta \in \left(0, \frac{\pi}{2}\right) \cup \left(\frac{\pi}{2}, \pi\right) \tag{10}$$

is not conserved.

In Fig. 4 the horizontal axis represents the angle θ, while the vertical axis represents the values of the Oblique-Length Contraction Factor $OC(v,\theta)$ for a fixed speed v. Hence $C(v)$ is thus a constant in this graph. The graph, for v fixed, is

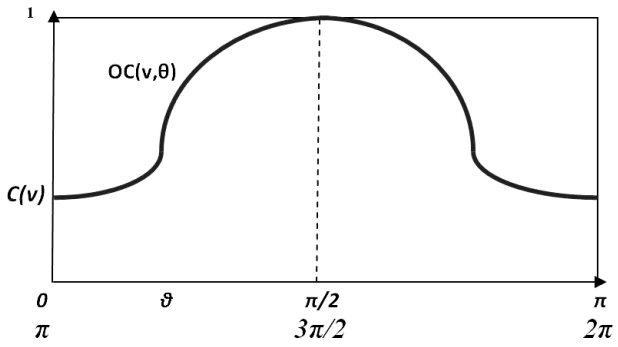

Fig. 4: The graph of the Oblique-Length Contraction Factor $OC(v,\theta)$

periodic of period π, since:

$$\begin{aligned} OC(v,\pi+\theta) &= \sqrt{C(v)^2\cos^2(\pi+\theta) + \sin^2(\pi+\theta)} \\ &= \sqrt{C(v)^2[-\cos\theta]^2 + [-\sin\theta]^2} \\ &= \sqrt{C(v)^2\cos^2\theta + \sin^2\theta} \\ &= OC(v,\theta). \end{aligned} \tag{11}$$

More exactly about the $OC(v,\theta)$ range:

$$OC(v,\theta) \in [C(v), 1] \tag{12}$$

but since $C(v) \in [0,1]$, one has:

$$OC(v,\theta) \in [0,1]. \tag{13}$$

The Oblique-Length Contractor

$$OC(v,\theta) = \sqrt{C(v)^2\cos^2\theta + \sin^2\theta} \tag{14}$$

is a generalization of Lorentz Contractor $C(v)$, because: when $\theta = 0$ or the length is moving along the motion direction, then $OC(v,0) = C(v)$. Similarly

$$OC(v,\pi) = OC(v,2\pi) = C(v). \tag{15}$$

Also, if $\theta = \frac{\pi}{2}$, or the length is perpendicular on the motion direction, then $OC(v,\pi/2) = 1$, i.e. no contraction occurs. Similarly $OC(v, \frac{3\pi}{2}) = 1$.

5 Angle Distortion

Except for the right angles $(\pi/2, 3\pi/2)$ and for the 0, π, and 2π, all other angles are distorted by the Lorentz transform.

Let's consider an object of triangular form moving in the direction of its bottom base (on the x-axis), with speed v, as in Fig. 5:

$$\theta \in \left(0, \frac{\pi}{2}\right) \cup \left(\frac{\pi}{2}, \pi\right) \tag{16}$$

is not conserved.

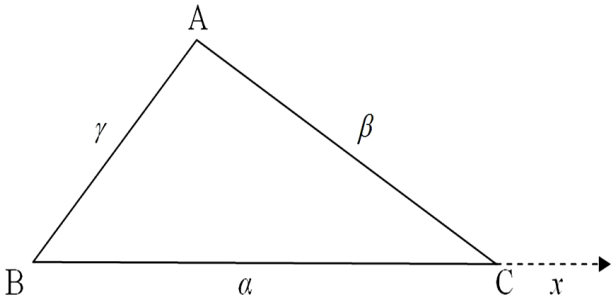

Fig. 5:

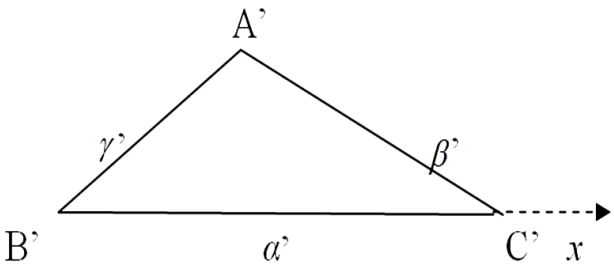

Fig. 6:

The side $|BC| = \alpha$ is contracted with the contraction factor $C(v)$ since BC is moving along the motion direction, therefore $|B'C'| = \alpha \cdot C(v)$. But the oblique sides AB and CA are contracted respectively with the oblique-contraction factors $OC(v, \measuredangle B)$ and $OC(v, \measuredangle \pi - C)$, where $\measuredangle B$ means angle B:

$$\left|A'B'\right| = \gamma \cdot OC(v, \measuredangle B) \tag{17}$$

and

$$\left|C'A'\right| = \beta \cdot OC(v, \measuredangle \pi - C) = \beta \cdot OC(v, \measuredangle A + B) \tag{18}$$

since

$$\measuredangle A + \measuredangle B + \measuredangle C = \pi. \tag{19}$$

Triangle ABC is shrunk and distorted to $A'B'C'$ as in Fig. 6.

Hence one gets:

$$\begin{aligned} \alpha' &= \alpha \cdot C(v) \\ \beta' &= \beta \cdot OC(v, \measuredangle A + B) \\ \gamma' &= \gamma \cdot OC(v, \measuredangle B) \end{aligned} \tag{20}$$

In the resulting triangle $A'B'C'$, since one knows all its side lengths, one applies the Law of Cosine in order to find each angle $\measuredangle A'$, $\measuredangle B'$, and $\measuredangle C'$. Therefore:

$$\measuredangle A' = \arccos \frac{-\alpha^2 \cdot C(v)^2 + \beta^2 \cdot OC(v, \measuredangle A + B)^2 + \gamma^2 \cdot OC(v, \measuredangle B)^2}{2\beta \cdot \gamma \cdot OC(v, \measuredangle B) \cdot OC(v, \measuredangle A + B)}$$

$$\measuredangle B' = \arccos \frac{\alpha^2 \cdot C(v)^2 - \beta^2 \cdot OC(v, \measuredangle A + B)^2 + \gamma^2 \cdot OC(v, \measuredangle B)^2}{2\alpha \cdot \gamma \cdot OC(v) \cdot OC(v, \measuredangle B)}$$

$$\measuredangle C' = \arccos \frac{\alpha^2 \cdot C(v)^2 + \beta^2 \cdot OC(v, \measuredangle A + B)^2 - \gamma^2 \cdot OC(v, \measuredangle B)^2}{2\alpha \cdot \beta \cdot OC(v) \cdot OC(v, \measuredangle A + B)}.$$

As we can see, the angles $\measuredangle A'$, $\measuredangle B'$, and $\measuredangle C'$ are, in general, different from the original angles A, B, and C respectively.

The distortion of an angle is, in general, different from the distortion of another angle.

Submitted on November 12, 2012 / Accepted on November 15, 2012

References

1. Einstein A. On the Electrodynamics of Moving Bodies. *Annalen der Physik*, 1905, v. 17, 891–921.
2. Smarandache F. Absolute Theory of Relativity and Parameterized Special Theory of Relativity and Noninertial Multirelativity. Somipress, Fes, 1982.
3. Smarandache F. New Relativistic Paradoxes and Open Questions. Somipress, Fes, 1983.

Caducity of Idea about Wave Function Collapse as well New Views on Schrödinger's Cat and Quantum Measurements

Spiridon Dumitru

(Retired) Department of Physics, "Transilvania" University, B-dul Eroilor 29, 500036 Brašov, Romania, Phone: +40 746 058 152.
E-mail: s.dumitru42@yahoo.com

Investigated idea was actuated by the old opinion that a measurement of a quantum observable should be regarded a as a single deterministic sampling. But, according to the last decades studies, such observables are veritable random variables and their measurements must imply significant sets of statistical samplings. So one finds the indubitable caducity of the approached idea. Contiguously the respective finding allows to put into a new light the controversial questions like the Schrödinger cat thought experiment or description of quantum measurements.

1 Introduction

A recent highly authorized opinion [1] points out the existing deadlock that: *"There is now ... no entirely satisfactory interpretation of Quantum Mechanics (QM)"*. As major question of that deadlock is recognized as being [2] the problem of Quantum Measurements (QMS), in whose center still stands [3] the Idea about Wave Function Collapse (IWFC). For IWFC, demarcated as above, the most known debates and mainstream publications are reported in [1–3].

Here, in discussing the IWFC question, we try to present a somewhat "unconventional" strategy based on viewpoints promoted in our modest researches about QM, developed over last few decades (see [4, 5] and references).

Firstly we note the fact that, historically, IWFC emerged at the same time with the inaugural ideas regarding the Conventional Interpretation of Uncertainty Relations (CIUR). In the main CIUR started [4, 5] by mixing the theoretical representation (modeling) of a a physical quantity regarding a quantum state/system with a "*fictitious observation*" (done through some thought (gedanken) measuring experiment) of the respective quantity. The mentioned mixing invented and promoted the widespread term of "*observable*" for such a quantity. Below, similarly to the nowadays publications, we will use also the respective term.

After the alluded start CIUR coagulates in a form of an apparent doctrine centered on two main pieces:

(i) Heisenberg's thought-experimental formula and

(ii) Robertson- Schrödinger theoretical relation.

The respective doctrine can be incorporated [4, 5] in few basic items (presumptions/ assertions). A deep analysis shows [4, 5] that the respective items, considered as single or grouped pieces, are incriminated by indubitable facts which are unsurmountable within the framework of CIUR. Then CIUR proves oneself to be deprived of necessary qualities for a valid scientific construction. Consequently, in spite of its apology in many modern texts (see references from [4]), CIUR must be abandoned as a wrong conception without any real value or scientific significance.

In its turn, IWFC continued to be present in important publications (see [1–3] and references), with explicit or implicit references to CIUR. It was aroused by the conflict between two items:

(i) The old opinion that a measurement of a quantum observable should be regarded a as a single deterministic sampling and

(ii) The agreement, enforced by theoretical practice, that studies of quantum systems use probabilistic (non-deterministic) entities (wave functions and observables/operators).

For avoiding conflict and breaking a deadlock it was devised the IWFC which, in different readings, was assumed in a large number of publications. But, as a rule, such assumptions were (and still are) not associated with adequate investigations regarding the truthfulness of the respective idea in relation with the QM questions. A modest investigation of that kind we will try to present below in the next sections.

Firstly, in Section 2, we point out the fact that in the main (i.e. irrespectively of its readings) IWFC is nothing but an useless fiction. Such a fact certainly shows the caducity and failure of the respective idea. In Section 3 we discuss the some aspects contiguous between failure of IWFC and famous subject of Schrödinger's cat thought experiment. Then within Section 4 we argue that alternatively to the IWFC we have to reconsider our views about QM theory in relation with QMS. So, for the readings of the respective theory, we must to consider either a restricted-QM (r-QM) or an extended-QM (e-QM) form. On the one hand the r-QM is essentially the version promoted by usual QM textbooks [6, 7] and it deals exclusively only with the modeling of intrinsic properties for the studied systems. On the other hand e-QM must to contain also obligatorily some additional elements regarding QMS descriptions (i.e. theoretical models about characteristics of measuring devices/procedures). Figuratively speaking e-QM consists in r-QM united with QMS descriptions. An simple exemplification of a QMS description, regarded in the mentioned sense, is presented in the end of the same Section 4. Fi-

nally, in Section 5, are given some concluding remarks about the views from this article.

2 Uselessness of IWFC

Now let us try to estimate the usefulness and truthfulness degrees of IWFC. Such an estimation can be obtained if IWFC is regarded through the details of its constituent elements. The before mentioned regard must be opened by observation that the starting purpose of IWFC was to harmonize the following two conflicting Items (***I***):

- ***I***$_1$ The old opinion (of the same time as CIUR) that a measurement of a quantum observable A, specific to a state/system at atomic scale, should be regarded as a single sampling which gives an unique deterministic result, say a_i;
- ***I***$_2$ The theoretical agreement that, due to the probabilistic character of wave function Ψ describing the alluded state/system, the observable A is endowed with a spectrum (set) of distinct values.

So came into an equivocal sight IWFC knew a lot of debates (see [1–3] and references). In essence, the solution promoted by the respective debates can be summarized within the following Subterfuge (***S***):

- ***S*** The unique result a_i and wave function Ψ, mentioned in items ***I***$_1$ and ***I***$_2$, should be seen (and described) through the wave function collapse $\Psi \longmapsto \psi_i$, where Ψ depicts the considered quantum state/system in its wholeness while ψ_i is the a_i-eigenfunction of the operator $\widehat{A}$ (associated to the observable A) — i.e $\widehat{A}\psi_i = a_i\psi_i$.

For a proper judgment of such a subterfuge we have to reconsider the correctness of the items ***I***$_1$ and ***I***$_2$. In the light of such a reason it must to note that studies from the last decades (see [4–7] and references) consolidated beyond doubt the fact that, mathematically, a quantum observable A (through of the operator $\widehat{A}$) is a true random variable. In a theoretical viewpoint, for a given quantum state/system, such a variable is regarded as endowed with a spectra of values associated with corresponding probabilities (more exactly probability amplitudes). Then, from an experimental perspective, a measurement of a quantum observable requires an adequate number of samplings finished through a significant statistical group of data (outcomes).

Previous opinions about the randomness of quantum observables can be consolidated indirectly by mentioning the quantum-classical probabilistic similarity (see [4, 8]) among the respective observables and macroscopic variables studied within phenomenolgical (thermodynamic) theory of fluctuations [4, 9–14]. In this way let us refer to such a macroscopic random observable $\widehat{\mathbb{A}}$. Its intrinsic (*in*) characteristics are given in details by a continuous spectra of values $\mathcal{A}$ inside of spectra (range) Ω_{in} (i.e. $\mathcal{A} \in \Omega_{in}$), associated with a probability density $w_{in} = w_{in}(\mathcal{A})$. Then for $\widehat{\mathbb{A}}$, in its fullness, a single experimental sampling delivering an unique (individual) result, say $\mathcal{A}_i$, is worthlessly. Such a sampling is not described as a collapse of the probability density $w_{in}(\mathcal{A})$. Moreover a true experimental evaluation of $\widehat{\mathbb{A}}$, in its wholeness and regarded equivalently with a stationary random process, requires [15] an adequate lot of samplings finished through a significant statistical set of individual recordings. In a plausible modeling [16, 17] the mentioned recordings (*rec*) can be described by another probability density $w_{rec} = w_{rec}(\mathcal{A})$.

The above notifications about quantum observables point out clearly the complete incorrectness of item ***I***$_1$. Consequently, even if in the main the item ***I***$_2$ is a true assertion, the subterfuge ***S*** supporting IWFC proves oneself to be nothing but an useless recommendation. Additionally note that, in the mainstream of publications (see [1–3] and references), the respective subterfuge is not fortified with thorough (and genuine) descriptions regarding the collapse $\Psi \longmapsto \psi_i$. Evidently that the above revealed facts ***point out the caducity and failure of IWFC***.

The previous discussions about IWFC lead us also to the following more general Remark (***R***)

- ***R*** A random variable should not be assessed (measured) by an unique deterministic sampling (trial) but by a statistical ensemble of samplings.

3 Contiguities with the Schrödinger's cat thought experiment

As it is well known [18] the famous Schrödinger's cat thought experiment is a subject often displayed in debates (more or less scientifically) about the significance/interpretations of QM constituents. The essential element in the respective experiment is represented by a killing single decay of a radioactive atom. But the radioactive decays are random (probabilistic) events. Then the mentioned killing decay is in fact a twin analogue of the single sampling noted above in item ***I***$_1$ in connection with IWFC.

The mentioned analogy motivates us to discuss on some contiguities among questions specific to the alluded experiment and those regarding IWFC. We think that, according to the above remark ***R***, the main point of such motivated discussions is to mark down the following Notification (***N***)

- ***N*** When the variable of interest has random characteristics it is useless (even forbidden) to design experiences or actions that relies solely on a single deterministic sampling of that variable.

In the light of such notification the Schrödinger experiment appears to be noting but just a fiction (figment) without any scientific value. That is why the statements like: "*the Schrödinger cat thought experiment remains a topical touchstone for all interpretations of quantum mechanics*", must be regarded as being worthlessly. (Note that such statements are

present in many science popularization texts, e.g. in the ones disseminated via the internet.)

The above notification ***N***, argued for quantum level, can be also of non-trivial significance (interest) at macroscopic scale. For illustrating such a significance let us refer to the thought experimental situation of a classical (macroscopic) cousin of the Schrödinger cat. The regarded situation can be depicted as follows. The cousin is placed in a sealed box together a flask of poison and an internal macroscopic hammer. The hammer is connected to an macroscopic uncontrollable (unobservable) sensor located within the circular error probable (CEP) of a ballistic projectile trajectory. Note that a ballistic projectile is a missile whose flight is governed by the laws of classical mechanics. CEP is defined as the radius of a circle, centered about the mean, whose boundary is expected to include the landing points of 50% of the launching rounds (for more details about ballistic terminology see [19]). The experiment consists in launching of a single projectile, without any possibility to observe the point where it hits the ground. Also the projectile is equipped with a radio transmitter which signals the flight time. If the sensor is smitten by projectile the hammer is activated releasing the poison that kills the cousin. But as the projectile trajectory has a probabilistic character (mainly due to the external ballistic factors) the hitting point is placed with the probability of 50% within the surface of CEP where the sensor is located. That is why, after the projectile time of flight and without opening the box, one can not know the state of living for the cousin. So the whole situation of the classical cousin is completely analogous with the one of quantum Schrödinger's cat. Therefore the thought experiment with classical cousin makes evident oneself as another fiction without any real significance.

We can add here another circumstance where the above notification ***N*** is taken into account (and put in practice) in a classical context. Namely we think that, in the last analysis, the respective notification is the deep reason of the fact that in practice of the traditional artillery (operating only with ballistic projectiles but not with propelled missiles) for destroying a military objective one uses a considerable (statistical) number of projectiles but not a single one.

4 Contiguities with descriptions of quantum measurements

It is easy to see the fact that the considerations from Section 2 are contiguous with the question of QMS descriptions. Such a fact require directly certain additional comments which we try to present here below. In our opinion the mentioned question must be regarded within a context marked by the following set of Topics (***T***):

$\boldsymbol{T}_1$ In its plenitude the QM theory must be considered in a r-QM respectively in an e-QM reading. Fundamentally, on the one hand, r-QM deals with theoretical models regarding intrinsic properties of quantum (atomically sized) systems. On the other hand e-QM has to take into account both the characteristics of measured observable/system and the peculiarities of measuring devices/procedures;

$\boldsymbol{T}_2$ Within r-QM a situation (state/system) is described completely by its intrinsic (*in*) wave function Ψ_{in} and operators $\widehat{A_k}$ ($k = 1, 2, \ldots, f$), associated to its specific observables A_k. Expression of Ψ_{in} is distinct for each situation while the operators $\widehat{A_k}$ have the same mathematical representation in many situations. The concrete mathematical expression for Ψ_{in} may be obtained either from theoretical studies (e.g. by solving the adequate Schrödinger equation) or from a priori considerations (not supported by factual studies). For a given state/system the observables A_k can be put into sight through a small number of global *in*-descriptors such are: *in*-mean values, *in*-deviations or second or higher order *in*-moments and correlations (for few examples see below);

$\boldsymbol{T}_3$ A true experimental evaluation of quantum observables can be obtained by means of an adequate numbers of samplings finished through significant statistical sets of individual recordings. For an observable the samplings must be done on the same occurrences (i.e. practically on very images of the investigated observable and state/system). As regards a lot of observables a global and easy sight of the mentioned evaluation can be done by computing from the alluded recordings some (experimental) *exp*-quantifiers (of global significance) such are: *exp*-mean, *exp*-deviation respectively *exp*-higher order moments;

$\boldsymbol{T}_4$ Usually, a first confrontation of theory versus experience, is done by comparing side by side the *in*-descriptors and *exp*-quantifiers mentioned above in $\boldsymbol{T}_2$ and $\boldsymbol{T}_3$. Then, if the confrontation is confirmatory, the investigations about the studied observable/system can be noticed as a fulfilled task. If the alluded confirmation does not appear the study may be continued by resorting to one or groups of the following upgradings (***u***):
$\boldsymbol{u}_1$) An amendment for expression of Ψ_{in}, e.g. through solving a more complete Schrödinger equation or using the quantum perturbation theory;
$\boldsymbol{u}_2$) Improvements of experimental devices and procedures;
$\boldsymbol{u}_3$) Addition of a theoretical description for the considered QMS;

$\boldsymbol{T}_5$ Through the extension suggested in above upgrading $\boldsymbol{u}_3$ the study changes its reading from a r-QM into an e-QM vision, in the sense mentioned in topic $\boldsymbol{T}_1$. Such an extension needs to be conceived as a stylized representation through a mathematic modeling so that it to include both intrinsic elements (regarding observables/states/systems) and measuring details. Also if the

upgrading $\boldsymbol{u}_3$ is adopted then a true confrontation of theory versus experience must be done not as it was mentioned in $\boldsymbol{T}_4$ but by putting face to face the predictions of QMS description with the experimental data.

For an illustration of the topics $\boldsymbol{T}_1$–$\boldsymbol{T}_5$ let us regard as a QM system a spin-less quantum particle in a rectilinear and stationary movement along the Ox axis. The QMS problems will be reported to the orbital observables momentum p_x and energy E, denoted generically by A.

In terms of $\boldsymbol{T}_2$ the probabilistic intrinsic (*in*) characteristics of such particle are depicted by orbital wave function $\Psi_{in} = \Psi_{in}(x)$ (where coordinate x covers the range Ω). The observables A are described by the associated operators $\widehat{A}$ according the QM rules [6,7] (i.e. by $\widehat{p}_x = -i\hbar\frac{\partial}{\partial x}$ respectively by the Hamiltonian $\widehat{H}$). Then from the class of global *in*-descriptors regarding such an observable A can be mentioned the *in*-mean-value $\langle A\rangle_{in}$ and *in*- deviation $\sigma_{in}(A)$ defined as follows

$$\left.\begin{aligned} \langle A\rangle_{in} &= \left(\Psi_{in},\ \widehat{A}\,\Psi_{in}\right) \\ \sigma_{in}(A) &= \sqrt{\left(\delta_{in}\widehat{A}\,\Psi_{in},\ \delta_{in}\widehat{A}\,\Psi_{in}\right)} \end{aligned}\right\}, \qquad (1)$$

where (f, g) denotes the scalar product of functions f and g, while $\delta_{in}\widehat{A} = \widehat{A} - \langle A\rangle_{in}$.

An actual experimental measurement of observable A in sense of $\boldsymbol{T}_3$ must be done through a set of statistical samplings. The mentioned set gives for A as recordings a collection of distinct values $\{\alpha_1, \alpha_2, \alpha_3, \ldots, \alpha_r\}$ associated with the empirical probabilities (or relative frequencies) $\{\nu_1, \nu_2, \nu_3, \ldots, \nu_r\}$. Usually, for a lower synthesized sight about the mentioned measurement, as experimental (*exp*) quantifiers are chosen the *exp*-mean $\langle A\rangle_{exp}$ and *exp*-deviation $\sigma_{exp}(A)$ given through the formulas:

$$\left.\begin{aligned} \langle A\rangle_{exp} &= \sum_{j=1}^{r} \nu_j \cdot \alpha_j \\ \sigma_{exp}(A) &= \sqrt{\sum_{j=1}^{r} \nu_j \cdot \left(\alpha_j - \langle A\rangle_{exp}\right)^2} \end{aligned}\right\}. \qquad (2)$$

The above considerations about an experimental QMS must be supplemented with the following Observations ($\boldsymbol{O}$):

$\boldsymbol{O}_1$ Note that due to the inaccuracies of experimental devices some of the recorded values $\{\alpha_1, \alpha_2, \alpha_3, \ldots, \alpha_r\}$ can differ from the eigenvalues $\{a_1, a_2, a_3, \ldots, a_s\}$ of the operator $\widehat{A}$.

$\boldsymbol{O}_2$ A comparison at first sight between theory and experiment can be done by putting side by side the corresponding aggregate (global) entities (1) and (2). When one finds that the values of compared entities are in near equalities, usually is admitted the following couple of linked beliefs ($\boldsymbol{b}$):

$\boldsymbol{b}_1$) Theory is pretty correct and

$\boldsymbol{b}_2$) Measuring devices/procedures are almost ideal.

Thus, practically, the survey of debated QMS can be regarded as a finished task.

$\boldsymbol{O}_3$ If instead of the mentioned equalities one detects (one or two) flagrant differences at least one of the alluded beliefs ($\boldsymbol{b}_1$) and ($\boldsymbol{b}_2$) is deficient (and unsustainable). Such a deadlock can be avoided by one or groups of the upgradings $\boldsymbol{u}_1$–$\boldsymbol{u}_3$ mentioned above within the topic $\boldsymbol{T}_4$.

Generally speaking the the upgradings $\boldsymbol{u}_1$–$\boldsymbol{u}_2$ are appreciated and worked (explicitly or implicitly) in mainstream literature (see [1–3] and references). But note that, as far as know, for $\boldsymbol{u}_3$ such an appreciation was neither taken into account nor developed in details in the respective literature. It is our modest task to present below a brief exemplification of upgrading $\boldsymbol{u}_3$ in relationship with the QMS question. The presentation is done in some simple terms of information transmission theory.

An information theory modeling for QMS description

In a QMS process the input information regarding the intrinsic (*in*) properties of the measured system is converted in predicted (*pd*) or output information incorporated within the data received on a device recorder. That is why a QMS appears as an *information transmission process* in which the measuring device plays the role of a *information transmission channel*. So the QMS considered above can be symbolized as $\Psi_{in} \Rightarrow \Psi_{pd}$ for the wave function while the operator $\widehat{A}$ remains invariant. Such symbolization is motivated by the facts that, on the one hand the wave function Ψ is specific for each considered situation (state/system) whereas, on the other hand the operator $\widehat{A}$ preserves the same mathematical expression in all (or at least in many) situations. Note that the (quantity of) information is connected with probability densities $\rho_\eta(x)$ and currents (fluxes) $j_\eta(x)$ ($\eta = in, pd$) defined in terms of $\Psi_\eta(x)$ as in usual QM [4–7]. Add here the fact that $\rho_\eta(x)$ and $j_\eta(x)$ refer to the positional respectively the motional kinds of probabilities. Experimentally the two kinds of probabilities can be regarded as measurable by distinct devices and procedures. Besides, as in practice, one can suppose that the alluded devices are stationary and linear. Then, similarly with the case of measurements regarding classical random observables [4, 16, 17], in an informational reading, the essence of here discussed QMS description can be compressed [4, 17] through the relations:

$$\left.\begin{aligned} \rho_{pd}(x) &= \int \Gamma(x, x')\,\rho_{in}(x')\,dx' \\ j_{pd}(x) &= \int \Lambda(x, x')\,j_{in}(x)\,dx' \end{aligned}\right\}. \qquad (3)$$

Here the kernels $\Gamma(x, x')$ and $\Lambda(x, x')$ include as noticeable parts some elements about the peculiarities of measuring devices/procedures. Mathematically, $\Gamma(x, x')$ and $\Lambda(x, x')$ are normalized in respect with both x and x'. Note that QMS becomes nearly ideal when both $\Gamma(x, x') \to \delta(x - x')$ and $\Lambda(x, x') \to \delta(x - x')$, ($\delta(x - x')$ being the Dirac's δ function). In all other cases QMS appear as non-ideal.

By means of the probability density $\rho_{pd}(x)$ and current $j_{pd}(x)$ can be computed [4] some useful expressions like $\Psi^*_{pd}(x)\,\widehat{A}\,\Psi_{pd}(x)$. Then, for observable A, it is possible to evaluate global indicators of predicted (pd) nature such are pd-mean $\langle A\rangle_{pd}$ and pd-deviation $\sigma_{pd}(A)$ defined, similarly with (1), as follows

$$\left.\begin{aligned} \langle A\rangle_{pd} &= \left(\Psi_{pd}, \widehat{A}\Psi_{pd}\right) \\ \sigma_{pd}(A) &= \sqrt{\left(\delta_{pd}\widehat{A}\Psi_{pd}, \delta_{pd}\widehat{A}\Psi_{pd}\right)} \end{aligned}\right\}. \tag{4}$$

If as regards a quantum observable A, besides a true experimental evaluation, for its measuring process one resorts to a (theoretical/informational) QMS description of the above kind the pd-indicators (4) must be tested by comparing them with their experimental (factual) correspondents (i.e. exp-quantifiers) given in (2).

When the test is confirmatory both theoretical descriptions, of r-QM intrinsic properties of system respectively of QMS, can be considered as adequate and therefore the scientific task can be accepted as finished. But, if the alluded test is of invalidating type, at least one of the mentioned descriptions must be regarded as inadequate and the whole question requires further investigations.

For an impressive illustration of the above presented informational QMS description we consider as observable of interest the energy $A = E = H$ regarding a QM harmonic oscillator. The operator $\widehat{H}$ associated to the respective observable is the Hamiltonian $\widehat{H} = -\frac{\hbar^2}{2m}\frac{d^2}{dx^2} + \frac{1}{2}m\,\omega^2 x^2$ (m and ω denote the mass respectively the angular frequency of oscillator). The oscillator is considered to be in its lower energetic level, whose intrinsic state is described by the wave function $\Psi_{in}(x) \propto \exp\left\{-\frac{x^2}{4\sigma^2}\right\}$ (here $\sigma = \sigma_{in}(x) = \sqrt{\frac{\hbar}{2m\omega}}$ denote the in-deviation of coordinate x). Then, because Ψ_{in} is a real function, for the considered state one finds $j_{in} = 0$ — i.e. the probability current is absent.

So for the regarded QMS description in (3) remains of interest only first relation dealing with the change $\rho_{in} \to \rho_{pd}$ of the probability density through the kernel $\Gamma(x, x')$. If the supposed measuring device has high performances $\Gamma(x, x')$ can be taken [4] of Gaussian form i.e. $\Gamma(x, x') \propto \exp\left\{-\frac{(x-x')^2}{2\gamma^2}\right\}$, γ being the error characteristic of the respective device. It can been seen that in the case when $\gamma \to 0$ the kernel $\Gamma(x, x')$ degenerates into the Dirac function $\delta(x - x')$. Then $\rho_{pd} = \rho_{in}$. Such a case corresponds to an ideal measurement. Differently, when $\gamma \neq 0$ one speaks of non-ideal measurements.

In the above modeling of QMS description for the energy $A = E = H$ one obtains [4] the following in respectively pd means and deviations

$$\langle H\rangle_{in} = \frac{\hbar\omega}{2}\,; \quad \sigma_{in}(H) = 0\,, \tag{5}$$

$$\langle H\rangle_{pd} = \frac{\omega\left[\hbar^2 + \left(\hbar + 2m\omega\gamma^2\right)^2\right]}{4\left(\hbar + 2m\omega\gamma^2\right)}\,, \tag{6}$$

$$\sigma_{pd}(H) = \frac{\sqrt{2}m\omega^2\gamma^2\left(\hbar + m\omega\gamma^2\right)}{\left(\hbar + 2m\omega\gamma^2\right)}\,. \tag{7}$$

Relations (5) and (7) show that even if Ψ_{in} has the quality of an eigenfunction for $\widehat{H}$ (as $\sigma_{in}(H) = 0$), due to the measurement Ψ_{pd} is deprived of such a quality (because $\sigma_{pd}(H) \neq 0$).

5 Concluding remarks

We point out, on the one hand, the historical emergence of the IWFC from the conflict between the items $\boldsymbol{I}_1$ and $\boldsymbol{I}_2$ mentioned in Section 2. Then we remind the fact that, on the other hand, the modern studies certify the random characteristics of quantum observables. Therefore a true measurement of such an observable requires a whole set of statistically significant samplings. The respective requirement invalidate indubitably the alluded item $\boldsymbol{I}_1$. So IWFC is proved as a caducous and useless recommendation.

Contiguously the respective proof allows to put into a new light the famous Schrödinger's cat thought experiment. We argue in Section 3 that Schrödinger's experiment is noting but just a fiction without any scientific value. The argumentation relies on the notification that: "When the variable of interest has random characteristics it is useless (even forbidden) to design experiences or actions that relies solely on a single deterministic sampling of that variable". The same notification is useful in appreciating of some non-quantum problems such are a Schrödinger's-type experiment with a classical cat or statistical practices in traditional artillery.

The question of IWFC caducity is contiguous also with the problem of QMS descriptions. That is why in Section 4 we present some brief considerations about the respective problem. Thus we propose that QM theory to be regarded either in a r-QM or in an e-QM reading, as it refers to the studied observables and systems without or with taking into account the QMS descriptions. The proposal is consolidated with simple illustration regarding a spin-less quantum oscillator in a rectiliniar and stationary movement along the Ox axis. Particularly we suggest an approach of QMS descriptions based on information transmission theory.

Of course that other different approaches about QMS descriptions can be imagined. They can be taken into account for extending QM theory towards an e-QM reading, as complete/convincing as possible.

Submitted on: November 15, 2012 / Accepted on: November 18, 2012

References

1. Weinberg S. Collapse of the state vector. *Physical Review A*, 2012, v. 85, 062116; arXiv: 1109.6462.
2. Ghirardi G. Collapse theories. *The Stanford Encyclopedia of Philosophy*, Winter 2011 Edition, Stanford.
3. Omnes R. Decoherence and wave function collapse. *Foundations of Physics*, 2011, v. 41, 1857–1880.
4. Dumitru S. Reconsideration of the uncertainty relations and quantum measurements. *Progress in Physics*, 2008, v. 2, 50–68.
5. Dumitru S. Do the uncertainty relations really have crucial significances for physics? *Progress in Physics*, 2010, v. 4, 25–29.
6. Cohen-Tannoudji C., Diu B., Laloe F. Quantum Mechanics. Vol. I. J. Wiley/Herman, NY–Paris, 1977.
7. Schwabl F. Quantum Mechanics. 2nd. rev. ed., Springer, Berlin, 1995.
8. Dumitru S. The Plank and Boltzmann constants as similar generic indicators of stochasticity: some conceptual implications of quantum-nonquantum analogies. *Physics Essays*, 1993, v. 6, 5–20.
9. Munster A. Statistical Thermodynamics. Vol. I, Springer, Berlin, 1969.
10. Landau L., Lifchitz E. Physique Statistique. Mir, Moscou, 1984.
11. Schwabl F. Statistical Mechanics. Springer, Berlin 2002.
12. Dumitru S. Fluctuations and thermodynamic inequalities. *Physica Scripta*, 1974, v. 10, 101–103.
13. Dumitru S., Boer A. Fluctuations in the presence of fields — phenomenological Gaussian approximation and a class of thermodynamic inequalities. *Physical Review E*, 2001, v. 64, 021108.
14. Boer A., Dumitru S. Higher order correlations in the presence of fields. *Physical Review E*, 2002, v. 66, 046116.
15. Korn G.A., Korn T.M. Mathematical Handbook for Scientists and Engineers. Chap. 19, McGraw Hill, New York 1968; Russian version — Nauka, Moscow, 1977.
16. Dumitru S. Phenomenological theory of recorded fluctuations. *Physics Letters A*, 1974, v. 48, 109–110.
17. Dumitru S., Boer A. On the measurements regarding random observables. *Romanian Journal of Physics*, 2008, v. 53, 1111–1116; http://www.nipne.ro/ rjp/2008_53_9-10.html
18. Schrödinger's cat. http://en.wikipedia.org/wiki/Schrödinger's_cat
19. Category: Ballistics. http://en.wikipedia.org/wiki/Category:Ballistics

Gravitational Field Shielding by Scalar Field and Type II Superconductors

B. J. Zhang*, T. X. Zhang†, P. Guggilia‡, and M. Dohkanian§

*Department of Physics and Astronomy, Vanderbilt University, Nashville, TN 37235. E-mail: bojun.zhang@vanderbilt.edu
*Department of Physics, Alabama A & M University, Normal, Alabama 35762.
†Department of Physics, Alabama A & M University, Normal, Alabama 35762. E-mail: tianxi.zhang@aamu.edu
‡Department of Physics, Alabama A & M University, Normal, Alabama 35762.
§Department of Physics, Alabama A & M University, Normal, Alabama 35762.

The gravitational field shielding by scalar field and type II superconductors are theoretically investigated. In accord with the well-developed five-dimensional fully covariant Kaluza-Klein theory with a scalar field, which unifies the Einsteinian general relativity and Maxwellian electromagnetic theory, the scalar field cannot only polarize the space as shown previously, but also flatten the space as indicated recently. The polarization of space decreases the electromagnetic field by increasing the equivalent vacuum permittivity constant, while the flattening of space decreases the gravitational field by decreasing the equivalent gravitational constant. In other words, the scalar field can be also employed to shield the gravitational field. A strong scalar field significantly shield the gravitational field by largely decreasing the equivalent gravitational constant. According to the theory of gravitational field shielding by scalar field, the weight loss experimentally detected for a sample near a rotating ceramic disk at very low temperature can be explained as the shielding of the Earth gravitational field by the Ginzburg-Landau scalar field, which is produced by the type II superconductors. The significant shielding of gravitational field by scalar field produced by superconductors may lead to a new spaceflight technology in future.

1 Introduction

Gravitation is one of the four fundamental interactions of nature. According to the Newtonian universal law of gravitation, any two objects in the universe attract each other with a force that is directly proportional to the product of their masses and inversely proportional to the square of the distance between them. According to the Einsteinian general theory of relativity, gravitation is directly related to the curvature of spacetime. The Schwarzschild solution of the general relativity for a static spherically symmetric body predicts the perihelion precession of planets, the deflection of distant star light by the Sun, the gravitational redshift of Sun's light, and the time delay of radar echoes, which have been well tested by the measurements [1-4].

To study the shielding of the gravitational field in analogous to the shielding of the electromagnetic field, Majorana [5] in 1920 modified the Newtonian gravitational field of an object with a nonzero extinction coefficient $h \neq 0$ as

$$g = g_N \exp\left[-h \int \rho(r) dr\right], \quad (1)$$

where $g_N \equiv G_0 M/r^2$ is the Newtonian gravitational field with G_0 the gravitational constant, M the mass of the object, and r the radial distance from the object center; ρ is the mass density of the object; h is the extinction coefficient. For a spherical object with a constant mass density and radius R, Eq. (1) after integrated becomes

$$g = g_N \exp\left(-\frac{3hM}{4\pi R^2}\right). \quad (2)$$

Laboratory measurements constrained $h \lesssim 10^{-15}$ m^2/kg [6-7]. Space measurements gave $h \lesssim 10^{-19}$ m^2/kg [8-9]. These measurements indicated that the gravitational field shielding is negligible or undetectable in the case of weak fields.

On the other hand, Kaluza [10] in 1921 proposed a five-dimensional (5D) theory to unify the Einsteinian general relativity and Maxwellian electromagnetic theory. The geometric structure and property of the 5D spacetime were then studied by Klein [11-12]. The early Kaluza-Klein (K-K) theory of unification was further developed with a scalar field [13], which can modify both the electromagnetic and gravitational fields. Some previous studies have shown that the scalar field can reduce the electromagnetic field of a charged object and thus polarize the space around the charged object or shield the electromagnetic field from the charged object [14-15]. It is equivalent to increase the free space permittivity constant. Recently, we has shown, in accord with a 5D fully covariant K-K theory, that the scalar field can also reduce the gravitational field of a body and thus flatten the space around the body or shield the gravitational field from the body [16]. It is equivalent to decrease the gravitational constant in and around the body [17].

The scalar field that was introduced to the cosmology in various models has also been considered as a candidate of dark energy for the acceleration of the universe. As the cosmic expansion, the scalar field of the universe changes over time and became repulsive about many years ago and then overcome the gravitational force to accelerate the expansion of the universe. In addition, we have recently shown that a

massive and compact neutron star can generate a strong scalar field, which can significantly shield or reduce its gravitational field, and thus can be more massive and more compact. The mass-radius relation developed under this type of modified gravity with a scalar field can be consistent with the measurements of neutron stars [18].

In this paper, we will investigate the gravitational field shielding by scalar field and type II superconductors. We suggest that the scalar field generated by the type II superconductors has the same physics and thus addable to the scalar field generated by any other types of matter. According to the five-dimensional fully covariant K-K theory with a scalar field, the scalar field of an object can shield its gravity or decrease the equivalent gravitational constant in or around the object. Therefore, the Ginzburg-Lanadu scalar field [19-20] generated by type II superconductors, if it has a similar physics and thus addable to the scalar field of the Earth, can cause a sample to lose a few percent of its weight or the Earth's gravity as detected by [21]. This study will quantitatively analyze the gravitational field shielding due to the scalar field generated by type II superconductors.

2 Gravitational Shielding by Scalar Field

In the 5D fully covariant K-K theory with a scalar field that has successfully unified the 4D Einsteinian general relativity and Maxwellian electromagnetic theory, the gravitational field of a static spherically symmetric object in the Einstein frame was obtained from the 5D equation of motion of matter as [16, 22]

$$g = \frac{c^2}{2\Phi^2}\left(\frac{d\Phi}{dr} + \Phi\frac{d\nu}{dr}\right)e^{\nu-\lambda}, \tag{3}$$

where the metric and scalar field solutions of the 5D fully covariant K-K theory are given by [23]

$$e^{\nu} = \Psi^2\Phi^{-2}, \tag{4}$$

$$e^{\lambda} = \left(1 - \frac{B^2}{r^2}\right)^2\Psi^{-2}, \tag{5}$$

$$\Phi^2 = -\alpha^2\Psi^4 + (1+\alpha^2)\Psi^{-2}, \tag{6}$$

with

$$\Psi = \left(\frac{r-B}{r+B}\right)^{1/\sqrt{3}}, \tag{7}$$

$$B = \frac{G_0 M}{\sqrt{3(1+\alpha^2)}c^2}, \tag{8}$$

$$\alpha = \frac{Q}{2\sqrt{G_0}M}. \tag{9}$$

Here M and Q are the mass and electric charge of the object.

For a neutral object (i.e., $\alpha = 0$ or $Q = 0$), the gravitational field Eq. (3) obtained from the 5D fully covariant K-K theory with a scalar field can be simplified to [17]

$$g = g_N\left(1 - \frac{B^2}{r^2}\right)^{-3}\Phi^{-7} = \frac{1}{64}\left(\Phi^{\sqrt{3}} + 1\right)^6\Phi^{-7-3\sqrt{3}}, \tag{10}$$

where the scalar field Φ and the critical or singular radius B of the K-K solution are simplified as

$$\Phi = \Psi^{-1}, \quad B = \frac{G_0 M}{\sqrt{3}c^2}. \tag{11}$$

The singular radius B of the K-K solution is a factor of $\sqrt{3}/6$ times smaller than the Schwarzschild radius. Eq. (10) indicates that the gravitational field obtained from the 5D fully covariant K-K theory with a scalar field is influenced by the scalar field Φ. This type of influence can be understood as the gravitational field shielding by scalar field.

In the case of weak fields (i.e., $B \ll r$ or in other words, when the gravitational potential energy of a particle is much smaller than the rest energy of the particle), we can approximately simplify g as

$$g = g_N\left(1 - \frac{14G_0 M}{3c^2 r}\right) = 1 - 7\delta\Phi. \tag{12}$$

Here we have replaced $\Phi = 1 + \delta\Phi$. Comparing the field at the surface of object between Eq. (2) and Eq. (12), we obtain the extinction coefficient as

$$h = \frac{56\pi G_0 R}{9c^2} \sim 1.5\times10^{-26}R, \tag{13}$$

which is about $h \sim 1.5\times10^{-26}$ m^2/kg for an object with radius of one meter and about $h \sim 10^{-19}$ m^2/kg for an object with the size of Earth. It is seen that the gravitational field shielding by scalar field is undetectable in a laboratory experiment since the extinction coefficient is very small for an object with laboratory scale size. For an object with Earth's radius $R \sim 6.4\times10^6$ m, the extinction coefficient is $h \sim 10^{-19}$, the order of the space measurements. This analysis is valid only for the case of weak fields.

The reason for the gravitational field to be shed is the significance of the scalar field, which rapidly increases as the radial distance approaches to the singular radius, i.e., $r \to B$ (Top panel of Figure 1). The gravitational field is inversely proportional to the scalar field with a power of $7 - 3\sqrt{3} \sim 1.8$ if $\Phi \gg 1$ as shown in Eq. (10). By writing Eq. (10) as the Newtonian form of the gravitational field

$$g = \frac{GM}{r^2}, \tag{14}$$

where the G is defined as an equivalent gravitational constant

$$G = G_0\left(1 - \frac{B^2}{r^2}\right)^{-3}\Phi^{-7} = \frac{1}{64}\left(\Phi^{\sqrt{3}} + 1\right)^6\Phi^{-7-3\sqrt{3}}. \tag{15}$$

This suggests that the gravitational field shielding occurs because the strong scalar field significantly varies or decreases the equivalent gravitational constant around the object.

To investigate the gravitational shielding by scalar field in the case of strong fields, we plot in the bottom panel of Figure 1 the gravitational field or constant ratio (g/g_N or G/G_0)

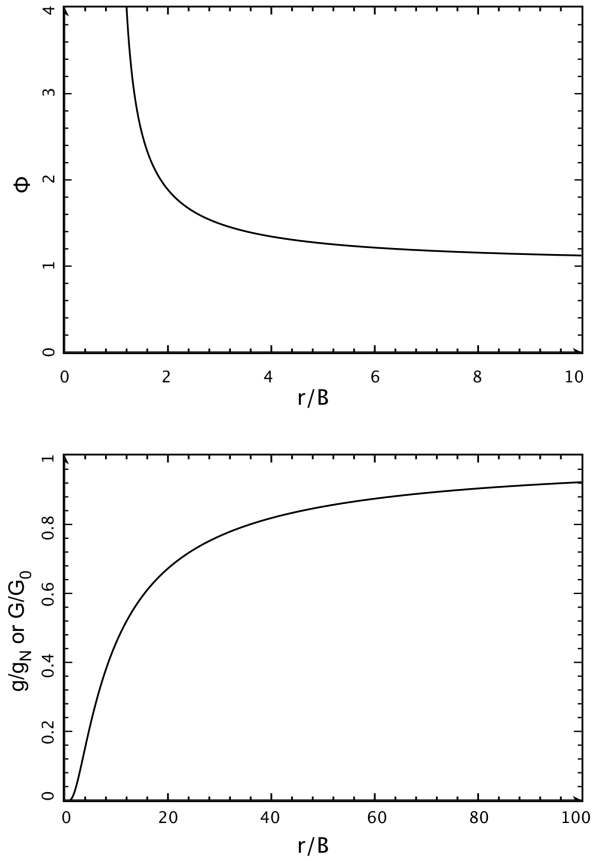

Fig. 1: Scalar field and gravitational field shielding by scalar field. Top panel: the scalar field (Φ) and bottom panel: the ratio between the K-K and Newtonian gravitational field or constant (g/g_N or G/G_0) of a neutral object vs. the normalized radial distance r/B [17].

as a function of the radius distance (r/B) [17]. It is seen that the gravitational field is significantly reduced (or shed) by the scalar field when r is comparable to B. For instances, the gravitational field is shed by $\sim$ 10% (or the percentage of weight loss for a sample object) at $r = 100B$, by $\sim$ 20% at $r = 35B$, by $\sim$ 40% at $r = 15B$, by $\sim$ 80% at $r = 5B$, and $\sim$ 100% at $r = B$. Therefore, for a weak field, the relative difference of the field is small and thus the shielding effect is negligible. For a strong field, however, the gravitational field or constant ratio is small or the relative difference of the field is large so that the shielding effect is significant. The gravitational field of an object, when $r = B$ or its mass-to-radius ratio is about $M/r \simeq 2 \times 10^{27}$ kg/m, is completely shed by the strong scalar field or by the huge amount of mass enclosed. As shown in the top panel of Figure 1, the scalar field increases as r approaches B. The scalar field is ~ 1.4 at $r = 4B$, ~ 4 at $r = 1.6B$, and tends to infinity when $r \to B$. When the scalar field is unity (i.e., $\Phi = 1$), we have $g/g_N = 1$, which refers to that the gravitational field is not shed. When the scalar field significantly departs from the unity, for instance, at $\Phi = 1.2$ or $\delta\Phi = 0.2$, we have $g/g_N \simeq 0.3$, which refers to that a 70% of gravitational field is shed by the scalar field.

3 Gravitational Shielding by Type II Superconductors

About two decades ago, Podkletnov and Nieminen [21] experimentally discovered that a bulk sintered ceramic (type II superconductor) disk of $YBa_2Cu_3O_{7-x}$ can have a moderate shielding effect against the gravitational field. This effect increases with the speed of disk rotation and also depends on the temperature. It was suggested that the shielding effect is the result of a certain state of energy that exists inside the crystal structure of the superconductor at low temperature. This state of energy changes the interactions between electromagnetic, nuclear, and gravitational fields inside a superconductor, and is responsible for the observational phenomena. But a shielding physics has not yet been developed.

Here, we propose a possible shielding physics to explain this phenomena. According to the Ginzburg-Landau theory, a rotating disk of type II superconductor at the phase transition with low temperature (e.g., 70K) generates a scalar field [19-20, 24-30] that varies the equivalent gravitational constant along with the Earth scalar field in and around the superconductor and thus shields the gravitational field of the Earth. According to the 5D fully covariant K-K theory and solution, the scalar field of the Earth at the surface is about the unity because $B \ll r$. Now, in the Podkletnov and Nieminen's experiment, the ceramic (or type II) superconductor can produce an extra scalar field $\delta\Phi$, which is responsible for the small weight loss of the sample.

Based on the previously-developed Landau theory of the second-order phase transition, Ginzburg and Landau [19, 30] showed that the free energy F of a superconductor per unit volume near the transition can be expressed in terms of a complex order parameter field ψ by

$$F = F_n + a|\psi|^2 + \frac{b}{2}|\psi|^4 + \frac{1}{2m}|(-i\hbar \bigtriangledown - 2e\vec{A})\psi|^2 + \frac{|\vec{B}|^2}{2\mu_0}, \quad (16)$$

where F_n is the free energy in the normal phase, a and b are phenomenological parameters, m is an effective mass, e is the charge of electron, $\vec{A}$ is the magnetic vector potential and $\vec{B}$ is the magnetic field. The absolute value of the complex order parameter field $|\psi|$ can be considered as a real scalar field called Ginzburd-Landau scalar field denoted here by $\Phi_{\rm GL} \equiv |\psi|$. Then, in Eq. (16), the second and third terms are the scalar field potential energy; the first part of the fourth term is the scalar field kinetic energy; and the other parts of the fourth term give the energy that couples the scalar field and magnetic field; and the last term is the energy of magnetic field.

By minimizing F with respect to fluctuations of ψ and $\vec{A}$, one can derive the Ginzburg-Landau equations [30-31]

$$a\psi + b|\psi|^2\psi + \frac{1}{2m}(-i\hbar \bigtriangledown - 2e\vec{A})^2\psi = 0, \quad (17)$$

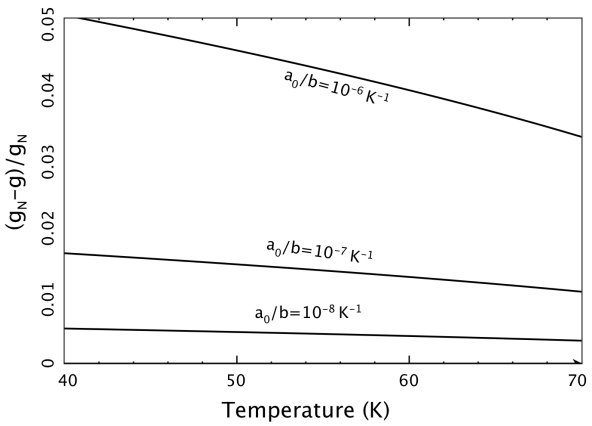

Fig. 2: Gravitational field shielding by scalar field associated with type II superconductor disk. The percentage of weight loss of the sample is plotted as a function of the temperature of the type II superconductors [17].

$$\vec{j} = \frac{2e}{m}\mathrm{Re}[\psi^*(-i\hbar\bigtriangledown - 2e\vec{A})\psi], \tag{18}$$

where $\vec{j}$ is the electrical current density, which is real.

For a homogeneous superconductor, in which $\vec{j} = 0$, Eq. (17) can be simplified to

$$a\psi + b|\psi|^2\psi = 0. \tag{19}$$

The solution $\psi = 0$ is trivial and corresponds to the normal state of the superconductor above the superconducting transition temperature T_c. The non-trivial solution of Eq. (19) determines the Ginzburg-Landau scalar field

$$\Phi_{\mathrm{GL}} \equiv |\psi| = \sqrt{-\frac{a}{b}} = \sqrt{-\frac{a_0}{b}(T - T_c)}. \tag{20}$$

Here, we have assumed the temperature dependence of a to be $a = a_0(T - T_c)$ with positive ratio a_0/b. For the YBCO superconductor, $T_c \sim 93$ K. Suggesting all types of scalar fields to be similar in physics and addable, we obtain the total scalar field in or around a type II superconductor,

$$\Phi_{\mathrm{total}} = \Phi_{\mathrm{Earth}} + \Phi_{\mathrm{GL}}$$
$$= 1 + \frac{2G_0M_{\mathrm{E}}}{3c^2R_{\mathrm{E}}} + \sqrt{-\frac{a_0}{b}(T - T_c)}, \tag{21}$$

where M_{E} and R_{E} are Earth's mass and radius.

To quantitatively study the gravitational field shielding by the Ginzburg-Landau scalar field along with the Earth scalar field, we plot in Figure 2 the weight relative loss of the sample or the gravitational field relative change at the sample as a function of the temperature of the type II superconductor. It is seen that the weight relative loss of the sample or the gravitational field relative change increases as the temperature decreases or as the ratio a_0/b increases. At $T \sim 70$ K and $a_0/b \sim 10^{-8} - 10^{-6}$, the weight relative loss or the gravitational field relative change is $\sim 0.5 - 3\%$, which can be the order of measurements [21].

4 Discussion and Conclusion

For a rotating disk of type II superconductor, the acceleration of inertially moving cooper pairs in the superconductor is equivalent to a gravitational field, which may couple with the Ginzburg-Landau scalar field to produce an extra shielding effect on gravity as shown in [21]. In future study, we will quantitatively analyze the rotation dependence for the gravitational field shielding by the Ginzburg-Landau scalar field of type II superconductors.

As a consequence, we have analytically studied the gravitational field shielding by scalar field and type II superconductors, in accord with the 5D fully covariant K-K theory with a scalar field and the Ginzburg-Landau theory for superconductors. The results have indicated that the gravitational field shielding by the scalar field of a body is very small at an undetectable level if the field is weak. The extinction coefficient derived from the comparison with the Majorana's gravitational field shielding theory is consistent with laboratory and space measurements. In the case of strong fields, however, the gravitational field shielding effect can be significant. This will have important applications in strong-field astrophysics and greatly impact the physics of supernova explosions, the models of neutron stars for their mass-radius relations, and the theory of black hole formations.

Detection of the gravitational field shielding is a challenge to a laboratory experiment, but possible especially when the object becomes a superconductor. A type II superconductor may produce a significant Ginzburg-Landau scalar field at the phase transition and thus may be used to shield gravity as claimed by [21]. The result obtained from this study can be consistent with the measurements. The significant shielding of gravitational field by scalar field produced by superconductors may lead to a new spaceflight technology in future. The gravitational field shielding by type II superconductors still need further experimentally confirmed.

Acknowledgements

This work was supported by the NASA EPSCoR grant (NNX 07AL52A), NSF CISM grant through Boston University, NS F REU program at AAMU, and AAMU Title III programs and by also the National Natural Science Foundation of China (G40890161). The authors thank reviewers and editors for their scientific reviews and editions.

Submitted on: November 19, 2012 / Accepted on November 23, 2012

References

1. Shapiro I. I. Fourth Test of General Relativity. *Physical Review Letters*, 1964, v. 13, 789–791.
2. Shapiro I. I. et al. Fourth Test of General Relativity: New Radar Result. *Physical Reviewer Letters*, 1971, v. 26, 1132–1135.

3. Will C. M. Theory and Experiment in Gravitational Physics, Cambridge Univ. Press, 1993.
4. Will C. M. The confrontation between general relativity and experiment. *Living Reviews in Relativity*, 2006, v. 9, 5–100.
5. Majorana Q. On gravitation: Theoretical and experimental researches. *Philosophical Magazine*, 1920, v. 39, 488–504.
6. Unnikrishnan C. S., Gillies G. T. New limits on the gravitational Majorana screening from the Zurich G experiment. *Physical Review D*, 2000, v. 61, id. 101101.
7. Caputo M. On new limits of the coefficient of gravitation shielding. *Journal of Astrophysics and Astronomy*, 2006, v. 27, 439–441.
8. Eckhardt D. H. Gravitational shielding. *Physical Review D*, 1990, v. 42, 2144–2145.
9. Yang X. S., Wang Q. S. Gravity anomaly during the Mohe total solar eclipse and new constraint on gravitational shielding parameter. *Astrophysics and Space Science*. 2002, v. 282, 245–253.
10. Kaluza T. On the problem of unity in physics. *Sitzungsber Preuss Aklad. Wiss. Berlin Math. Phys.* K1, 1921, 966–972.
11. Klein O. Quantum theory and five-dimensional theory of relativity. *Zeitschrift für Physik*, 1926a, v. 37, 895–906.
12. Klein O. The atomicity of electricity as a quantum theory law. *Nature*, 1926b, v. 118, 516–516.
13. Jordan P. Erweiterung der projektiven relativitastheorie. *Annual Physics* (Leipzig), 1947, v. 1, 219–228.
14. Nodvik J. S. Suppression of singularities by the g^{55} field with mass and classical vacuum polarization in a classical Kaluza-Klein theory. *Physical Review Letters*, 1985, v. 55, L2519–L2522.
15. Dragilev V. M. Vacuum polarization of a scalar field in anisotropic multidimensional cosmology. *Theoretical Mathematics in Physics*, 1990, v. 84, 887–893.
16. Zhang T. X. Gravitational field shielding and supernova explosion. *Astrophysical Journal Letters*, 2010, v. 725, L117–L121.
17. Zhang B. J. Gravitational field shielding and neutron star mass-radius relation. *Research Report* (Alabama A & M University), 2011.
18. Zhang B. J., Zhang, T. X., Guggila, P., Dokhanian, M. Neutron star mass-radius relation with gravitational field shielding by scalar field-Gravitational field shielding by scalar field and neutron star. *Research in Astronomy and Astrophysics*, 2011, Submitted.
19. Ginzburg V. l., Landau L. D. On the theory of superconductivity. *Zh. Eksp. Teor. Fiz.*, 1950, v. 20, 1064–1082.
20. Robertson G. A. Manipulating the vacuum scalar field with superconductor: A search for exotic material. *AIP Conference Proceedings*, 2005, v. 746, 1371–1378.
21. Podkletnov E., Nieminen R. A possibility of gravitational force shielding by bulk $YBa_2Cu_3O_{7-x}$. *Physica C*, 1992, v. 203, 441–444.
22. Zhang T. X. Gravitationless black hole. *Astrophysics and Space Science*, 2011, v. 334, 311–316.
23. Zhang T. X. Electric redshifts and Quasars. *Astrophysical Journal Letters*, 2006, v. 636, L61–L64.
24. Kajantie K., Karjalainen M., Laine M., Peisa J. Masses and phase structure in the Ginzburg-Landau model. *Physical Review B*, 1998, v. 57, 3011–3016.
25. Kiometzis M., Kleinert H., Schakel A. M. J. Critical exponents of the superconducting phase transition. *Physical Review Letters*, 1994, v. 73, 1975–1977.
26. Rosenstein B., Li D. P. Ginzburd-Landau theory of type II superconductors in magnetic field. *Reviews of Modern Physics*, 2010, v. 82, 109–168. bibitem Li N., Noever D., Robertson T., Koczer R., Brantley, W. Static test for a gravitational force coupled to type II YBCO superconductor, *Physica C*, 1997, v. 281, 260–267.
27. Unnikrishan C. S. Does a superconductor shield gravity? *Physica C*, 1996, v. 266, 133–137.
28. Wu N. Gravitational shielding effect in gauge theory of gravity. *Communications in Theoretical Physics*, 2004, v. 41, 567–572.
29. Rosenstein B., Li D. P. Ginzburd-Landau theory of type II superconductors in magnetic field. *Reviews of Modern Physics*, 2010, v. 82, 109–168.
30. Wikipedia, Ginzburg-Landau theory.
31. Cyrot M. Ginzburg-Landau theory for superconductors. *Reports on Progress in Physics*, 1973, v. 36, 103–158.

Progress in Physics is an American scientific journal on advanced studies in physics, registered with the Library of Congress (DC, USA): ISSN 1555-5534 (print version) and ISSN 1555-5615 (online version). The journal is peer reviewed and listed in the abstracting and indexing coverage of: Mathematical Reviews of the AMS (USA), DOAJ of Lund University (Sweden), Zentralblatt MATH (Germany), Scientific Commons of the University of St.Gallen (Switzerland), Open-J-Gate (India), Referential Journal of VINITI (Russia), etc. Progress in Physics is an open-access journal published and distributed in accordance with the Budapest Open Initiative: this means that the electronic copies of both full-size version of the journal and the individual papers published therein will always be acessed for reading, download, and copying for any user free of charge. The journal is issued quarterly (four volumes per year).

Electronic version of this journal: http://www.ptep-online.com

Postal address:
Department of Mathematics and Science,
University of New Mexico, 705 Gurley Avenue, Gallup, NM 87301, USA

Printed in the United States of America